

PHYSICAL AND CHEMICAL MODIFICATION OF MEDICAL METAL ALLOYS TO ENHANCE SURFACE FUNCTIONALISATION FOR ANTIMICROBIAL PEPTIDE IMMOBILISATION

by

Mohadeseh Zare

A thesis submitted to the **University of Birmingham** for the degree of

DOCTOR OF PHILOSOPHY

School of Metallurgy and Materials

College of Engineering and Physical Science

University of Birmingham

October 2024

UNIVERSITY OF
BIRMINGHAM

University of Birmingham Research Archive

e-theses repository

This unpublished thesis/dissertation is copyright of the author and/or third parties. The intellectual property rights of the author or third parties in respect of this work are as defined by The Copyright Designs and Patents Act 1988 or as modified by any successor legislation.

Any use made of information contained in this thesis/dissertation must be in accordance with that legislation and must be properly acknowledged. Further distribution or reproduction in any format is prohibited without the permission of the copyright holder.

Abstract

The rise of antibiotic-resistant bacterial infections has become a significant concern in implant failure. A promising strategy to combat peri-implant infections involves the use of antimicrobial peptides (AMPs), which exhibit broad-spectrum activity against Gram-positive and Gram-negative bacteria, fungi, and viruses, while also demonstrating a low propensity for inducing bacterial resistance. Recently, various strategies have been applied for the chemical and physical immobilisation of AMPs on surfaces. These approaches vary in terms of binding strength, modularity, stability, and complexity. While physical binding methods often result in weak immobilisation and the potential detachment of bioactive molecules, chemical integration of AMPs into biomaterials provides a more robust immobilisation, ensuring that the peptides remain stable and optimally oriented on the surfaces. However, chemical integration is a complex process involving multiple steps that can impact overall efficiency. Among the numerous techniques available for chemical immobilisation, plasma nitriding has gained attention for its time- and energy-efficient process, as well as the use of nontoxic materials. The primary objective of this study was to develop innovative antimicrobial surfaces for titanium alloys by incorporating AMPs and utilising advanced surface engineering techniques. In this study KR-12 peptide has been employed as an AMP derived from the human cathelicidin LL-37, known for its broad-spectrum activity against bacteria by disrupting microbial membranes. Titanium implants were functionalised with the KR-12 peptide using two approaches: titanium surface plasma treatment and silanisation, both aimed at generating amine groups on the surface to facilitate subsequent reactions with KR-12. Additionally, the study investigated how different linking arms -Polyethylene Glycol (PEG) and human-elastin-like-polypeptide (HELP)- affect the antimicrobial activity of the peptides through comprehensive surface characterisations, biological assays, and antimicrobial evaluations.

In the initial phase of this study, plasma treatment was utilised to further immobilise the KR-12 peptide on titanium implant surfaces, and polyethylene-glycol (PEG) was employed as a linker to impart antifouling properties and enhance peptide mobility, thereby improving antimicrobial efficacy. Plasma treatment was chosen for its ability to introduce functional groups, streamline chemical reactions, and reduce processing time. The primary amine groups (NH_2) generated during plasma treatment could form strong attachments to titanium surfaces, serving as anchors for immobilising bioactive agents. In this study, our first objective was to

optimise plasma treatment parameters to achieve surface-bound amine group levels comparable to those obtained through chemical techniques like silanisation. X-ray photoelectron spectroscopy (XPS) analysis revealed that the distribution and density of primary amine groups could be finely tuned by adjusting plasma parameters, reaching a maximum of 9.18% without altering the titanium surface morphology or bulk properties.

Following the generation of primary amine groups, PEG and KR-12 were immobilised on the surface at specific concentrations. The antimicrobial activity of these coatings against four pathogenic bacterial strains demonstrated over 90% inhibition of bacterial adhesion and colonisation. The enhanced activity was due to the improved orientation of linker-grafted AMPs compared to directly immobilised peptides. Also, the plasma-treated surfaces were proven to enhance cell proliferation and adhesion. These results underscored the potential of combining plasma treatment with the covalent bonding of AMPs, exploiting both the antimicrobial properties of the AMPs and the cell-promoting effects of the plasma-treated surface.

In the second phase of the study, silanisation was employed to introduce primary amine groups onto the surface, serving as anchor points for the immobilisation of the KR-12. This study introduced an enzyme-responsive antimicrobial coating for orthopaedic devices, utilising KR-12 in conjunction with Human Elastin-Like Polypeptide (HELP) as a biomimetic, stimuli-responsive linker that emulates the ECM. Upon implantation, these tailored interfaces interacted with the innate immune response, leading to the release of elastase. The biodegradation of the HELP biopolymer by elastase facilitated the controlled release of KR-12. The antimicrobial activity of the KR-12-HELP-functionalised titanium surface was evaluated against four pathogenic bacterial strains (*Staphylococcus aureus, Staphylococcus epidermidis, Escherichia coli*, and *Pseudomonas aeruginosa*), demonstrating an inhibition of bacterial adhesion and colonisation exceeding 91.86% for all tested strains. When compared to a titanium surface functionalised directly with KR-12 without the HELP linker, the antimicrobial efficacy was significantly enhanced. This improvement was due to the increased mobility of KR-12 when coupled with HELP and its stimuli-responsive controlled release.

Plasma treatment demonstrated superior efficiency, introducing 9.18% primary amine groups on titanium surfaces compared to 4.67% with silanisation. Both methods achieved comparable peptide immobilisation levels (59.67 nmol and 61.34 nmol respectively), although plasma treatment offered additional advantages, such as enhanced surface energy, improved protein

adsorption, reduced toxicity, and lower costs. Plasma-treated surfaces maintained biocompatibility, promoting cell adhesion and proliferation without altering surface morphology.

This study highlights plasma treatment as a cost-effective and efficient alternative to silanisation, particularly when combined with advanced linker systems such as PEG and HELP. The integration of these methods offers a promising pathway for developing next-generation antimicrobial coatings for orthopaedic implants, enhancing both bacterial resistance and tissue integration.

Acknowledgements

First and foremost, I would like to express my gratitude to my main supervisor, Prof Artemis Stamboulis. Her guidance and advice have been instrumental, and this project would not have been possible without her support. I would like to extend my thanks to my co-supervisors, Prof Sarah Kuehne and Prof Zubair Ahmed, for their invaluable assistance throughout this study.

I am also deeply thankful for the funding provided by the European Union's Horizon 2020 research and innovation programme under the Marie Skłodowska-Curie grant agreement No 861138 AIMed, which made this research possible.

I am also grateful to everyone in the Biomaterials group, whose friendship and support have significantly enriched my time at the university.

I would also like to show my gratitude to the staff at the School of Metallurgy and Materials, the School of Dentistry, and the Institute of Inflammation and Ageing. I am particularly grateful to Dr. Melissa Grant and Dr. Abhinav Thareja for their invaluable guidance during the experiments.

Additionally, I wish to acknowledge Dr Bogdan Butoi, Dr Ion N. Mihailescu, and Dr Corneliu Porosnicu from the National Institute for Laser, Plasma & Radiation Physics in Romania for their support with the plasma treatment.

Last but certainly not least, I am deeply grateful to my husband, Dr Pooya Davoodi, for his support and patience, which has helped me pursue my passion.

Publications

- Riccio, P., **Zare, M.**, Gomes, D., Green, D., Stamboulis, A. (2022). Antimicrobial Bioceramics for Biomedical Applications. In: Choi, A.H., Ben-Nissan, B. (eds) Innovative Bioceramics in Translational Medicine I. Springer Series in Biomaterials Science and Engineering, vol 17. Springer, Singapore. https://doi.org/10.1007/978-981-16-7435-8_5

- **Zare M**., Colomina Alfaro L., Bandiera A., Mutlu E., Grossin D., Albericio F., A. Kuehne S., Ahmed Z., Stamboulis A. (2024). Enzyme-Responsive Coatings Supporting Dual Functionality: Osteoblast Promotion and Antimicrobial Activity for Orthopaedic Implants; Submitted and under review.

- **Zare M**., Butoi B., Porosnicu C., N. Mihailescu I., Grossin D., A. Kuehne S., Ahmed Z., Stamboulis A. (2024). Optimised Amine Density via Plasma Treatment for Covalent immobilisation of AMPs to Promote Osteoblasts and Enhance Antimicrobial Activity; In preparation.

Conference Presentations and Posters:

- "Covalent immobilisation of Peptides Antimicrobial Coating for Orthopaedic Implants" M. Zare, Kuehne S., Ahmed Z., and Stamboulis A., 31st Annual Conference of the European Society for Biomaterials (ESB) 2021.

- "Antimicrobial Coating for Orthopaedic Implants Using Covalent Immobilisation of Peptides" M. Zare, Kuehne S., Ahmed Z., Stamboulis A., Tissue Engineering and Regenerative Medicine International Society (TERMIS) European Chapter Meeting 2022.

- "Surface Functionalisation of Medical Devices by Plasma Treatment and Peptide Immobilisation for Antimicrobial Coatings" M. Zare, A. Stamboulis, 33rd Annual Conference of the European Society for Biomaterials (ESB) 2023.

Table of Contents

List of Figures x

List of Tables xiii

Abbreviations xiv

Chapter One: General Introduction 1

1.1. Bacterial infections 2

1.2. Antimicrobial peptides (AMPs) and their mechanisms 2

1.3. AMP-based antimicrobial coatings 6

1.3.1 Polymer brushes 6

1.3.2 Polydopamine (PDA) layers 8

1.3.3 Physical adsorption 9

1.3.4 Chemical binding on functionalised surfaces 10

1.4. Covalent immobilisation of AMPs on titanium implants 13

1.4.1 Silanisation of titanium surfaces 14

1.4.2 Plasma treatment of titanium surfaces 17

1.4.3 Direct immobilisation of AMPs 20

1.4.4 Linker incorporated immobilisation of AMPs 21

1.4. Aims and objectives 23

1.5. References 27

Chapter Two: Optimised Amine Density via Plasma Treatment for Covalent Immobilisation of AMPs to Promote Osteoblasts and Enhance Antimicrobial Activity 39

2.1. Introduction 41

2.2. Experimental methods 45

2.2.1 Sample preparation 45

2.2.2 Plasma treatment 46

2.2.3 PEG attachment 48

2.2.4 Covalent immobilisation of KR-12 48
2.2.5 Thermal and mechanical stability of plasma-treated surfaces 49
2.2.6 Surface characterisation 49
2.2.7 Concentration of immobilised KR-12 51
2.2.8 KR-12 release rate 51
2.2.9 Antimicrobial activity assay 52
2.2.10 Bacterial growth inhibition 53
2.2.11 Bacterial morphology assay 54
2.2.12 Confocal Laser Scanning Microscopy (CLSM) 54
2.2.13 Cell viability and compatibility assessment 55
2.2.14 Statistical analyses 56
2.3. Results and discussion 56
2.3.1 Optimisation of plasma parameters and stability of treated surfaces 57
2.3.2 Surface characterisation by XPS, AFM, FTIR, and WCA 61
2.3.3 Concentration of the immobilised KR-12 and release rate 68
2.3.4 Antimicrobial activity assay 70
2.3.5 Cytocompatibility and cell adhesion 75
2.4. Conclusions 78
2.5. References 79
Chapter Three: Enzyme-Responsive Coatings Supporting Dual Functionality: Osteoblast Promotion and Antimicrobial Activity for Orthopaedic Implants 91
3.1. Introduction 93
3.2. Experimental methods 96
3.2.1 Sample preparation 96
3.2.2 Silanisation of titanium substrates 98
3.2.3 Production and purification of the HELP biopolymer 98
3.2.4 HELP attachment 99

3.2.5 Covalent immobilisation of KR-12 100
3.2.6 Surface characterisation 101
3.2.7 Concentration of immobilised KR-12 102
3.2.8 KR-12 release triggered by elastase degradation of HELP 103
3.2.9 Antimicrobial activity assay 104
3.2.10 Bacterial growth inhibition 104
3.2.11 Bacterial morphology assay 105
3.2.12 Confocal Laser Scanning Microscopy (CLSM) 106
3.2.13 Cell viability and compatibility assessment 106
3.2.13 Quantification of cell viability using MTT assay 107
3.2.14 Statistical analyses 107
3.3 Results and discussion 108
3.3.1 Surface characterisation by SEM, FTIR, AFM, XPS and WCA 108
3.3.2 Calculation of the peptide density 117
3.3.3 KR-12 release triggered by elastase 117
3.3.4 Antimicrobial activity assay 118
3.3.5 Cytocompatibility and cell adhesion 123
3.4 Conclusions 126
3.5 References 127
Chapter Four: General Discussion 136
4.1. Research steps and objectives 137
4.2. Phase one: 137
4.3. Phase two: 139
4.5. Overall comparison of findings 141
4.6. References 146
Chapter Five: Conclusions and Future Perspective 151

5.1. Conclusions 152

5.2. Future perspective..... 153

Appendix..... i

List of Figures

Figure 1-1. (a) Immune modulation of cells including neutrophils, t-cells and macrophages to regulate inflammation and facilitate bacterial clearance as well as directly kill planktonic bacteria by AMPs [27]. (b) The antibiofilm properties of AMPs and the underlying cellular mechanisms involved to hinder bacterial adhesion to surfaces, which prevents the initial formation of biofilms and disrupts those that are already established. [28]. 4

Figure 1-2. The schematic illustration of (a) polymer brush strategy and (b) dopamine-based coating to prevent bacteria attachment.....8

Figure 1-3. Schematic illustration of the structure of an APTES molecule, its activation. process, and its reaction with a hydroxylated oxide surface.....16

Figure 1-4. (a) Schematic representation of a plasma nitriding reactor illustrating the placement of the forming tool at the cathodic potential [128]. (b) Townsend breakdown and electron avalanche formation between two electrodes [129].....18

Figure 2-1. Schematic illustration of the step-by-step process of A. plasma treatment, B. PEG attachment, and KR-12 immobilisation, outlining the preparation of C. antimicrobial coating for titanium surfaces....45

Figure 2-2. Plasma treatment evaluation: (a) Scheme of purpose-designed plasma reactor with adjustable parameters. (b-d) Concentration of primary amine groups measured by XPS as a function of varying plasma parameters to determine optimal conditions. (e) Ambient stability of primary amine groups on plasma-treated discs at room temperature over a period of up to 14 days, with XPS analyses used to monitor changes in NH_2 concentration. (f) Mechanical stability of primary amine groups within 30 minutes of ultrasonication. Error bars represent the standard deviation from three independent experiments 59

Figure 2-3. XPS results of surface elemental composition after the modification steps during the plasma treatment, PEG attachment and KR-12 immobilisation: (a) XPS survey spectra, (b) Relative atomic ratios of chemical compositions, (c) high-resolution C1 s spectra, and (d) high-resolution N 1s spectra of different surface modifications. See Table 2.1 for abbreviations. 64

Figure 2-4. Characterisation of titanium surfaces after plasma treatment, PEG attachment and KR-12 immobilisation: (a) Surface morphology and mean roughness (Ra) analysed via AFM 3D imaging. (b) ATR-FTIR spectra of different coatings (c) Quantitative water contact angle measurements along with representative images of water droplets. Results are presented as the mean ± standard deviation (SD) of three independent experiments performed in triplicate. Statistical significance is indicated by * for $p < 0.05$, ** for $p < 0.01$, and *** for $p < 0.001$ between UTi and all modified surfaces. 66

Figure 2-5. KR-12 release rates from KR12-NTi and KR12-PNTi in PBS at 37 °C for 168 hours. Results are presented as the mean ± standard deviation (SD) of independent experiments performed in triplicate.70

Figure 2-6. Assessment of antimicrobial activity; (a) Bacterial growth inhibition of the various surface coatings against *E. coli*, *P. aeruginosa*, *S. aureus*, and *S. epidermidis* with UTi samples serving as controls

showing 0.00% inhibition. Statistical significance is denoted by * for $p < 0.05$, ** for $p < 0.01$, and *** for $p < 0.001$. Error bars represent the standard deviation from three independent experiments, each performed in triplicate. (b) The fluorescence live/dead assay and SEM images of (b) *S. aureus* and (c) *E. coli* cultured on different coatings (Live/Dead assay scale bars = 10 μm, green bacteria: live, red bacteria: dead); (SEM images scale bars = 5 μm). All assessments were taken after 24 hours of surface incubation. Both KR12-NTi and KR12-PNTi surfaces exhibited higher bacterial affinity than NH_2-Ti and PEG-NTi. The inclusion of PEG as a linker appeared to reduce bacterial adhesion. AMPs attached to KR12-NTi and KR12-PNTi demonstrated effective bactericidal activity, disrupting the membranes of both *E. coli* and *S. aureus* bacteria. 74

Figure 2-7. Cytocompatibility and cell morphology analyses: (a) Cell viability results from the MTT assay of hFOB cells cultured on various substrates over 3, 5, and 7 days, no significant difference was observed compared to UTi; Statistical significance is denoted by * for $p < 0.05$. (b) SEM micrographs depicting the morphology of hFOB cells on day 5 (Scale bars = 20 μm); By day 5, cells displayed a spread morphology with filopodia extending towards neighbouring cells. 77

Figure 3-1. Schematic representation of (a) step-by-step procedure of silanisation, HELP attachment, and KR-12 immobilisation to prepare enzyme-responsive antimicrobial coating for titanium implant surfaces, and (b) the chemical reactions occurred in each step at the interface of the titanium surface and the reagents. The diagram is not drawn to scale, and symbols are just utilised to elucidate the underlying concepts; APTES = (3-aminopropyl) triethoxysilane, HELP = Human elastin-like polypeptide, EDC = 1-ethyl-3-diaminopropyl carbodiimide hydrochloride, sulfo-NHS = sulfo-N-hydroxysuccinimide. 97

Figure 3-2. Surface characterisation of coated titanium surfaces; (a) SEM micrographs depicting the surface morphology, with a scale bar of 10 μm, (b) ATR-FTIR spectra, and (c) mean roughness (Ra) and morphology analysed by AFM 3D imaging. *** denotes statistical significance ($p < 0.001$) between the polished titanium (PTi) and all modified surfaces. 109

Figure 3-3. XPS analysis results for characterisation of surface elemental composition after the modification steps during the silanisation, HELP attachment and KR-12 immobilisation; (a) high-resolution C1 s spectra and (b) N 1s spectra of PTi, Sil-PTi, KR12-STi, HELP-STi, and KR12-HTi, (c) relative atomic ratios of chemical compositions, and d) ratios of different elements to Ti 2p% for all samples. 115

Figure 3-4. The quantitative measurement of (a) the water contact angle of each titanium substrate (**$P < 0.01$, ***$P < 0.001$) and representative images of the water drops on the different coatings, and (b) KR-12 release from coating in the absence and presence of elastase. Reactions were carried out at 37 °C for 24 hours. Following incubation, the proteolytic activities were detected by absorbance readings at 585 nm. Results were the mean ± standard deviation (SD) of three independent experiments performed in triplicate. 116

Figure 3-5. Assessment of antimicrobial activity; (a) bacterial growth inhibition ratio of the indicated surface coatings against *E. coli*, *P. aeruginosa*, *S. aureus*, and *S. epidermidis*, PTi samples were considered

as controls showing 0.00% inhibition ratio. * Denotes $p < 0.05$, ** denotes $p < 0.01$, *** denotes $p < 0.001$ (all error bars denote the standard deviations over triplicate measurements), and fluorescence live/dead assay images of (b) *E. coli* and (c) *S. aureus* cultured on different coatings (Scale bars = 6 µm, green bacteria: live, red bacteria: dead). Both HELP-STi and KR12-HTi surfaces exhibited higher bacterial affinity than Sil-PTi. The inclusion of HELP as a linker appeared to amplify bacterial adhesion. However, a significant portion of bacteria that adhered to KR12-HTi were found to be deceased. 120

Figure 3-6. SEM characterisation of bacterial growth of substrates. SEM images of (a) *E. coli* and (b) *S. aureus* on indicated substrates. All results were taken after 24 hours of incubation with the surface. Scale bars = 5 µm. AMPs attached to KR12-HTi and KR12-STi showed adequate bactericidal activity to disrupt the membranes of both *E. coli* and *S. aureus* bacteria. 122

Figure 3-7. Cytocompatibility and cell morphology study; (a) cell viability results of MTT test of hFOB cells cultured on different substrates after 3, 5, and 7 days of culturing, * denotes significant differences ($p < 0.05$) compared with PTi, and (b) SEM micrographs showing the morphology of the seeded hFOB cells on day 3 and 7. Scale bars = 20 µ m. By Day 7, the cells exhibited a spread morphology with filopodia extending towards adjacent cells, accompanied by the formation of mineralised deposits (depicted by arrows) on KR-STi, HELP-STi, and KR-HTi surfaces. 125

Figure 4-1. Comparison of two methods for functionalising surfaces—silanisation and plasma treatment—the results of surface roughness, water contact angle, cell viability, and bacteria inhibition ratio for prepared samples from both phases of the study 142

Figure S1. a) Calibration curve of dibenzofulvene-base adduct (µM) vs. absorbance, using 20% piperidine (Panel B) in DMF, b) Mechanism for Fmoc group removal from immobilised KR-12. ii

Figure S2. XPS survey spectra of modified surfaces PTi, Sil-PTi, KR12-STi, HELP-STi, and KR12-HTi with characteristic peaks of carbon (C), oxygen (O), nitrogen (N), silicon (Si), and titanium (Ti). iii

List of Tables

Table 1-1. A summary of recent studies on the immobilisation of AMPs on different forms of medical implants for various applications. 10
Table 2-1. Description of sample names corresponding to various surface modifications. 45
Table 2-2. Range of Plasma Parameters Investigated for Pulsed DC Power Supply. 48
Table 3-1. Description of sample names indicating different surface modifications. 96
Table 4-1. Optimised plasma parameters to maximise the primary amine groups.....138

Abbreviations

AC	Alternating Current
AFM	Atomic Force Microscopy
AMP	Antimicrobial Peptide
APMA	N-(3-aminopropyl)-methacrylamide hydrochloride
DMA	N,N-dimethylacrylamide
APTES	3-Aminopropyltriethoxysilane
ATR-FTIR	Attenuated Total Reflectance Fourier-Transform Infrared
ATRP	Atom-transfer Radical Polymerisation
CFU	Colony Forming Units
CW	Continuous Wave
Cys-LL37	Cysteine-LL37
DBF	9,9-Dimethylfluorene
DC	Direct Current
DCC	Dicyclohexylcarbodiimide
DCT	Disk Contact Test
DI	Deionised
DMSO	Dimethyl Sulfoxide
ECM	Extracellular Matrix
EDC	1-Ethyl-3-(3-dimethyl-aminopropyl) carbodiimide
E. coli	*Escherichia coli*
FBS	Fetal Bovine Serum
FMOC	Fluorenyl methyloxy carbonyl

FTIR	Fourier-Transform Infrared
F. nucleatum	*Fusobacterium nucleatum*
GPTS	(3-Glycidyloxypropyl)-trimethoxysilane
HA	Hyaluronic acid
HAp	Hydroxyapatite
HELP	Human Elastin-Like Polypeptide
hFOB 1.19	Human Fetal Osteoblast 1.19 cell line
ISO	International Organisation for Standardisation
LTP	Low temperature plasma
MES	2-(N-morpholino) ethanesulfonic acid
MIC	Minimum inhibitory concentration
μM	Micromolar
MTT	3-(4, 5-dimethylthiazolyl-2)-2, 5-diphenyltetrazolium bromide
MW	Microwave
$NaBH_4$	Sodium borohydride
NHS	N-Hydroxysuccinimide
OD_{600}	Optical Density at 600 nm
P. aeruginosa	*Pseudomonas aeruginosa*
PBS	Phosphate-Buffered Saline
PDA	Polydopamine
PEG	Polyethylene glycol
P. gingivalis	*Porphyromonas gingivalis*
R_a	Mean Roughness
RGD	Arginine-glycine-aspartate

RF	Radio Frequency
S. aureus	*Staphylococcus aureus*
S. epidermidis	*Staphylococcus epidermidis*
S. mutans	*Streptococcus mutans*
S. typhimurium	*Salmonella typhimurium*
SCCM	Standard Cubic Centimeters per Minute
SEM	Scanning Electron Microscopy
t-Bu	Tert-Butyl
TEM	Transmission Electron Microscopy
TCP	Tissue Culture Plastic
UV	Ultraviolet
WCA	Water Contact Angle
XPS	X-ray photoelectron spectroscopy

Chapter One:

General Introduction

1.1. Bacterial infections

Medical devices have been advanced significantly to save lives, but they also pose a considerable risk due to the potential for infection resulting from bacterial colonisation and biofilm formation [1]. Microbial biofilms, which are complex, multicellular communities surrounded by a self-produced extracellular matrix (ECM) consisting of polysaccharides, extracellular DNA, and proteins, can develop on the implanted device surfaces [2]. The development of biofilms at the implant-tissue interface can significantly compromise immune responses, prolong the duration of antibiotic therapy, and, in some cases, require multiple surgical procedures [3-5]. Within biofilms, bacterial cells can exhibit a dramatic increase in antibiotic resistance. This elevated resistance persists even with the application of aseptic surgical techniques and systemic antibiotic treatments, leading to hospital acquired infections associated with implants that contribute substantially to patient morbidity and mortality [6]. Preventing bacterial colonisation on biomedical surfaces, such as implants, is a critical step in reducing infection spread. Various surface treatment methods, including the application of polymers, metallic compounds, quaternary ammonium salts, and other agents, have been explored to create novel antimicrobial surfaces. However, most of these agents come with significant limitations including the risk of cytotoxicity to target tissues, limited efficacy, and narrow antimicrobial spectra. These issues are particularly concerning when these agents are used against antibiotic-resistant bacteria [7, 8].

1.2. Antimicrobial peptides (AMPs) and their mechanisms

AMPs, which are naturally produced by the innate immune systems of all multicellular organisms, represent a promising category of molecules, addressing the challenge of antibiotic resistance [9]. These peptides are recognised for their strong and broad-spectrum antimicrobial activity against bacteria, fungi, and parasites, with the ability to inactivate certain viruses as well [10]. AMPs operate through a unique mechanism of action, which results in rapid activity against bacteria and fungi [11]. One promising application of AMPs is their incorporation into coatings that can be applied to implant surfaces, delivering targeted antimicrobial action precisely where it is most required [12]. Furthermore, immobilising AMPs onto implant surfaces can overcome the limitations associated with free-circulating AMPs, such as their short half-life and cytotoxicity at high concentrations [3]. This immobilisation can be obtained physically, through methods like layer-by-layer

assembly or adsorption, or chemically, through covalent bonding [13].

AMPs typically consist of a short, amphiphilic sequence of 12 to 50 amino acid residues and generally possess a net positive charge ranging from +2 to +9, primarily due to the presence of arginine and lysine residues [14]. This positive charge enhances their interaction with negatively charged bacterial membranes, a key factor in their antimicrobial activity [15]. AMPs disrupt bacterial cell membranes, leading to cell lysis. They do so by electrostatic interactions with bacterial membranes, as these membranes carry a negative charge, unlike mammalian cell membranes, which are neutral. This higher net negative charge of bacterial membranes is attributed to the acidic phospholipids in their outer membrane layer, whereas mammalian cell membranes contain cholesterol and phosphatidylcholine, which reduce interaction with AMPs [16],[17]. Consequently, AMPs can achieve effective antimicrobial concentrations while maintaining biocompatibility with adjacent tissues, even at elevated concentrations [18].

Various models have been proposed to elucidate the microbicidal mechanisms of AMPs through their interaction with bacterial cell membranes [19, 20]. A detailed examination of these models is presented in the review by Brodgden [21].

One model highlights the role of strong electrostatic interactions between AMPs and bacterial membranes [22]. These interactions can lead to direct bacterial cell lysis, facilitate self-uptake of AMPs, or induce pore formation. This pore formation allows AMPs to penetrate further into the bacterial cell, disrupting several intracellular processes like protein synthesis, transcription factor binding to nucleic acids, DNA replication, and cell wall synthesis [19, 23].

Additionally, the antimicrobial efficacy of AMPs is influenced by their secondary structure (e.g., α-helix, β-sheet), the presence of aromatic amino acids, notably tryptophan, hydrophobicity, and amphipathicity [24, 25].

The intricate and multifaceted mechanisms by which AMPs act against bacterial cells may explain the low rate of resistance development observed in bacteria exposed to these peptides. Unlike conventional antibiotics, AMPs employ diverse microbial killing strategies and have the potential to work synergistically with other antibiotics and AMPs, thereby reducing the likelihood of resistance emergence.

In addition to their roles in immune modulation and direct killing of planktonic bacteria

(Figure 1-1(a)), AMPs have emerged as promising agents for combating chronic bacterial biofilms (Figure 1-1(b)). For example, Fuente-Nunez et al screened a synthetic peptide library to identify peptides with optimised antibiofilm activity [26]. Their findings revealed that direct antimicrobial activity against planktonic bacteria did not necessarily align with effectiveness against biofilms. A notable lead peptide discovered in this study was the KRFRIRVRV-NH_2, which exhibited activity against *Burkholderia cenocepacia* biofilms despite the bacterium's resistance to AMP action in its planktonic form.

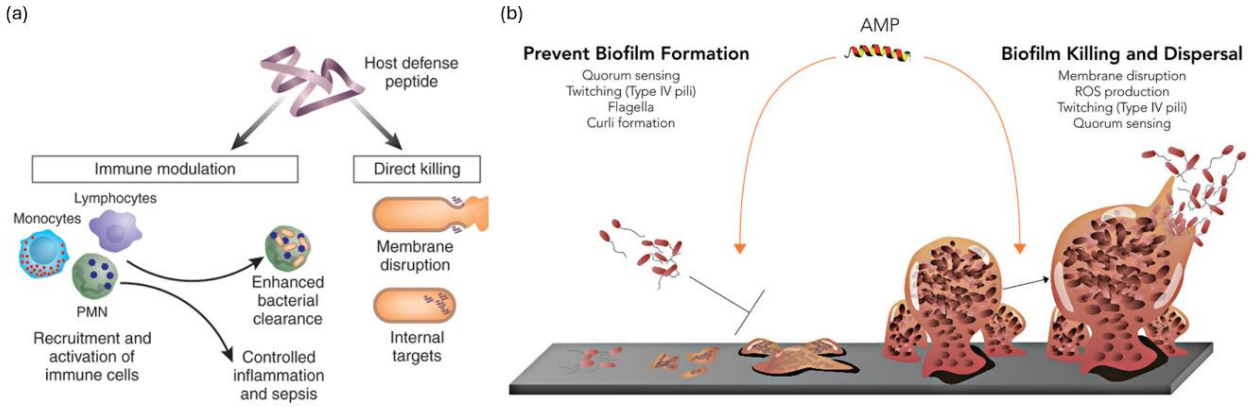


Figure 1-1. (a) Immune modulation of cells including neutrophils, t-cells and macrophages to regulate inflammation and facilitate bacterial clearance as well as directly kill planktonic bacteria by AMPs [27]. (b) The antibiofilm properties of AMPs and the underlying cellular mechanisms involved to hinder bacterial adhesion to surfaces, which prevents the initial formation of biofilms and disrupts those that are already established. [28].

Among many studied peptides, derivatives of peptide LL-37 have been shown to exhibit broad-spectrum antimicrobial activity. These derivatives not only prevent the formation of biofilms but also effectively eradicate existing biofilms of *Staphylococcus epidermidis* [29]. Further research has explored the incorporation of additional biological functionalities into the LL-37 sequence. For instance, Nagant et al. developed a library of 12 truncated LL-37 fragments, varying in length from 19 to 31 amino acids and identified eight peptides with significant activity against *Pseudomonas aeruginosa* biofilms [30]. Additionally, various peptide derivatives of LL-37 have been developed to target MRSA in skin burn models [31].

Current efforts are focused on developing smaller peptides to reduce synthesis and fabrication costs. One example is the 12-mer peptide 1018 (VRLIVAVRIWRR), which was created using the amino acid sequence of the cattle neutrophil peptide bactenecin as a basis.

This peptide has demonstrated efficacy in inhibiting and eradicating biofilms formed by various Gram-negative pathogens and Gram-positive, drug-resistant pathogens [32].

Alterations in peptide sequences can sometimes lead to molecules with heightened cytotoxicity. To address this, structure–activity relationship models and computer-aided AMPs can offer predictive insights into the biological activity of candidate sequences prior to synthesis. *De novo* design approaches influence statistical analysis tools and machine learning algorithms to create and refine new therapeutic molecules, enabling the development of AMPs with optimised efficacy and reduced toxicity [33, 34]. For instance, two short AMP candidates, HHC36 (Tet127) and Tet213, were identified through an extensive Quantitative Structure-Activity Relationship study. Both peptides exhibited strong broad-spectrum antimicrobial activity. For example, HHC36 was noted for its comparatively lower cytotoxicity, making it a suitable candidate for peptide-loaded calcium phosphate coatings for titanium implants [35, 36].

LL-37 is the only cathelicidin AMP present in humans, playing a crucial role in the innate immune system [37]. In 2008, Wang identified an active fragment of this peptide, named 'KR-12' . This fragment corresponds to the amino acid sequence KRIVQRIKDFLR-NH2, specifically spanning residues 18 to 29 of the parent peptide [37]. Similar to its precursor peptide LL-37, KR-12 offers several therapeutic advantages. KR-12 and its derivatives, such as KR-12-a5 and KR-12-a4, have been shown to promote osteogenic differentiation, which is critical for bone growth and repair [38]. Additionally, research by Liu et al., 2019 demonstrated that when KR-12 was loaded onto hyaluronic acid-coated eggshell membranes, it enhanced re-epithelialisation and angiogenesis, contributing to wound healing by fostering blood vessel formation [39]. KR-12 and its analogues also exhibit anti-inflammatory properties. For instance, Jacob et al.,2013 assessed the anti-endotoxic effects of KR-12 and its variants by measuring their ability to inhibit the production of tumour necrosis factor-α (TNF-α) in LPS-stimulated macrophage cells [40]. Furthermore, Fabisiak et al 2021 tested KR-12's efficacy against bowel diseases, demonstrating that KR-12 exhibited superior anti-inflammatory activity compared to its original peptide, LL-37. While several analogues and modifications of KR-12 showed enhanced antimicrobial properties, the unmodified KR-12 was selected for this research. The decision to use unmodified KR-12 was based on its strong clinical familiarity as an AMP, making it the most reasonable option.

Although AMPs exhibit strong antimicrobial properties, the recent research proved that bacteria can develop resistance through adaptations involving cell wall modifications and alterations in cellular metabolism [41, 42]. For instance, non-ribosomal AMPs (nrAMPs) like vancomycin inhibit bacterial cell wall synthesis by binding to the d-Ala-d-Ala terminus of Lipid II. However, resistance can emerge when bacteria modify this precursor, substituting d-Ala-d-Ala with d-Ala-d-Ser or d-Ala-d-Lac, which reduces vancomycin's binding affinity and effectiveness [43]. On the other hand, ribosomally synthesized cationic AMPs (rAMPs), which rapidly disrupt bacterial membranes, are considered less prone to resistance [41, 42, 44]. Nevertheless, bacteria can still develop resistance by altering membrane charge to become more positive, incorporating neutral membrane components, modifying membrane fluidity, or employing proteases and efflux pumps to degrade the AMPs. Despite these potential resistance mechanisms, both nrAMPs and rAMPs, including synthetic AMPs, are generally less susceptible to resistance compared to conventional antibiotics [41, 42].

1.3. AMP-based antimicrobial coatings

To achieve specific antimicrobial properties, AMPs can be immobilised or conjugated to polymer-functionalised surfaces, polymer vesicles, micelles, hydrogels, and similar substrates, contributing to the development of advanced multi-functional biomedical coatings [78]. Techniques for covalent attachment of AMPs to the coatings, such as the formation of amide-bonds and click chemistry, require compatible functional groups on both the AMPs and the polymers chains [79]. Alternatively, AMP immobilisation can be accomplished through methods including Michael addition/Schiff base reactions, photo crosslinking, and oxidation reactions [78]. The following sections will inspect the prevalent strategies for AMPs incorporation on titanium surfaces.

1.3.1 Polymer brushes

A polymer brush is an arrangement of densely packed polymer chains chemically bonded to a surface at one end [45]. This configuration results in a "brush" structure where the chains extend outward, creating a high-density layer that fills the space above the surface and prevents chain intermingling [46, 47]. The polymer brush acts as a flexible linker between the implant surface and AMPs, minimising the effects of surface restriction. Numerous studies have explored the use of polymer brushes as linkers between AMPs and titanium implant surfaces during immobilisation (Figure 1-2(a)). For instance, Gallardo et

al demonstrated the covalent attachment of hLF1-11 (GRRRRSVQWCA), to a co-polymer brush made from Dimethylacrylamide (DMA) and Acryloylaminopropyl Methacrylate (APMA) [48]. This polymer brush-hLF1-11 chain was subsequently attached onto a titanium surface that had been functionalised with an Atom Transfer Radical Polymerisation (ATRP) initiator. The bacterial inhibition of the resulting antimicrobial coating was analyzed using two oral bacterial strains, Streptococcus sanguinis and Lactobacillus salivarius, showing inhibition rates of 15.7% and 30.4%, respectively. Further testing revealed that the bio-functionalised surfaces exhibited antibacterial properties, reducing bacterial adhesion by 70% as confirmed by live and dead staining assays [87]. Additionally, the hLF1-11 releasing surfaces were found to prevent early-stage biofilm formation by both bacterial strains.

Gao et al. employed a similar approach to tether AMPs containing terminal cysteine residues e.g., Tet-20, Tet-213, 1010cys to titanium surfaces [49]. To tether the AMPs, the titanium surface was modified with an ATRP initiator, while the DMA and APMA copolymer underwent functionalisation [49]. The titanium surfaces functionalised with various AMPs were evaluated for their activity against *P. aeruginosa*. Polymer brush coatings also allow for functionalisation with multiple peptides that possess diverse functionalities. For instance, Muszanska et al utilised Pluronic F-127, as a block copolymer, immobilised on silicone [50]. The polymer brushes were functionalised with ILPWRWPWWPWRR-NH_2 as an AMP and an RGD-containing peptide, to combine anti-adhesive, bactericidal, and tissue-integrating properties. This peptide releasing coating demonstrated both antifouling and bactericidal effects against *Staphylococcus aureus (S. aureus)*, *Staphylococcus epidermidis (S. epidermidis)*, and *Pseudomonas aeruginosa (P. aeruginosa)*, nearly completely preventing bacterial adhesion on the treated silicone rubber surface. Additionally, the incorporation of RGD moieties on the AMP-coated surface enhanced fibroblast coverage, promoting better tissue integration.

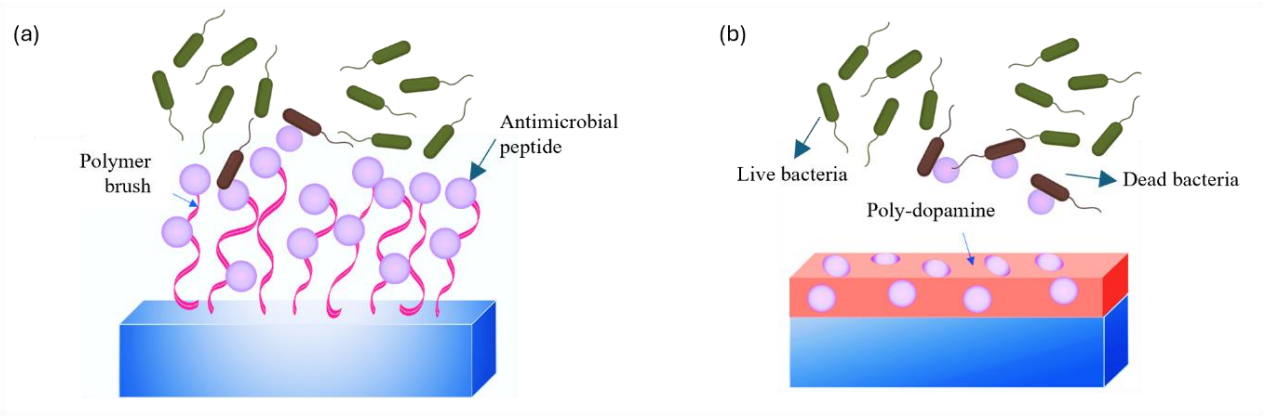


Figure 1-2. The schematic illustration of (a) polymer brush strategy and (b) dopamine-based coating to prevent bacteria attachment.

1.3.2 Polydopamine (PDA) layers

PDA is a remarkable material endowed with unique properties, most notably its ability to adhere to virtually any surface, including those submerged in water [51]. This exceptional adhesive capability is primarily attributed to the catechol groups present in its monomeric building blocks, which facilitate strong binding interactions with a wide variety of substrates [52]. The dopamine self-polymerisation method has been introduced to form thin, surface-adherent polydopamine coatings via simple dip-coating on a variety of inorganic and organic substrates [53]. The field has expanded significantly, leading to the development of numerous PDA-based coatings tuned by incorporating various additives during synthesis (Figure 1-2(b)). These additives can influence material characteristics through covalent cross-linking, physical entrapment, or non-covalent interactions. [54].

In a related approach, Lee et al. developed a self-polymerising dopamine film inspired by mussel adhesive proteins [55]. This polydopamine film can be applied onto various organic or inorganic surfaces, including polymers, ceramices, and noble metals by easily immersing the surface in an aqueous solution of dopamine. The polydopamine coating functions as a multifunctional platform for a range of applications, with its significant role being the delivery of AMPs. One study utilised this polydopamine coating strategy to immobilise a synthetic AMP, CWR11 (CWFWKWWRRRRR-NH_2), onto commercial silicone coated Foley-catheter surfaces [56]. Firstly, catheters were coated with polydopamine by dipping them into a dopamine solution. The polydopamine-functionalised silicone catheter was then soaked in a CWR-11 peptide solution for three days at 25°C. The resulting CWR-11 coated catheter demonstrated no bacterial colonies when incubated for three hours with a

suspension of *Escherichia coli* (*E. Coli)* on an agar plate. Furthermore, the study demonstrated that the antimicrobial functionality of the coating was retained for up to 21 days.

1.3.3 Physical adsorption

This section has been adapted from the book chapter written by Zare et al. (2022). Antimicrobial Bioceramics for Biomedical Applications. Innovative Bioceramics in Translational Medicine I. Springer Series in Biomaterials Science and Engineering, vol 17. Springer, Singapore. The specific sections used here were authored by Mohadeseh Zare as a contributing writer to the chapter.

There are a variety of strategies for AMPs immobilisation physically or chemically on implant surfaces which are different in binding strength and complexity. Poor binding would lead to an inefficient uncontrolled release. Contrarily, strong anchoring provides a controlled release of AMPs but may hinder biological activities. Since a balance between controlled release and stable attachment is demanded for preparing an ideal antimicrobial surface, many studies have examined different strategies of AMP immobilisation to provide antimicrobial coatings [57].

The most straightforward and naturally occurring method for immobilising AMPs is physical adsorption. This technique involves the weak attachment of AMPs to surfaces through electrostatic or hydrophobic interactions. It can be easily performed by immersing the implant in peptide solutions, allowing the AMPs to become entrapped during processing [58]. To achieve a more controlled release of AMPs, some studies have employed layer-by-layer deposition of cationic and anionic molecules to form films on the surface, enabling gradual peptide release [59].

Additionally, AMPs can be engineered with affinity domains to enhance their electrostatic and hydrophobic interactions with surfaces. Surface-binding peptides utilise these electrostatic interactions, where their binding affinity can be significantly increased by incorporating repeated sequences rich in basic amino acids. This modification strengthens the attachment of AMPs to surfaces, thereby improving their stability and effectiveness in various applications. Physical adsorption is more applicable for clinical approaches, although it results in poor orientation, low stability, and poor activity compared to covalent interactions [60]. Recently, surface-binding peptides composed of histidine and lysine were developed which can directly assemble onto the biomaterials with high affinity. These self-

assembly peptides can be utilised to integrate various peptides, principally AMPs, onto biomaterials [61]. Chen et al. integrated a surface-binding peptide at the N-terminal of AMP Tet213 and utilised it to prepare antimicrobial implants made of titanium, gold, Hydroxyapatite (HAp), and polymethyl methacrylate [62].

1.3.4 Chemical binding on functionalised surfaces

This section has been adapted from the book chapter written by Zare et al. (2022). Antimicrobial Bioceramics for Biomedical Applications. Innovative Bioceramics in Translational Medicine I. Springer Series in Biomaterials Science and Engineering, vol 17. Springer, Singapore. The specific sections used here were authored by Mohadeseh Zare as a contributing writer to the chapter.

In order to prepare more stable and durable immobilisation compared to the physical adsorption method, covalently binding of AMPs using functionalisation of surfaces with varied functional groups can be applied [3]. Following the surface functionalisation, different biomolecules, including AMPs, can be directly grafted onto the implant surface. After the surface functionalisation step, AMPs can be attached to the surface through various strategies, either directly or via covalently bound linkers. The most effective strategy depends on the compatibility of the peptide sequences, where the inclusion of active functional groups within the sequence allows for chemical reactions without the need for additional steps to functionalise the peptides [3].

Different forms of the chemically immobilised AMPs, and the immobilisation strategies which have been used in recent studies in the last 10 years have been summarised in Table 1-1. According to the studies reported in Table 1-1, the most common strategy used for AMP immobilisation to implant surfaces is the physical adsorption method because of its simplicity and non-toxicity. Among chemical techniques, silanisation is the most general method for the peptide immobilisation.

Table 1-1. A summary of recent studies on the immobilisation of AMPs on different forms of medical implants for various applications.

AMP name	Substrate	Immobilisation strategy	Bacteria tested	Application	Research team
KR-12	Polymer (2-methacryloyloxyethyl	Silanisation	*E. coli*	Orthopaedics	Kozuka et al. 2024 [63]

	phosphorylcholine)				
KR-12	Gold nanoparticles	Silanisation	*E. coli*	Drug delivery system	Romero et al. 2023 [64]
KR-12	Silica particles	Physical adsorption	*E. coli*	Drug delivery system	Ki et al. 2023 [65]
KR-12	Polyethylene-glycol	Physical adsorption	*P. aeruginosa*	Orthopaedics	Ajish et al. 2022 [66]
Nisin	Polydopamine	Plasma treatment	*E. coli* & *S. aureus*	Orthopaedics	Mondal et al. 2021 [67]
GL13K	Collagen fibril/ Hydroxyapatite	Physical adsorption	*E. coli* & *S. gordonii*	Dentin scaffold	Ye et al. 2021 [68]
Nisin	Silicon wafers	Plasma treatment	*E. coli* & *S. Aureus*	Orthopaedics	Vanslambrouck et al. 2020 [69]
HHC-36	silk fibroin/ Hydroxyapatite	PDA coating	*E. coli* & *S. aureus*	Orthopaedics	Abbasizadeh et al. 2020 [70]
LL-37	Polydopamine/ Hydroxyapatite	Ceramic binding peptide	*E. coli* & *Streptococcus mutans*	Bone substitute	Fateme et al. 2020 [71]
Nisin	Polydopamine/ hydroxyapatite	PDA coating	*S. aureus*	Bone implants & drug delivery	Wang et al. 2020 [72]
Protamine	Hydroxyapatite	Physical adsorption by batch method	*E. coli* & *S. aureus*	Bone substitute	Honda et al. 2020 [73]
Melittin	Silica nanoparticles	Physical adsorption	*P. aeruginosa*	Drug delivery system	Yu et al. 2020 [74]
LL-37	Calcium Phosphate Nanoparticles	Physical adsorption	*E. coli* & *S. pneumoniae*	Drug delivery	Tsikourkitoudi et al. 2020 [75]
Mel4	Quartz glass slides	Surface functionalisation	*P. aeruginosa*	Medical devices	Yasir et al. 2019 [76]
Protamine	Calcium phosphates	Physical adsorption	*Streptococcus mutans*	Dental field	Fujiki et al. 2019 [77]
BP100 DD K	Alumina nanoparticles	Surface functionalisation	*E. coli & S. aureus & Salmonella typhimurium*	Medicine & orthopaedics	Torres et al. 2019 [78]
Tet127	Titanium	Ceramic binding peptide	*E. coli* & *Streptococcus mutans*	Bone implant	Yazici et al. 2019 [79]
HAL-2	Calcium phosphate cement	Physical adsorption	*S. aureus, S. epidermidis* & *P. aeruginosa*	Bone implant	Melichercik et al. 2018 [80] [81]
BP100	Alumina	Silanisation	*E. coli* & *Salmonella typhimurium*	Biological applications	Torres et al. 2018 [82]

Tet213	Polymethyl methacrylate/ hydroxyapatite	Ceramic binding peptide	*E. coli* & *S. aureus*	Bone implant	Chen et al. 2017 [62]
Human defensins	Hydroxyapatite	Physical adsorption & Surface functionalisation	*S. aureus, S. epidermidis & P. aeruginosa*	Orthopaedics	Townsend et al. 2017 [83]
Cysteinylated Lipopeptides	Titanium/ glasss/ silicon	Silanisation	*P. aeruginosa* & *E. coli*	Medical implants	De Zoysa et al. 2017 [84]
GL13K	Titanium oxide	Physical adsorption	*Fusobacterium nucleatum* & *Porphyromonas gingivalis*	Orthopaedics	Li et al. 2017 [85]
Inverso-cyshhc10	Calcium aluminum oxide/ hydroxyapatite	Alkene-thiol reaction	*E. coli*	Bone implant	Buckholtz et al. 2016 [86]
LL-37	Silica nanoparticles	Physical adsorption	*E. coli*	Drug delivery	Braun et al. 2016 [87]
KSLW	Hydroxyapatite	Ceramic binding peptide	*S. mutans*	Oral infection	Huang et al. 2016 [88]
PSI 10	Magnesium alloy/ hydroxyapatite	Physical adsorption	*S. aureus*	Orthopaedics	Tian et al. 2015 [89]
HHC-36	Natural trabecular bon	Physical adsorption	*S. aureus*	Bone scaffold	Kazemzadeh et al. 2014 [90]
HHC-36	Titanium	Physical adsorption	*S. aureus and P. aeruginosa*	Bone implant	Kazemzadeh et al. 2013 [91]
GL13K	Titanium	Silanisation	*Porphyromonas gingivalis*	Dental application	Holmberg et al. 2013 [92]
HHC-36 Tet213	Titanium	Physical adsorption	*P. aeruginosa* & *S. aureus*	Orthopaedics	Kazemzadeh et al. 2012 [36]
HHC-36	Titanium oxide	Vacuum-assisted physical adsorption	*S. aureus*	Orthopaedics	Ma et al. 2012 [59]
Nisin	β-tricalcium phosphate/ monocalcium phosphate cement	Physical adsorption	*S. aureus*	Bone cement	Van Staden et al. 2012 [93]

1.4. Covalent immobilisation of AMPs on titanium implants

Modern biomaterials can be modified through surface functionalisation or coating to minimise the risks of inflammation and infection, particularly before biofilm formation occurs [94]. Traditionally, the management of implant-associated infections has relied on embedding antibiotics or biocides within these materials. However, the prolonged use of antibiotics can lead to the development of antibiotic-resistant bacteria, while biocides carry potential cytotoxic risks, raising concerns about their safety for patients. Consequently, there is growing interest in alternative antimicrobial approaches. As discussed in previously, AMPs present a promising alternative to conventional antimicrobial agents. AMPs function through mechanisms that lessen the potential for microbial resistance. However, achieving effective infection control may require high concentrations of AMPs, which can pose cytotoxic risks due to the rapid degradation of natural AMPs by proteases. Therefore, enhancing the stability of free AMPs against degradation in vivo and improving the binding efficiency of immobilised AMPs on biomaterial surfaces are crucial steps in developing non-toxic, durable antimicrobial surfaces. By reducing the need for implant removal due to AMP inactivity, patient outcomes can be improved, and healthcare costs can be significantly reduced [95].

Titanium is widely used for implants due to its excellent biocompatibility, corrosion resistance, and mechanical properties, making it suitable for long-term integration with human tissues. Its surface forms a stable oxide layer (mainly titanium dioxide), which enhances osseointegration by promoting bone growth [96-98]. The surface characteristics of titanium, including roughness, chemical composition, and surface energy, significantly impact peptide binding. Surface roughness provides physical anchoring points, while its oxide layer enables chemical interactions like covalent bonding or electrostatic interactions with peptides. Surface functionalisation techniques can modify these surface properties, increasing reactivity for peptide immobilisation for enhanced antimicrobial or biological functionality [84]. Numerous strategies have been investigated for the chemical functionalisation of metallic implant surfaces, with titanium being a primary focus [96-98]. Among these, silanisation and plasma treatment are two of the most extensively studied methods [97, 98]. The following sections will provide a detailed explanation of these techniques, allowing for a better comparison of their effectiveness and applications.

1.4.1 Silanisation of titanium surfaces

Silanisation has emerged as the most widely utilised method for immobilising AMPs on titanium implants [84]. This process begins by modifying the hydroxyl groups present on the titanium surface with alkoxysilane, which introduces amino groups. The surface can then be further modified, either directly or through the use of a crosslinker, to facilitate the immobilisation of thiol-containing peptides. Depending on the functional groups present on the surface and the reactive groups of the AMPs, peptides can be covalently attached to these functionalised surfaces using various chemical reactions, such as those between amine and carboxyl groups or through azide-alkyne cycloaddition reactions [99-102].

Gabriel et al. demonstrated the conjugation of the peptide cysteine-LL37 with added N-terminal cysteine residues onto amino-silanised titanium surfaces using a three-step procedure [103]. Initially, the samples were silanised with amino silane (3-aminopropyl triethoxysilane). Following this, the amino-silanised surfaces were treated with N-maleimidopropionic acid succinimide ester, and finally, the samples were incubated with Cysteine-LL37. This resulted in coatings that were significantly more effective, eradicating 50 times more *E. coli* than control coatings.

Similarly, Li et al conjugated the AMP GL13K onto silanised titanium surfaces [81]. The process involved sequential treatment of titanium samples with sodium hydroxide and (3-chloropropyl) triethoxysilane, which prepared the surfaces for effective peptide attachment and enhanced their antimicrobial properties. AMPs were covalently attached to silanised titanium surfaces through immersion in a GL13K peptide solution. The resulting GL13K-coated surfaces effectively eradicated *Streptococcus gordonii* and prevented biofilm formation and growth in a simulated salivary environment, demonstrating steady AMP release, even in the presence of continuous shear forces.

Also, another recent study reported a melamine coating grafted onto titanium surfaces for the antibacterial activity [104]. The titanium sample was first amine functionalised with 3-Aminopropyltriethoxysilane (APTES) and then reacted with the linker 4-(N-maleimidomethyl) cyclohexane-1-carboxylic-3-sulfo-N-hydroxysuccinimide ester to create a functionalised maleimide surface. Melamine was then tethered to the substrate via a thio-ether linkage formed through a Michael-addition reaction between the cysteine at the N-terminus of melamine and the maleimide moiety on the surface. The coating effectively decreased bacterial adhesion and biofilm formation of P. aeruginosa by as much as 62%

and S. aureus by up to 84% in vitro. Moreover, in vivo studies using subcutaneous infection models showed a reduction in bacterial load by 2 log units when compared to surfaces without the coating.

In a recent study, Makihira et al immobilised the AMP JH8194, known for its osteogenic as well as antibacterial properties, onto titanium surfaces using a method that involved successive immersion in 5% γ-aminopropyltriethoxysilane followed by treatment with sodium borohydride ($NaBH_4$) to reduce imines to amine groups [105]. Carboxyl groups on the surface were activated with NHS and 1-Ethyl-3-(3-dimethyl-aminopropyl) carbodiimide (EDC), and the samples were subsequently reacted with the AMP. The JH8194-Ti immobilisation significantly contained *Porphyromonas gingivalis (P. gingivalis)* colonisation and enhanced osteogenic mRNA expression in the MC3T3-E1 cell line.

In a recent study, antibacterial and antifungal agents were effectively delivered by attaching them to stainless steel surfaces using a grafted chitosan polymer layer [106]. The peptides magainin I, known for its efficacy against a range of bacteria and fungi, and nisin, which targets Gram-positive bacteria, were covalently linked to the surface. The peptides magainin I, which is effective against various bacteria and fungi, and nisin, effective against Gram-positive bacteria, were covalently bound to the surface. The covalent binding of bioactive peptides was performed using a three-step functionalisation process, based on two successive amination reactions. In this approach, a dialdehyde crosslinker, either glutaraldehyde (GA) or terephthalaldehyde (Tere), was introduced between the chitosan-modified stainless-steel surface and the peptides. The magainin- and nisin-coated surfaces demonstrated significant antibacterial activity, killing more than 90% of *Listeria ivanovii* and 70% of *E. coli*.

To summarise the silanisation technique, the metal surface is immersed in a silane solution APTES to create amine groups on the surface. In this process, the first hydrolysis happens by cleaving off ethyl residues. Then, silane molecules attach to the hydroxyl groups on the surface via hydrogen bonds. Eventually, this condensation leads to the covalent bonds linking silane and surface (Figure 1-3). After silanisation, the metals can be added to a peptide solution to obtain a reaction between carboxyl groups of the peptides and the amine groups of the APTES activated by EDC and NHS. With this common activation process, the carbodiimide carbons of EDC couple to carboxylic groups and form reactive

intermediate where NHS can finally bind. This creates a semi stable NHS ester with reactive amine groups. Finally, this forms amide bonds between peptides amino groups and NHS esters [107]. The silanisation method can be applied for most metals and some studies used this technique for titanium surfaces, where coupling with APTES and EDC/NHS activation was applied to attach AMP KR-12. This effort resulted in 90% antimicrobial activity against *S. epidermidis*. They also used a linker, polyethylene glycol (PEG), between APTES amine groups and amine terminus of peptides, resulting in increased flexibility and consequently 100% antimicrobial activity against *S. epidermidis* [108].

In addition to the activation by EDC/NHS, the coupling can also be done by other chemical reactions. For instance, the immobilisation can be done by Michael-addition reaction of the peptide cysteine and maleimide. In one study, alumina was incubated in a solution of succinimidyl-3-maleimidopropionate and then underwent peptide immobilisation by the same technique [109]. Moreover, coupling of 3-(maleimido)propionic acid N-hydroxysuccinimide ester to APTES is also applied. In one study, peptides were coupled to tantalum and titanium by modifying the n-terminals with 3-mercaptopropionic acid and 6-aminohexanoic acid tetramer [110]. This strategy resulted in nucleophilic substitution using the immobilised iodine and thiol group of peptides which brought peptides binding to the surface.

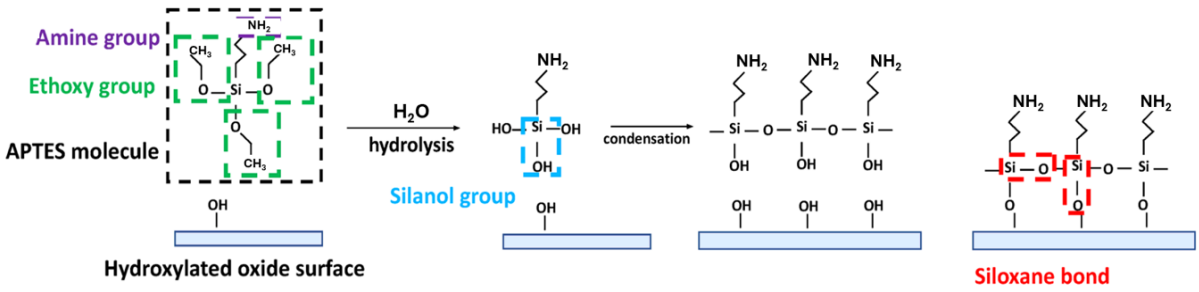


Figure 1-3. Schematic illustration of the structure of an APTES molecule, its activation. process, and its reaction with a hydroxylated oxide surface.

Similar to APTES, APTMS can also produce amine groups on metal surfaces activated by EDC/NHS [111]. There are also other silanes with different functional groups such as (3-Glycidyloxypropyl)-trimethoxysilane (GPTS). In one study, GPTS combined with PEG was used to coat a titanium surface with carboxyl groups. To bind AMPs (LL-37), the carboxyl groups were activated by Dicyclohexylcarbodiimide (DCC) and NHS [103].

The silanisation strategy is also applicable to create thiol rich surfaces by cysteine coupled

APTES. In this case, cysteine containing peptides can be coupled using a disulfide bond [78]. Moreover, another kind of silanes, 3-Mercaptopropyltrimethoxysilane, can be paired with sodium azide. Therefore, peptides modified with 2-aminopent-4-ynoic acid can undergo a copper-catalysed azide-alkyne cycloaddition [78]. Halogen-containing silanes, such as BPTCS[1], can be used for AMP immobilisation where halogens act as initiators for polymer brushes to polymerise in-situ on the surface [48].

Overall, silanisation provides a wide range of functional groups such as amine, carboxyl, thiol, azide, halogen, and epoxy. Moreover, this strategy can be used for a variety of metals as well as glasses [112, 113]. The drawback for this strategy is the requirement for the pre functionalisation and the use of EDC/NHS activation.

1.4.2 Plasma treatment of titanium surfaces

Plasma consists of gases that are either fully or partially ionised [114]. When enough energy is imparted to a gas, electrons are stripped away from atoms, resulting in a mixture containing free electrons, neutral particles, free radicals, and positively charged ions [114]. These free electrons continue to interact with other particles, sustaining or increasing the density of charged species within the plasma. Despite the presence of charged particles, plasmas often remain electrically neutral overall, a characteristic that helps define them as the fourth state of matter [115]. The properties of plasma, such as electron density and temperature, can vary significantly depending on the energy source and its intensity [116]. Non-thermal plasmas, which are not in thermodynamic equilibrium, include what is known as "cold plasma," where electron temperatures are significantly higher than those of ions and neutral particles [117].

Plasma technology is currently demonstrating significant potential across various applications, particularly in the degradation of macromolecules, pollution control, sterilisation, and chemical synthesis [118-121]. During plasma discharge, electrons emitted from the electrode interact with nearby molecules [122]. These interactions can be categorised into two types: elastic and inelastic collisions. In elastic collisions, no new chemical reactions take place, and the energy is merely redistributed among the particles. In contrast, in inelastic collisions, the electrons transfer their energy to the internal energy states of surrounding molecules or atoms. This energy transfer can excite the molecules or

[1] 1-(2-bromo-2-methyl)-propionyloxyundecenyltrichlorosilane

atoms, causing them to transition from their ground state to an excited state, which makes them more chemically reactive and capable of inducing further dissociation or initiating additional reactions [123, 124].

Chemically reactive species generated during plasma treatment can undergo interconversions. The plasma discharge process is complicated, producing a wide range of reactive species, each with distinct generation mechanisms and specific roles in the treatment process [122]. Due to their strong oxidative properties, these reactive species make plasma technology a form of advanced oxidation technology, particularly effective in the degradation of macromolecules. Numerous studies have focused on the application of plasma technology for the degradation of polysaccharides, which have diverse physicochemical properties and biological activities. The degradation process can alter these properties, potentially enhancing the biological activities of the polysaccharides [125, 126].

Plasma treatment is typically performed in an evacuated chamber, and a mixture of gases can flow into the chamber at a controlled pressure, and then any electrical energy is applied (Figure 1-4(a)). A plasma consists of electrons, neutral gas atoms, positive ions, excited gas molecules, and atoms, along with Ultraviolet (UV) light carrying a high amount of internal energy [127]. When all these components interact with a surface, plasma treatment can be initiated. The effects of plasma treatment on any surface can be tuned precisely by controlling a special gas mixture, temperature, pressure, or even power. During plasma nitriding, energetic nitrogen ions can bombard surfaces in the electric field, and therefore entrapment of nitrogen into the surface and heating the targeted surface happen [127]. The edge effect can occur due to the electric-field distributions around the corners of samples. Generally, in the conventional DC plasma nitriding, the furnace wall has an anodic potential, and the samples are treated in a cathodic potential [127].

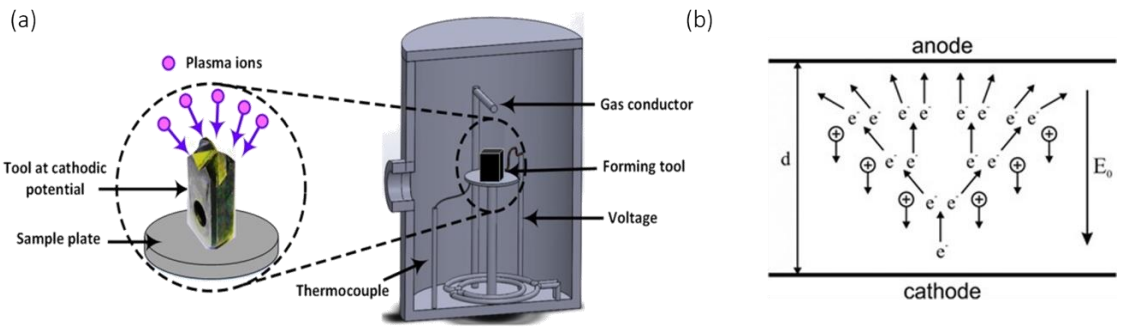


Figure 1-4. (a) Schematic representation of a plasma nitriding reactor illustrating the

placement of the forming tool at the cathodic potential [128]. (b) Townsend breakdown and electron avalanche formation between two electrodes [129].

Plasma surface modification can be used to modify the surface properties by functionalisation of the surface with different functional groups [130]. The surface modification based on plasma treatments is typically used to introduce functional groups onto material surfaces through the plasma adsorption and diffusion, which consists of ionised gas mixtures. The type of formed functional groups depends on the working gas injected to generate the plasma. For instance, plasma nitriding, also known as glow-discharge nitriding, employs a mixture of nitrogen (N_2) and hydrogen (H_2) gases to introduce nitrogen-based functional groups onto the surface [131]. These newly formed functional groups can subsequently serve as anchors for further surface modifications, as explored in this work. Plasma nitriding provides numerous benefits compared to conventional nitriding techniques, such as nitrocarburising (salt bath nitriding) and gas nitriding with ammonia, which involve hazardous chemicals like caustic cyanides and toxic gases [132, 133]. In contrast, plasma nitriding utilises nitrogen-hydrogen gas directly for surface functionalisation and requires significantly less gas, making it more efficient. Additionally, plasma nitriding provides enhanced control and consistency in surface treatment, as the process parameters, including applied voltage and gas ratios, can be precisely controlled, leading to a uniform surface modification [132, 134]. Moreover, the by-products of plasma treatment using nitrogen/hydrogen gas are non-toxic, contributing to its reputation as an environmentally friendly technology [135, 136]. This non-toxic nature has led to increased industrial interest in plasma nitriding since its introduction.

Up to the present, different functionalities have been provided by plasma treatment, such as carboxyl, hydroxyl, and primary amine [137, 138]. In order to immobilise the peptides, primary amine ($-NH_2$) groups can initiate the covalent immobilisation of AMPs using chemical reactions between carboxyl groups (-COOH) of peptides and primary amine groups ($-NH_2$) [139]. Moreover, protonated amines can create a localised positive charge in an aqueous solution at the physiological pH, which can potentially be beneficial for electrostatic interactions with negatively charged cells and proteins and is advantageous to promote cell adhesion and proliferation [139].

In addition to surface functionalisation, plasma technology can be applied to sterilise biomaterials. The bombardment of the material surface with ionised gas mixtures during

plasma treatment can effectively remove impurities, such as dust and particles left after polishing [140]. Plasma nitriding also offers the advantage of enhancing mechanical properties, achieving surface functionalisation without the need for wet chemical processes, with faster processing times, and a reduced environmental impact [141]. Plasma nitriding of polymers is usually conducted in either vacuum or ambient atmospheric conditions, with the treatment temperature restricted by the polymer's melting point. [142]. As a result, plasma treatment of polymers is generally impacted just a few microns in depth, with the physical and chemical changes mainly confined to the surface or near-surface layers, having lowest effect on the bulk properties of the material.

For stable plasma formation, it is crucial to maintain steady ionisation of the injected gas between the anode and cathode. In highly ionised plasma, collisions among active molecules are predominant, while in plasma with lower ionisation, interactions between active and neutral species dominate. The level of ionisation primarily depends on the pressure at which the plasma is produced, as this influences the mean free path of the ionised molecules [143]. At atmospheric pressure, the mean free path of the gas molecules is relatively short, limiting their momentum and resulting in fewer molecular collisions. Conversely, at extremely low pressures around 0.01 Pa, the mean free path is extended, but the large distances between molecules reduce collision frequency. In both atmospheric and very low-pressure environments, it becomes challenging to sustain consistent ionisation between the anode and cathode. Optimal plasma formation typically occurs at lower pressures, around 10 Pa, where the mean free path is sufficient to allow frequent collisions, facilitating the development of self-sustained plasma [143].

The ability of plasma to maintain self-sustainability is described by the Townsend avalanche process, a simplified schematic of which is shown in Figure 1-4(b). Briefly, the electric field between the anode and cathode accelerates free electrons, causing them to collide with gas molecules in the working gas, which in turn releases secondary electrons. This chain reaction of electron collisions leads to an "avalanche" effect, where the multiplication of free electrons allows for continuous electrical conduction through the working gas, thereby sustaining the plasma [143].

1.4.3 Direct immobilisation of AMPs

In order to immobilise AMPs on the implant surfaces, after the process of biomaterial surface functionalisation, activating agents including EDC and NHS, are employed to

promote the formation of amide bonds between peptides and surfaces, thereby avoiding the creation of carboxylic salts with amines [144]. Other molecules can serve as alternatives to NHS and EDC for coupling similar functional groups. Moreover, cysteines or thiols are frequently used for efficient chemo-selective conjugation of AMPs to a range of polymeric substrates [145]. Humblot et al investigated the antimicrobial activity of Magainin-1 by directly immobilizing it onto a mixed self-assembled monolayer of thiol compounds. The effectiveness of this setup was tested against *S. aureus, Listeria ivanovii,* and *Enterococcus faecalis* [146].

The orientation of the AMPs during immobilisation cannot be precisely controlled, as the coupling chemistry facilitates the attachment of any available amine group in the peptides to the functional groups present on the surface. Due to the restricted lateral orientation and mobility of the directly immobilised AMPs, they are unable to fully engage their natural membrane-targeting mechanisms [147].

1.4.4 Linker incorporated immobilisation of AMPs

Direct immobilisation may limit AMP mobility, potentially reducing the effectiveness of membrane permeabilization or polarisation. Therefore, many advancements utilise linkers between the surface functional groups and the AMP. Research indicated that the length of linkers, which refers to the distance between the surface and the peptide, plays a crucial role in influencing the activity of surface-immobilized AMPs, particularly concerning the density of AMPs on the surface [69]. Additionally, the degradation of polymers can result in the cleavage of linker chains, facilitating the controlled release of immobilized AMPs [148, 149].

The increased activity observed with linkers is generally attributed to the enhanced lateral mobility of AMPs, which increases the likelihood of membrane permeabilization and microbial cell death [69]. This hypothesis assumes that AMPs function similarly to their free-form counterparts. However, some AMPs, when immobilised, may disrupt the cytoplasmic membrane and electron transport, leading to partial membrane permeabilization and cell death [150].

Gabriel et al. conducted a comprehensive study on silanised titanium surfaces to assess the impact of linker specifications and orientation on the antimicrobial efficacy of LL-37 [103]. Their research compared direct immobilisation and spacer-incorporated immobilisation, using PEG-based linkers, through various multi-step coupling chemistries. Direct

immobilisation of LL-37 on silanised titanium did not yield observable antimicrobial activity. Similarly, LL-37 remained inactive when linked to a flexible PEG linker at its C-terminal. In contrast, conjugation of LL-37 to PEG through its N-terminal resulted in effective killing of *E. coli*. This suggests that LL-37 requires sufficient lateral freedom to interact with microbial membranes, which was achieved using a long, flexible linker positioned in a specific orientation. PEG's antifouling properties offer additional benefits, including the creation of non-adhesive surfaces and improved peptide solubility and stability against protease degradation and aggregation [151, 152]. Exploiting the antifouling characteristics of linkers alongside the antimicrobial properties of AMPs presents a promising strategy to mitigate biofilm formation.

The Varieties of surface functionalisation techniques, coupling chemistries, linker designs, and available AMPs, underscores the complexity in developing antimicrobial biomaterial surfaces. Comparing these approaches is challenging due to the variability in reactants, biomaterial surfaces, and AMPs, which can influence the observed antimicrobial efficacy. A thorough comprehension of structure-function relationships is essential for improving the effectiveness of surface-immobilised AMPs. It is also important to understand the kinetics of leaching, as degradation of materials and coupling agents can compromise structural integrity and result in the release of AMPs or debris, potentially causing negative biological responses. Despite these challenges, AMPs offer considerable potential as alternatives to conventional biocides and antibiotics for the development of advanced antimicrobial surfaces in medical devices.

While direct coupling offers a quick and straightforward approach, incorporating linkers is essential to enhance the flexibility of AMPs. The close attachment of AMPs to the surface and the limited spacing between them can restrict their functional activity.

After functionalising surfaces, various polymer chains can be utilised as linkers between peptides and functional groups to enhance their mobility and flexibility. For instance, Diaz-Rodriguez et al. employed glutaric anhydride as a linker in their research [153, 154]. Initially, they created an amine-rich surface using plasma treatment, followed by immersion in a glutaric anhydride solution, which resulted in the formation of carboxylic anhydride groups. Subsequently, EDC activation in MES (2-(N-morpholino) ethanesulfonic acid) buffer (pH = 4.5) was used to facilitate peptide binding to the carboxyl groups of the linker chains [111]. The only limitation of applying such linkers is the need for an additional

activation step. An ideal approach for immobilising AMPs on titanium implants could involve extracellular matrix (ECM) inspired linkers, such as the human elastin-like polypeptide (HELP) [49, 50]. HELP is a recombinant biopolymer that mimics the natural human tropoelastin, providing advantages such as enhanced biocompatibility, improved cell adhesion, and additional anchoring sites for effective immobilisation [51, 52]. Importantly, HELP can be degraded through physiological pathways, reducing the potential for harmful byproducts [53-55]. Previous research has explored the proteolytic susceptibility of HELP matrices, indicating their potential for enzyme-triggered release of model compounds [56-59]. The elastolytic activity found in both prokaryotic and eukaryotic organisms is linked to various pathological conditions, including pulmonary emphysema, cystic fibrosis, infections, inflammation, chronic wounds, and atherosclerosis [60, 61]. Building on this concept, HELP polypeptides offer potential as proteolytic stimuli-responsive linker for the controlled release of AMPs [53]. The application of HELP as a linker for peptide immobilisation has not been proposed in previous studies and is explored for the first time here.

1.4. Aims and objectives

In this chapter various strategies for AMP immobilisation on different forms of implants were presented, including scaffolds, coatings, composites, and micro/nanoparticles, to impart antimicrobial properties for specific biomedical applications. The literature review, conducted in this study, identified silanisation and plasma treatment as two of the most reliable methods for AMP immobilisation on titanium implants [97, 98]. Consequently, this research focuses on utilising these two techniques and evaluating them through surface characterisation, antimicrobial analysis, and biological assessment. A main concern about peptide immobilisation is that AMPs need complete flexibility and freedom in order to interact with bacteria efficiently. Moreover, AMPs need enough space between each other to form a secondary structure. Therefore, an optimised concentration of AMPs must be immobilised on the surface [107, 155].

As previously discussed, achieving optimal antimicrobial activity requires careful consideration of not only the peptide structure but also the immobilisation strategy and the available functional groups for immobilisation. Additionally, optimising AMP concentration on titanium implants depends on several factors, including the surface functionalisation method (which involves optimising the number of functional groups on

the surface), the choice of linkers, and the specific chemical reactions employed.

Accordingly, this study is divided into two main phases, each focusing on surface functionalisation of titanium surfaces using silanisation or plasma treatment methods in conjunction with the application of different linkers. The key steps of these methodologies are as follows:

Phase One:

Enzyme-Responsive antimicrobial coating based on silanisation technique for surface functionalisation and HELP linking arms. (Zare et al., (2024). Enzyme-Responsive Coatings Supporting Dual Functionality: Osteoblast Promotion and Antimicrobial Activity for Orthopaedic Implants)

- In the first step, plasma treatment is employed to introduce primary amine functional groups onto the surface using a gas mixture of nitrogen and hydrogen. To achieve optimal antimicrobial activity, both the parameters of the plasma treatment and the conditions of the subsequent chemical reactions must be carefully optimised. These amine groups can react with carboxyl groups of the AMPs (or PEG linkers) for covalent immobilisation.
- In the second step, the AMPs are directly bonded to the primary amine groups on the treated titanium surfaces using EDC/NHS reactions.
- In the third step, PEG is attached directly to the titanium surfaces as a linker before attaching AMPs to enhance their mobility and subsequently their activity.
- After the PEG linker attachment, the fourth step is peptide immobilisation. Generally, peptides can be attached chemically by their either C-terminus or N-terminus. In this project, C-terminus of the AMPs are used to react with. To activate the reaction, the NHS and EDC are used as activating agents.

Phase Two:

Optimisation of plasma treatment for covalent immobilisation of amps and peg linkers with antifouling properties (Zare et al.,. (2024). Optimised Amine Density via Plasma Treatment for Covalent immobilisation of AMPs to Promote Osteoblasts and Enhance Antimicrobial Activity)

- In the first step, the silanisation technique using APTES is employed to introduce primary amine functional groups onto the surface. To facilitate this, the surface must first be equipped with hydroxyl groups, which are generated through a chemical reaction with Piranha solution. As in the initial phase, primary amine groups are introduced to the surface to enable subsequent reactions with carboxyl groups of AMPs.

- In the second step, the AMPs are directly attached to the primary amine groups on the treated titanium surfaces through EDC/NHS coupling reactions.

- In the third step, HELP is attached directly to the titanium surfaces as a linker to enhance the mobility and activity of the subsequently immobilised AMPs as well as mimicking the ECM.

- After the HELP attachment, the fourth step is peptide immobilisation on the HELP-attached titanium surface using their C-terminus. To activate the reaction, the NHS and EDC are used as activating agents.

To assess the efficacy of plasma treatment and silanisation techniques for surface functionalisation, a series of physical and chemical characterisations are conducted following surface functionalisation, linker attachment, and AMP immobilisation. These characterisation methods include Fourier-Transform Infrared (FTIR) spectroscopy, X-ray Photoelectron Spectroscopy (XP, Atomic Force Microscopy (AFM), Scanning Electron Microscopy (SEM), and Water Contact Angle (WCA) measurement. Furthermore, after AMP immobilisation, the antimicrobial properties of the surface are evaluated using four different bacteria strains: *E. coli, P.* a*eruginosa, S. epidermidis, S. aureus*. Given that the implant surface will interact with the biological environment, its characteristics significantly influence cell-material interactions. Thus, biological assessment, including cell viability on human osteoblast cell line (hFOB) based on MTT (3-(4, 5-dimethylthiazolyl-2)-2, 5-diphenyltetrazolium bromide) assay, morphological assessment using SEM, are performed to correlate these properties with the biocompatibility of the materials.

In brief, this study is structured around the following aims and objectives:

Aims:

- To enhance the antimicrobial activity and biocompatibility of titanium implants

through optimised functionalisation strategies and AMP immobilisation.

- To evaluate and compare the effectiveness of plasma treatment and silanisation as the two most robust techniques for surface functionalisation.

Objectives:

- To assess the efficiency of plasma treatment and silanisation in introducing functional groups for AMP attachment.
- To characterise functionalised titanium surfaces using advanced surface analysis methods.
- To optimise AMP immobilisation by ensuring sufficient flexibility to preserve antimicrobial efficacy.
- To investigate the role of PEG linkers in enhancing AMP mobility, antifouling properties, and bacterial inhibition.
- To explore the potential of HELP-based linkers for controlled AMP release in response to enzymatic activity.
- To evaluate the antimicrobial performance of functionalised surfaces against clinically significant pathogens, including *S. aureus, S. epidermidis, E. coli,* and *P. aeruginosa*.
- To validate the biocompatibility and cell adhesion properties of the modified surfaces using in vitro assays.
- To compare the cost, toxicity, and efficiency of plasma treatment and silanisation as functionalisation techniques for titanium implants.

The subsequent chapters will provide a comprehensive explanation of these methodologies, facilitating a thorough comparison of their effectiveness and applications.

1.5. References

1. Phillips, K.S., D. Patwardhan, and G. Jayan, *Biofilms, medical devices, and antibiofilm technology: Key messages from a recent public workshop.* American journal of infection control, 2015. **43**(1): p. 2-3.
2. Vertes, A., V. Hitchins, and K.S. Phillips, *Analytical challenges of microbial biofilms on medical devices*. 2012, ACS Publications.
3. Costa, F., et al., *Covalent immobilisation of antimicrobial peptides (AMPs) onto biomaterial surfaces.* Acta biomaterialia, 2011. **7**(4): p. 1431-1440.
4. Cheng, H., et al., *Long-lasting in vivo and in vitro antibacterial ability of nanostructured titania coating incorporated with silver nanoparticles.* Journal of biomedical materials research Part A, 2014. **102**(10): p. 3488-3499.
5. Bargon, R., et al., *General assembly, research caveats: proceedings of international consensus on orthopedic infections.* The Journal of arthroplasty, 2019. **34**(2): p. S245-S253. e1.
6. Wang, Y., et al., *Antimicrobial and Anti-Biofilm Medical Devices: Public Health and Regulatory Science Challenges*. 2017, Springer International Publishing: Cham. p. 37-65.
7. Cloutier, M., D. Mantovani, and F. Rosei, *Antibacterial coatings: challenges, perspectives, and opportunities.* Trends in biotechnology, 2015. **33**(11): p. 637-652.
8. Hasan, J., R.J. Crawford, and E.P. Ivanova, *Antibacterial surfaces: the quest for a new generation of biomaterials.* Trends in Biotechnology, 2013. **31**(5): p. 295-304.
9. Guaní-Guerra, E., et al., *Antimicrobial peptides: general overview and clinical implications in human health and disease.* Clinical immunology, 2010. **135**(1): p. 1-11.
10. Wang, G., et al., *Antibacterial peptides-loaded bioactive materials for the treatment of bone infection.* Colloids and Surfaces B: Biointerfaces, 2023. **225**: p. 113255.
11. Asif, F., et al., *Antimicrobial peptides as therapeutics: Confronting delivery challenges to optimise efficacy.* The Microbe, 2024. **2**: p. 100051.
12. Riool, M., et al., *Antimicrobial Peptides in Biomedical Device Manufacturing.* Front Chem, 2017. **5**: p. 63.
13. Onaizi, S.A. and S.S.J. Leong, *Tethering antimicrobial peptides: Current status and potential challenges.* Biotechnology Advances, 2011. **29**(1): p. 67-74.

14. Jenssen, H.v., P. Hamill, and R.E.W. Hancock, *Peptide Antimicrobial Agents.* Clinical Microbiology Reviews, 2006. **19**(3): p. 491-511.
15. Yeaman, M.R. and N.Y. Yount, *Mechanisms of antimicrobial peptide action and resistance.* Pharmacological reviews, 2003. **55**(1): p. 27-55.
16. Zasloff, M., *Antimicrobial peptides of multicellular organisms.* nature, 2002. **415**(6870): p. 389-395.
17. Aoki, W. and M. Ueda, *Characterisation of antimicrobial peptides toward the development of novel antibiotics.* Pharmaceuticals, 2013. **6**(8): p. 1055-1081.
18. Hurdle, J.G., et al., *Targeting bacterial membrane function: an underexploited mechanism for treating persistent infections.* Nature Reviews Microbiology, 2011. **9**(1): p. 62-75.
19. WK Mok, W. and Y. Li, *Therapeutic peptides: new arsenal against drug resistant pathogens.* Current pharmaceutical design, 2014. **20**(5): p. 771-792.
20. Laverty, G., S.P. Gorman, and B.F. Gilmore, *The potential of antimicrobial peptides as biocides.* International journal of molecular sciences, 2011. **12**(10): p. 6566-6596.
21. Brogden, K.A., *Antimicrobial peptides: pore formers or metabolic inhibitors in bacteria?* Nature Reviews Microbiology, 2005. **3**(3): p. 238-250.
22. Jean-François, F., et al., *Pore formation induced by an antimicrobial peptide: electrostatic effects.* Biophysical journal, 2008. **95**(12): p. 5748-5756.
23. J Afacan, N., et al., *Therapeutic potential of host defense peptides in antibiotic-resistant infections.* Current pharmaceutical design, 2012. **18**(6): p. 807-819.
24. Takahashi, D., et al., *Structural determinants of host defense peptides for antimicrobial activity and target cell selectivity.* Biochimie, 2010. **92**(9): p. 1236-1241.
25. Chan, D.I., E.J. Prenner, and H.J. Vogel, *Tryptophan-and arginine-rich antimicrobial peptides: structures and mechanisms of action.* Biochimica et Biophysica Acta (BBA)-Biomembranes, 2006. **1758**(9): p. 1184-1202.
26. De La Fuente-Núñez, C., et al., *Inhibition of bacterial biofilm formation and swarming motility by a small synthetic cationic peptide.* Antimicrobial agents and chemotherapy, 2012. **56**(5): p. 2696-2704.
27. Hancock, R.E. and H.-G. Sahl, *Antimicrobial and host-defense peptides as new anti-infective therapeutic strategies.* Nature biotechnology, 2006. **24**(12): p. 1551-1557.
28. Grassi, L., et al., *Combination Strategies to Enhance the Efficacy of Antimicrobial Peptides against Bacterial Biofilms.* Frontiers in Microbiology, 2017. **8**.

29. Molhoek, E.M., et al., *A cathelicidin-2-derived peptide effectively impairs Staphylococcus epidermidis biofilms.* International Journal of Antimicrobial Agents, 2011. **37**(5): p. 476-479.
30. Nagant, C., et al., *Identification of Peptides Derived from the Human Antimicrobial Peptide LL-37 Active against Biofilms Formed by Pseudomonas aeruginosa Using a Library of Truncated Fragments.* Antimicrobial Agents and Chemotherapy, 2012. **56**(11): p. 5698-5708.
31. Haisma Elisabeth, M., et al., *LL-37-Derived Peptides Eradicate Multidrug-Resistant Staphylococcus aureus from Thermally Wounded Human Skin Equivalents.* Antimicrobial Agents and Chemotherapy, 2014. **58**(8): p. 4411-4419.
32. Mansour, S.C., C. de la Fuente-Núñez, and R.E.W. Hancock, *Peptide IDR-1018: modulating the immune system and targeting bacterial biofilms to treat antibiotic-resistant bacterial infections.* Journal of Peptide Science, 2015. **21**(5): p. 323-329.
33. Cardoso, M.H., et al., *Computer-Aided Design of Antimicrobial Peptides: Are We Generating Effective Drug Candidates?* Front Microbiol, 2019. **10**: p. 3097.
34. Müller, A.T., J.A. Hiss, and G. Schneider, *Recurrent Neural Network Model for Constructive Peptide Design.* Journal of Chemical Information and Modeling, 2018. **58**(2): p. 472-479.
35. Fjell, C.D., et al., *Identification of Novel Antibacterial Peptides by Chemoinformatics and Machine Learning.* Journal of Medicinal Chemistry, 2009. **52**(7): p. 2006-2015.
36. Kazemzadeh-Narbat, M., et al., *Drug release and bone growth studies of antimicrobial peptide-loaded calcium phosphate coating on titanium.* Journal of Biomedical Materials Research Part B: Applied Biomaterials, 2012. **100B**(5): p. 1344-1352.
37. Wang, G., *Structures of human host defense cathelicidin LL-37 and its smallest antimicrobial peptide KR-12 in lipid micelles.* Journal of Biological Chemistry, 2008. **283**(47): p. 32637-32643.
38. Li, H., et al., *The antimicrobial peptide KR-12 promotes the osteogenic differentiation of human bone marrow stem cells by stimulating BMP/SMAD signaling.* RSC advances, 2018. **8**(28): p. 15547-15557.
39. Liu, M., et al., *Fabrication of KR-12 peptide-containing hyaluronic acid immobilised fibrous eggshell membrane effectively kills multi-drug-resistant bacteria, promotes angiogenesis and accelerates re-epithelialisation.* Int J Nanomedicine, 2019. **14**: p. 3345-3360.

40. Jacob, B., et al., *Short KR-12 analogs designed from human cathelicidin LL-37 possessing both antimicrobial and antiendotoxic activities without mammalian cell toxicity.* Journal of peptide science, 2013. **19**(11): p. 700-707.
41. Lim, K., et al., *Immobilisation Studies of an Engineered Arginine–Tryptophan-Rich Peptide on a Silicone Surface with Antimicrobial and Antibiofilm Activity.* ACS Applied Materials & Interfaces, 2013. **5**(13): p. 6412-6422.
42. Zhao, B. and W.J. Brittain, *Polymer brushes: surface-immobilised macromolecules.* Progress in Polymer Science, 2000. **25**(5): p. 677-710.
43. Ayres, N., *Polymer brushes: Applications in biomaterials and nanotechnology.* Polymer Chemistry, 2010. **1**(6): p. 769-777.
44. Godoy-Gallardo, M., et al., *Antibacterial properties of hLf1–11 peptide onto titanium surfaces: A comparison study between silanisation and surface initiated polymerisation.* Biomacromolecules, 2015. **16**(2): p. 483-496.
45. Gao, G., et al., *The biocompatibility and biofilm resistance of implant coatings based on hydrophilic polymer brushes conjugated with antimicrobial peptides.* Biomaterials, 2011. **32**(16): p. 3899-3909.
46. Muszanska, A.K., et al., *Antiadhesive polymer brush coating functionalised with antimicrobial and RGD peptides to reduce biofilm formation and enhance tissue integration.* Biomacromolecules, 2014. **15**(6): p. 2019-2026.
47. Pan, G., et al., *Biomimetic Design of Mussel-Derived Bioactive Peptides for Dual-Functionalisation of Titanium-Based Biomaterials.* Journal of the American Chemical Society, 2016. **138**(45): p. 15078-15086.
48. Li, F., et al., *Polymerisation of dopamine catalysed by laccase: Comparison of enzymatic and conventional methods.* Enzyme and microbial technology, 2018. **119**: p. 58-64.
49. Li, M., et al., *Dopamine modified organic–inorganic hybrid coating for antimicrobial and osteogenesis.* ACS applied materials & interfaces, 2016. **8**(49): p. 33972-33981.
50. Li, Y., et al., *Targeted polydopamine nanoparticles enable photoacoustic imaging guided chemo-photothermal synergistic therapy of tumour.* Acta biomaterialia, 2017. **47**: p. 124-134.
51. Lee, H., et al., *Mussel-inspired surface chemistry for multifunctional coatings.* science, 2007. **318**(5849): p. 426-430.

52. Lim, K., et al., *Development of a catheter functionalised by a polydopamine peptide coating with antimicrobial and antibiofilm properties.* Acta biomaterialia, 2015. **15**: p. 127-138.
53. Costa, F., P. Gomes, and M.C.L. Martins, *Antimicrobial peptides (AMP) biomaterial coatings for tissue repair*, in *Peptides and Proteins as Biomaterials for Tissue Regeneration and Repair*. 2018, Elsevier. p. 329-345.
54. Riccio, P., et al., *Antimicrobial Bioceramics for Biomedical Applications*, in *Innovative Bioceramics in Translational Medicine I: Fundamental Research*, A.H. Choi and B. Ben-Nissan, Editors. 2022, Springer Singapore: Singapore. p. 159-193.
55. Ma, M., et al., *Local delivery of antimicrobial peptides using self-organised TiO2 nanotube arrays for peri-implant infections.* J Biomed Mater Res A, 2012. **100**(2): p. 278-85.
56. Wronska, M.A., et al., *Adding Functions to Biomaterial Surfaces through Protein Incorporation.* Advanced Materials, 2016. **28**(27): p. 5485-5508.
57. Micksch, T., et al., *A modular peptide-based immobilisation system for ZrO2, TiZr and TiO2 surfaces.* Acta Biomaterialia, 2015. **12**: p. 290-297.
58. Chen, J., et al., *Preparation of an antimicrobial surface by direct assembly of antimicrobial peptide with its surface binding activity.* J Mater Chem B, 2017. **5**(13): p. 2407-2415.
59. Kozuka, Y., et al., *Antimicrobial Peptide Assembly on Zwitterionic Polymer Films to Slow Down Biofilm Formation.* Langmuir, 2024. **40**(13): p. 7029-7037.
60. He, X., et al., *One-step self-assembly of biogenic Au NPs/PEG-based universal coatings for antifouling and photothermal killing of bacterial pathogens.* Chemical Engineering Journal, 2021. **421**: p. 130005.
61. Ki, M.-R., et al., *Self-entrapment of antimicrobial peptides in silica particles for stable and effective antimicrobial peptide delivery system.* International Journal of Molecular Sciences, 2023. **24**(22): p. 16423.
62. Ajish, C., et al., *A novel hybrid peptide composed of LfcinB6 and KR-12-a4 with enhanced antimicrobial, anti-inflammatory and anti-biofilm activities.* Scientific Reports, 2022. **12**(1): p. 4365.
63. Mondal, A., et al., *A Synergistic New Approach Toward Enhanced Antibacterial Efficacy via Antimicrobial Peptide Immobilisation on a Nitric Oxide-Releasing Surface.* ACS Applied Materials & Interfaces, 2021. **13**(37): p. 43892-43903.

64. Ye, Z., et al., *Biomimetic mineralised hybrid scaffolds with antimicrobial peptides.* Bioact Mater, 2021. **6**(8): p. 2250-2260.
65. Vanslambrouck, S., et al., *Effect of linking arm hydrophilic/hydrophobic nature, length and end-group on the conformation and the RGD accessibility of surface-immobilised fibronectin.* Materials Science and Engineering: C, 2020. **107**: p. 110335.
66. Abbasizadeh, N., et al., *HHC-36 antimicrobial peptide loading on silk fibroin (SF)/hydroxyapatite (HA) nanofibrous-coated titanium for the enhancement of osteoblast and bactericidal functions.* International Journal of Polymeric Materials and Polymeric Biomaterials, 2020. **69**(10): p. 629-639.
67. Fateme, R., et al., *New Engineered Fusion Peptide with Dual Functionality: Antibacterial and Strong Binding to Hydroxyapatite.* International Journal of Peptide Research and Therapeutics, 2020. **26**(3): p. 1629-1639.
68. Wang, N., et al., *Nisin-loaded polydopamine/hydroxyapatite composites: Biomimetic synthesis, and in vitro bioactivity and antibacterial activity evaluations.* Colloids and Surfaces A: Physicochemical and Engineering Aspects, 2020. **602**: p. 125101.
69. Honda, M., M. Matsumoto, and M. Aizawa, *Potential Application of Protamine for Antimicrobial Biomaterials in Bone Tissue Engineering.* International Journal of Molecular Sciences, 2020. **21**(12).
70. Yu, Q., et al., *Supramolecular Assemblies of Heterogeneous Mesoporous Silica Nanoparticles to Co-deliver Antimicrobial Peptides and Antibiotics for Synergistic Eradication of Pathogenic Biofilms.* ACS Nano, 2020. **14**(5): p. 5926-5937.
71. Tsikourkitoudi, V., et al., *Flame-Made Calcium Phosphate Nanoparticles with High Drug Loading for Delivery of Biologics.* Molecules, 2020. **25**(7).
72. Yasir, M., et al., *Mechanism of Action of Surface Immobilised Antimicrobial Peptides Against Pseudomonas aeruginosa.* Front Microbiol, 2019. **10**: p. 3053.
73. Fujiki, M., et al., *Antimicrobial Activity of Protamine-Loaded Calcium Phosphates against Oral Bacteria.* Materials (Basel), 2019. **12**(17).
74. Torres, L., et al., *Antimicrobial alumina nanobiostructures of disulfide- and triazole-linked peptides: Synthesis, characterisation, membrane interactions and biological activity.* Colloids Surf B Biointerfaces, 2019. **177**: p. 94-104.
75. Yazici, H., et al., *Self-assembling antimicrobial peptides on nanotubular titanium surfaces coated with calcium phosphate for local therapy.* Mater Sci Eng C Mater Biol Appl, 2019. **94**: p. 333-343.

76. Melichercik, P., O. Nesuta, and V. Cerovsky, *Antimicrobial Peptides for Topical Treatment of Osteomyelitis and Implant-Related Infections: Study in the Spongy Bone.* Pharmaceuticals (Basel), 2018. **11**(1).
77. Melichercik, P., et al., *Testing the efficacy of antimicrobial peptides in the topical treatment of induced osteomyelitis in rats.* Folia Microbiol (Praha), 2018. **63**(1): p. 97-104.
78. Torres, L., et al., *Nanobiostructure of fibrous-like alumina functionalised with an analog of the BP100 peptide: Synthesis, characterisation and biological applications.* Colloids Surf B Biointerfaces, 2018. **163**: p. 275-283.
79. Townsend, L., et al., *Antimicrobial peptide coatings for hydroxyapatite: electrostatic and covalent attachment of antimicrobial peptides to surfaces.* J R Soc Interface, 2017. **14**(126).
80. De Zoysa, G.H. and V. Sarojini, *Feasibility Study Exploring the Potential of Novel Battacin Lipopeptides as Antimicrobial Coatings.* ACS Applied Materials & Interfaces, 2017. **9**(2): p. 1373-1383.
81. Li, T., et al., *Antibacterial activity and cytocompatibility of an implant coating consisting of TiO2 nanotubes combined with a GL13K antimicrobial peptide.* International journal of nanomedicine, 2017. **12**: p. 2995.
82. Buckholtz, G.A., et al., *Reducing Escherichia coli growth on a composite biomaterial by a surface immobilised antimicrobial peptide.* Mater Sci Eng C Mater Biol Appl, 2016. **65**: p. 126-34.
83. Braun, K., et al., *Membrane interactions of mesoporous silica nanoparticles as carriers of antimicrobial peptides.* Journal of colloid and interface science, 2016. **475**: p. 161-170.
84. Huang, Z.-b., et al., *Design of a hydroxyapatite-binding antimicrobial peptide with improved retention and antibacterial efficacy for oral pathogen control.* Scientific Reports, 2016. **6**(1): p. 38410.
85. Tian, J., et al., *Investigation of the antimicrobial activity and biocompatibility of magnesium alloy coated with HA and antimicrobial peptide.* J Mater Sci Mater Med, 2015. **26**(2): p. 66.
86. Kazemzadeh-Narbat, M., et al., *Antimicrobial Peptide Delivery from Trabecular Bone Grafts.* Journal of Biomaterials and Tissue Engineering, 2014. **4**(11): p. 967-972.

87. Kazemzadeh-Narbat, M., et al., *Multilayered coating on titanium for controlled release of antimicrobial peptides for the prevention of implant-associated infections.* Biomaterials, 2013. **34**(24): p. 5969-5977.
88. Holmberg, K.V., et al., *Bio-inspired stable antimicrobial peptide coatings for dental applications.* Acta Biomater, 2013. **9**(9): p. 8224-31.
89. van Staden, A.D., A.M. Brand, and L.M. Dicks, *Nisin F-loaded brushite bone cement prevented the growth of Staphylococcus aureus in vivo.* J Appl Microbiol, 2012. **112**(4): p. 831-40.
90. Richards, R.G., et al., *Advances in biomaterials and surface technologies.* J Orthop Trauma, 2012. **26**(12): p. 703-7.
91. Hao, Z., et al., *Antimicrobial peptides for bone tissue engineering: Diversity, effects and applications.* Front Bioeng Biotechnol, 2022. **10**: p. 1030162.
92. Egghe, T., et al., *Silanisation of Plasma-Activated Hexamethyldisiloxane-Based Plasma Polymers for Substrate-Independent Deposition of Coatings with Controlled Surface Chemistry.* ACS Applied Materials & Interfaces, 2022. **14**(3): p. 4620-4636.
93. Akdoğan, E. and H.T. Şirin, *Plasma surface modification strategies for the preparation of antibacterial biomaterials: A review of the recent literature.* Materials Science and Engineering: C, 2021. **131**: p. 112474.
94. Álvarez-López, A., et al., *Improved cell adhesion to activated vapor silanisation-biofunctionalised Ti-6Al-4V surfaces with ECM-derived oligopeptides.* Biomaterials Advances, 2022. **133**: p. 112614.
95. Hou, R., et al., *Novel osteogenic growth peptide C-terminal pentapeptide grafted poly(d,l-lactic acid) improves the proliferation and differentiation of osteoblasts: The potential bone regenerative biomaterial.* International Journal of Biological Macromolecules, 2018. **119**: p. 874-881.
96. Maia, F.R., et al., *Hydrogel depots for local co-delivery of osteoinductive peptides and mesenchymal stem cells.* Journal of Controlled Release, 2014. **189**: p. 158-168.
97. Li, S., et al., *Enhanced osteogenic activity of poly(ester urea) scaffolds using facile post-3D printing peptide functionalisation strategies.* Biomaterials, 2017. **141**: p. 176-187.
98. Soultan, A.H., et al., *Synthesis and peptide functionalisation of hyperbranched poly(arylene oxindole) towards versatile biomaterials.* Polymer Chemistry, 2018. **9**(20): p. 2775-2784.

99. Gabriel, M., et al., *Preparation of LL-37-Grafted Titanium Surfaces with Bactericidal Activity.* Bioconjugate Chemistry, 2006. **17**(2): p. 548-550.

100. Chen, R., et al., *Antimicrobial peptide melimine coating for titanium and its in vivo antibacterial activity in rodent subcutaneous infection models.* Biomaterials, 2016. **85**: p. 142-151.

101. Makihira, S., et al., *Titanium Immobilised with an Antimicrobial Peptide Derived from Histatin Accelerates the Differentiation of Osteoblastic Cell Line, MC3T3-E1.* International Journal of Molecular Sciences, 2010. **11**(4).

102. Héquet, A., et al., *Optimised grafting of antimicrobial peptides on stainless steel surface and biofilm resistance tests.* Colloids and Surfaces B: Biointerfaces, 2011. **84**(2): p. 301-309.

103. Mauchauffé, R., et al., *Robust bio-inspired antibacterial surfaces based on the covalent binding of peptides on functional atmospheric plasma thin films.* Journal of Materials Chemistry B, 2014. **2**(32): p. 5168-5177.

104. Nie, B.e., et al., *A comparative analysis of antibacterial properties and inflammatory responses for the KR-12 peptide on titanium and PEGylated titanium surfaces.* RSC Advances, 2017. **7**(55): p. 34321-34330.

105. Leary Swan, E.E., K.C. Popat, and T.A. Desai, *Peptide-immobilised nanoporous alumina membranes for enhanced osteoblast adhesion.* Biomaterials, 2005. **26**(14): p. 1969-1976.

106. Vreuls, C., et al., *Prevention of bacterial biofilms by covalent immobilisation of peptides onto plasma polymer functionalised substrates.* Journal of Materials Chemistry, 2010. **20**(37): p. 8092-8098.

107. Duday, D., et al., *Atmospheric pressure plasma modified surfaces for immobilisation of antimicrobial nisin peptides.* Surface and Coatings Technology, 2013. **218**: p. 152-161.

108. Bekmurzayeva, A., et al., *Surface modification of stainless steel for biomedical applications: Revisiting a century-old material.* Materials Science and Engineering: C, 2018. **93**: p. 1073-1089.

109. Magalhães, S., et al. *Brief Overview on Bio-Based Adhesives and Sealants*. Polymers, 2019. **11**, DOI: 10.3390/polym11101685.

110. Chen, Z., et al., *Cold atmospheric plasma delivery for biomedical applications.* Materials Today, 2022. **54**: p. 153-188.

111. Drummond, J.E., *Plasma physics*. 2013: Courier Corporation.

112. Gurnett, D.A. and A. Bhattacharjee, *Introduction to plasma physics: with space and laboratory applications*. 2005: Cambridge university press.
113. Misra, N., O. Schlüter, and P.J. Cullen, *Cold plasma in food and agriculture: fundamentals and applications*. 2016: Academic Press.
114. He, Y., et al., *Recent advances of emerging organic pollutants degradation in environment by non-thermal plasma technology: A Review.* Water, 2022. **14**(9): p. 1351.
115. Laureano-Anzaldo, C.M., et al., *Plasma-enhanced modification of polysaccharides for wastewater treatment: A review.* Carbohydrate Polymers, 2021. **252**: p. 117195.
116. Ma, F., et al., *Effect of solution plasma process with bubbling gas on physicochemical properties of chitosan.* International journal of biological macromolecules, 2017. **98**: p. 201-207.
117. Pan, Y., J.H. Cheng, and D.W. Sun, *Oxidative lesions and post-treatment viability attenuation of listeria monocytogenes triggered by atmospheric non-thermal plasma.* Journal of Applied Microbiology, 2022. **133**(4): p. 2348-2360.
118. Chokradjaroen, C., et al., *Cytotoxicity against cancer cells of chitosan oligosaccharides prepared from chitosan powder degraded by electrical discharge plasma.* Carbohydrate polymers, 2018. **201**: p. 20-30.
119. Hertel, I.V. and C.-P. Schulz, *Inelastic Collisions – A First Overview*, in *Atoms, Molecules and Optical Physics 2: Molecules and Photons - Spectroscopy and Collisions*. 2015, Springer Berlin Heidelberg: Berlin, Heidelberg. p. 453-513.
120. Jiang, Y.-H., J.-H. Cheng, and D.-W. Sun, *Effects of plasma chemistry on the interfacial performance of protein and polysaccharide in emulsion.* Trends in Food Science & Technology, 2020. **98**: p. 129-139.
121. Primc, G., *Generation of Neutral Chemically Reactive Species in Low-Pressure Plasma.* Frontiers in Physics, 2022. **10**.
122. Wong, K.S., et al., *Plasma-Activated Water: Physicochemical Properties, Generation Techniques, and Applications.* Processes, 2023. **11**(7): p. 2213.
123. Tsujita, H., et al., *Effect of Plasma Treatment on Titanium Surface on the Tissue Surrounding Implant Material.* Int J Mol Sci, 2021. **22**(13).
124. Araújo, A.G.F., et al., *Design, manufacturing and plasma nitriding of AISI-M2 steel forming tool and its performance analysis.* Journal of Materials Research and Technology, 2020. **9**(6): p. 14517-14527.

125. Ollegott, K., et al., *Fundamental Properties and Applications of Dielectric Barrier Discharges in Plasma-Catalytic Processes at Atmospheric Pressure.* Chemie Ingenieur Technik, 2020. **92**.
126. Strauss, L., et al., *Plasma surface modification and three-dimensional structuring of additively manufactured polyetheretherketone implants for improvement of osseointegration.* Plasma Processes and Polymers, 2024. **21**(3): p. 2300082.
127. Kaklamani, G., et al., *Effect of plasma surface modification on the biocompatibility of UHMWPE.* Biomedical Materials, 2010. **5**(5): p. 054102.
128. Mittemeijer, E.J. and M. Somers, *Thermochemical Surface Engineering of Steels: Improving Materials Performance.* 2014: p. 1-792.
129. Bell, T. and Y. Sun, *Low-temperature plasma nitriding and carburising of austenitic stainless steels.* Heat Treatment of Metals, 2002. **29**: p. 57-64.
130. Huang, J.K., et al., *Effect of N2/H2 plasma treatment on the moisture adsorption of MOCVD–TiN films.* Thin Solid Films, 2011. **519**(15): p. 4948-4951.
131. Michlíček, M., S. Hamaguchi, and L. Zajíčková, *Molecular dynamics simulation of amine groups formation during plasma processing of polystyrene surfaces.* Plasma Sources Science and Technology, 2020. **29**(10): p. 105020.
132. Roliński, E., *Nitriding of Titanium Alloys*, in *Heat Treating of Nonferrous Alloys*, G.E. Totten, Editor. 2016, ASM International. p. 0.
133. Aziz, G., N. De Geyter, and R. Morent, *Incorporation of primary amines via plasma technology on biomaterials.* Advances in bioengineering, 2015: p. 21-48.
134. Oehr, C., et al., *Plasma grafting — a method to obtain monofunctional surfaces.* Surface and Coatings Technology, 1999. **116-119**: p. 25-35.
135. Yang, Z., et al., *The covalent immobilisation of heparin to pulsed-plasma polymeric allylamine films on 316L stainless steel and the resulting effects on hemocompatibility.* Biomaterials, 2010. **31**(8): p. 2072-2083.
136. Deepanjana, A. and B. Raghunath, *Plasma Based Approaches to Achieve Self-Cleaning Surfaces*, in *Nature-Inspired Self-Cleaning Surfaces in the Nanotechnology Era*, V.P. Phuong, Editor. 2023, IntechOpen: Rijeka. p. Ch. 5.
137. Booth, J.-P., et al., *Foundations of plasma surface functionalisation of polymers for industrial and biological applications.* Plasma Sources Science and Technology, 2022. **31**(10): p. 103001.
138. Levchenko, I., et al., *Plasma and Polymers: Recent Progress and Trends.* Molecules, 2021. **26**(13).

139. Francis F, C., *Introduction to plasma physics and controlled fusion*. 2016, Springer.
140. Hasan, A., et al., *Surface Design for Immobilisation of an Antimicrobial Peptide Mimic for Efficient Anti-Biofouling.* Chemistry – A European Journal, 2020. **26**(26): p. 5789-5793.
141. Gevrek, T.N., et al., *Thiol-Reactive Polymers for Titanium Interfaces: Fabrication of Antimicrobial Coatings.* ACS Applied Polymer Materials, 2019. **1**(6): p. 1308-1316.
142. Humblot, V., et al., *The antibacterial activity of Magainin I immobilised onto mixed thiols Self-Assembled Monolayers.* Biomaterials, 2009. **30**(21): p. 3503-3512.
143. Shen, L., et al., *Determination of conformation and orientation of immobilised peptides and proteins at buried interfaces.* Chemical Physics Letters, 2015. **619**: p. 247-255.
144. Ikonomova, S.P., et al., *Effect of linkers on immobilisation of scFvs with biotin-streptavidin interaction.* Biotechnol Appl Biochem, 2018. **65**(4): p. 580-585.
145. Nie, T., et al., *Sustained Release Systems for Delivery of Therapeutic Peptide/Protein.* Biomacromolecules, 2021. **22**(6): p. 2299-2324.
146. Bagheri, M., M. Beyermann, and M. Dathe, *Mode of action of cationic antimicrobial peptides defines the tethering position and the efficacy of biocidal surfaces.* Bioconjugate chemistry, 2012. **23**(1): p. 66-74.
147. Chen, Q., et al., *Impact of Antifouling PEG Layer on the Performance of Functional Peptides in Regulating Cell Behaviors.* Journal of the American Chemical Society, 2019. **141**(42): p. 16772-16780.
148. Banerjee, I., R.C. Pangule, and R.S. Kane, *Antifouling Coatings: Recent Developments in the Design of Surfaces That Prevent Fouling by Proteins, Bacteria, and Marine Organisms.* Advanced Materials, 2011. **23**(6): p. 690-718.
149. Diaz-Rodriguez, S., et al., *Comparison of the linking arm effect on the biological performance of a CD31 agonist directly grafted on L605 CoCr alloy by a plasma-based multistep strategy.* Biointerphases, 2019. **14**(5): p. 051009.
150. Diaz-Rodriguez, S., P. Chevallier, and D. Mantovani, *Low-pressure plasma treatment for direct amination of L605 CoCr alloy for the further covalent grafting of molecules.* Plasma Processes and Polymers, 2018. **15**(7).
151. Wang, T., et al., *The effect of structural modification of antimicrobial peptides on their antimicrobial activity, hemolytic activity, and plasma stability.* Journal of Peptide Science, 2021. **27**(5): p. e3306.

Chapter Two:

Optimised Amine Density via Plasma Treatment for Covalent Immobilisation of AMPs to Promote Osteoblasts and Enhance Antimicrobial Activity

---

Mohadeseh Zare [a*], Bogdan Butoi [b], Corneliu Porosnicu [b], Ion N. Mihailescu [b], David Grossin [c], Sarah A. Kuehne [d], Zubair Ahmed [e], Artemis Stamboulis [a*].

[a] Biomaterials Research Group, School of Metallurgy and Materials, University of Birmingham, Edgbaston, Birmingham, B15 2TT, UK

[b] INFLPR, 409 Atomistilor Street, Magurele, RO-077125, ROMANIA

[c] CIRIMAT, Toulouse INP, Université Toulouse 3 Paul Sabatier, CNRS, Université de Toulouse, 4 Allée Emile Monso - BP44362, 31030 Toulouse Cedex 4, France

[d] School of Science and Technology, Nottingham Trent University, Nottingham, NG11 8NS, UK

[e] Neuroscience and Ophthalmology, Institute of Inflammation and Ageing, College of Medical and Dental Sciences, University of Birmingham, Edgbaston, Birmingham, B15 2TT, UK

*Corresponding authors: a.stamboullis@bham.ac.uk; zare.mohadeseh@gmail.com

M.Z. conceived and designed the experiment, conducted the experimental work, interpreted the data, and drafted the manuscript. C.P. and I.N.M. contributed to the experimental design and data interpretation. D.G. was involved in the experimental design. A.S. provided overall supervision of the project. S.A.K. and Z.A. oversaw the microbiological analyses and biological assessments.

Abstract

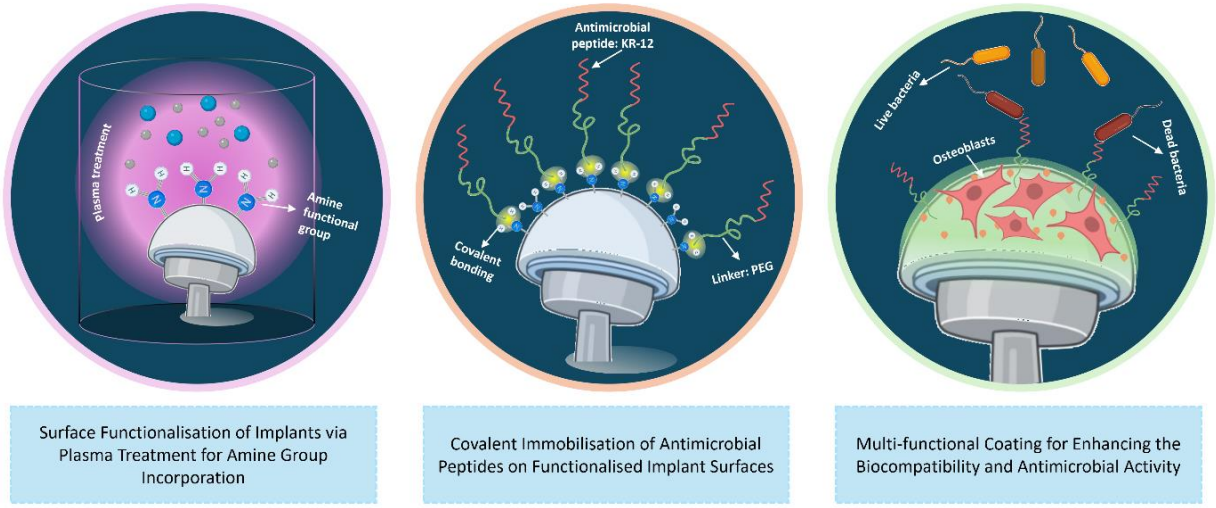
Biomedical implants, although capable of establishing functional connections with living tissues, are susceptible to bacterial infections, often leading to implant failure. Biomedical surface science employs different strategies, using bactericidal agents to prevent initial bacterial attachment, or antifouling agents to induce cell death by disrupting bacterial cell membranes or diffusing through them. However, bacterial resistance limits the efficacy of certain bactericidal agents like antibiotics. Recent research suggests that antimicrobial peptides (AMPs) can be promising alternatives to traditional antimicrobial agents.

To effectively inhibit bacterial biofilm formation, combining antifouling and bactericidal properties while promoting tissue integration is crucial. Our approach involves immobilising the KR-12 peptide as a bactericidal agent on titanium implant surfaces using Polyethylene glycol (PEG) as a linker, providing antifouling properties and enhancing peptide mobility for improved antimicrobial efficacy. Various methods exist for grafting PEG and peptide molecules onto titanium surfaces, including wet chemical and low-pressure plasma processes. We focus on plasma treatment due to its ability to introduce functional groups, simplify chemical reactions, and minimise process time requirements. Additionally, plasma treatment increases surface energy and wettability, facilitating protein adsorption and promoting favourable cell behaviour without altering surface topography. Primary amine groups generated during the treatment can strongly attach to titanium surfaces, acting as anchors for bioactive agents and positively impacting cell adhesion and signalling processes. Despite being a well-established technique for covalent binding, plasma treatment has seen limited success in immobilising antimicrobial agents compared to wet chemical methods, often due to the low efficiency of functional group creation. In this study, the first aim was to optimise the plasma treatment parameters to achieve comparable levels of surface-bound amine groups as with chemical techniques like silanisation. X-ray photoelectron spectroscopy (XPS) results revealed that the distribution and density of primary amine groups could be adjusted with plasma parameters, reaching a maximum of 9.18% nitrogen atoms associated with primary amines without altering the titanium surface morphology or bulk properties. Following the creation of primary amine groups, PEG and AMP were immobilised on the surface, sequentially and then the characterisation of the peptide-immobilised coatings was conducted using Atomic Force Microscopy (AFM), static Water Contact Angle (WCA) measurements, and XPS to analyse surface morphology and chemistry. Antimicrobial

testing against four pathogenic bacterial strains showed more than 90% of inhibition of bacterial adhesion and colonisation, with enhanced activity attributed to the improved orientation of linker-grafted AMPs compared to directly immobilised peptides. Additionally, the impact of the plasma-treated surface on cell promotion and adhesion was demonstrated by cell viability assay and Scanning Electron Microscopy (SEM). Cell viability results from the MTT assay of hFOB cells cultured on various substrates over 3, 5, and 7 days, no significant difference was observed compared to UTi. These findings emphasise the potential of integrating plasma treatment with the covalent bonding of AMPs to benefit from both the antimicrobial activity of the AMPs and the cell promotion properties of the plasma-treated surface.

Keywords: Antimicrobial Peptide, Plasma treatment, Antifouling properties, KR-12, Osteoblast promotion, Bacterial growth inhibition.

Graphical abstract:



2.1. Introduction

The successful long-term function of biomedical implants depends not only on their biocompatibility, encompassing hemocompatibility and osteoconductivity, but also on their inherent or acquired antibacterial efficacy [1]. Upon implantation, the surface undergoes protein adsorption, forming a layer that can serve as a potential receptor for bacterial adhesins, thereby promoting further colonisation and biofilm formation [2, 3].

To effectively prevent bacterial biofilm formation on medical device surfaces, the development of surface modifications that incorporate antimicrobial coatings is essential.

Ideally, these coatings should exhibit a trifecta of functionalities: 1) antifouling properties: to repel or resist initial bacterial attachment through physicochemical properties like electrostatic repulsion and surface energy manipulation [4, 5], 2) bactericidal activity: using incorporated antimicrobial agents to interact with the bacterial membrane to induce cell death [6], and 3) biocompatibility: to promote host cell adhesion and minimise cytotoxicity to ensure proper tissue integration [7].

Current research on bactericidal agents for antimicrobial coatings emphasises the development of multifaceted structures with tuneable toxicity and improved bioengineering functionalities to achieve desired antimicrobial properties. In this pursuit, antimicrobial peptide (AMP)-based systems have emerged as particularly promising candidates [8, 9]. AMPs are naturally occurring molecules found across diverse organisms. These peptides possess unique structural characteristics, typically containing both cationic and amphiphilic domains. These domains are crucial for their membrane-disruptive activity against bacteria [10]. Unlike traditional antibiotics, AMPs exhibit a broad spectrum of activity, targeting a wide range of microorganisms including bacteria, fungi, and viruses [11, 12]. Notably, AMPs display a reduced tendency to bacterial resistance compared to traditional antibiotics. This advantage stems from their distinct mechanism of action where the AMPs primarily disrupt bacterial membranes, bypassing common resistance pathways employed by bacteria to evade antibiotics [13, 14].

Among the diverse documented AMPs, the human cathelicidin peptide LL-37 stands out for its potent antimicrobial activity and multifaceted immunomodulatory properties [15]. A shorter fragment of LL-37, the cationic KR-12 peptide, offers lower cytotoxicity and improved cost-effectiveness owing to lower length, making KR-12 an attractive candidate for various biomedical applications including orthopaedic implants [16, 17]. The α-helical conformation and positive charge of KR-12 facilitate favourable interactions with bacterial membranes, leading to antimicrobial activity while minimising cytotoxicity. Structural studies suggest that AMPs like KR-12 exert their antibacterial effects by creating nanoscale pores or inducing membrane micellisation [18]. Furthermore, recent research demonstrates that controlled concentrations of KR-12 not only possess bactericidal properties but also promote osteogenic differentiation in human bone marrow-derived mesenchymal stem cells [19-21].

To immobilise AMPs on implants such as titanium alloys, two main strategies, physical

adsorption and covalent immobilisation, have been explored [22, 23]. Physical adsorption, while simpler, suffers from lower stability compared to covalent attachment. This leads to rapid release of AMPs from the surface, resulting in a decline in antimicrobial activity over time [24-26]. Conversely, covalent immobilisation establishes a strong chemical bond between the AMP and the implant surface, ensuring long-term stability and preservation of AMP activity [27, 28]. However, this method can restrict the mobility of the AMP and potentially hinder its interaction with bacteria due to steric hindrance [29]. To overcome this limitation, researchers have explored the use of flexible linker molecules between the AMP and the implant surface [30, 31]. These linkers provide the AMPs with increased flexibility and exposure, facilitating better bacterial interaction and penetration, and ultimately enhancing the overall antimicrobial efficacy [31, 32].

Concurrently, imparting antifouling properties to inhibit initial bacterial adhesion is crucial which typically involves two strategies: those that resist bacteria adhesion through the formation of a hydration layer and those that repel bio-contaminants due to low surface energy [4]. Among many different methods, the PEG and PEG-copolymers are widely utilised as anti-fouling coatings [33-35]. Although PEG exhibits antifouling characteristics against bacteria, it demonstrates favourable biocompatibility with fibroblasts and osteoblasts [36, 37]. The antifouling attributes of PEG are presumed to arise from steric repulsion mechanisms, which result from an entropic loss when proteins endeavour to adsorb onto surfaces [36, 37]. Despite significant experimental research and molecular dynamic simulations into PEG's applications on surfaces, its mechanism of action is still not fully understood [38-40]. PEG's efficacy is influenced by various factors, such as grafting density (higher densities correlating with increased protein repellence), chain length, and the specific branching architecture of PEG [39, 41, 42]. Considering the antifouling properties and biocompatibility of PEG, it can be regarded as a flexible linker for the covalent immobilisation of AMPs [43].

In order to chemically attach both the PEG and KR-12 peptide onto the surface, it is necessary to prepare functional groups, as anchors, through wet chemical or low-pressure plasma processes [43-47]. Comparing these methods suggests that plasma treatment holds superior advantages due to its ability to eliminate toxic multi-step chemical reactions, while also increasing surface energy and wettability without altering surface topography, thereby accelerating protein adsorption and promoting cell biological responses. Plasma treatment has the capability to create functional groups such as hydroxyl, carboxyl, or

amine groups on surfaces [48-50]. When modifying titanium alloys through plasma treatment, amine functional groups facilitate robust cross-linking and adhesion to the surface, while also exhibiting positive charges upon protonation in aqueous solutions at physiological pH levels [51-54]. In this instance, the carboxyl group of KR-12 peptides, initially activated by carbodiimide and succinimide-based compounds, can then covalently attach to the primary amine groups on the titanium surface induced by plasma treatment [54, 55].

Despite its numerous advantages, plasma treatment is not commonly used for AMP immobilisation. This discrepancy may arise from an insufficient number of anchor points available for immobilising AMPs. To achieve the highest amount of primary amine groups on the surface, the optimisation of plasma treatment parameters becomes crucial to achieve the highest amount of amine groups on the surface, a process requiring interdisciplinary knowledge encompassing physics, chemistry, and materials science [56]. Furthermore, the uniformity and stability of functional groups generated by plasma treatment must be considered throughout the entire process of immobilisation, sterilisation, and subsequent reactions between the surface and biological environment after the implantation [45, 57, 58].

The proposed approach can be utilised to create a multifunctional, antimicrobial, and biocompatible coating for all biomaterial implants. However, this study focuses on titanium alloys as the initial attempt, as preferred choices for orthopaedic, bone surgery, and dental applications owing to their remarkable mechanical strength, chemical inertness, and compatibility with biological systems [36, 59, 60]. Despite their capability for osseointegration, bacterial infections on titanium surfaces persist as a significant challenge, frequently leading to implant failure and complicating patient treatment [60-64]. Therefore, this study begins by optimising plasma treatment parameters to maximise the density of primary amine groups on the titanium surfaces. The surface density of $-NH_2$ groups, among other nitrogen-containing functional groups, can be fine-tuned by adjusting factors such as gas mixture (N_2/H_2) feed ratio, power input, sample position (glow or afterglow), and frequency, among others.

Here, we introduce a trifunctional coating that combines: i) the cell adhesive potential of plasma-treated surfaces; ii) the antifouling capabilities of PEG; and iii) the antimicrobial properties of the KR-12 peptide. For this purpose, we propose a rapid and straightforward

method involving plasma treatment of titanium alloy, followed by the immobilisation of PEG and subsequent attachment of the KR-12 peptide. The antimicrobial efficacy of the coating against various pathogenic bacteria was evaluated, and the cytocompatibility of the coating was assessed using human osteoblast bone cells.

2.2. Experimental methods

2.2.1 Sample preparation

The process of creating an antimicrobial coating for titanium substrates involved a systematic three-step procedure. First, plasma treatment was used to add primary amine groups to the substrates. Next, PEG linkers were attached, followed by the immobilisation of KR-12 peptides. Each stage of this sequential process is thoroughly explained in the following sections. An overview of the processing steps can be found in Figure 2-1. Table 2-1 provides descriptions of the sample names used in the experimental study.

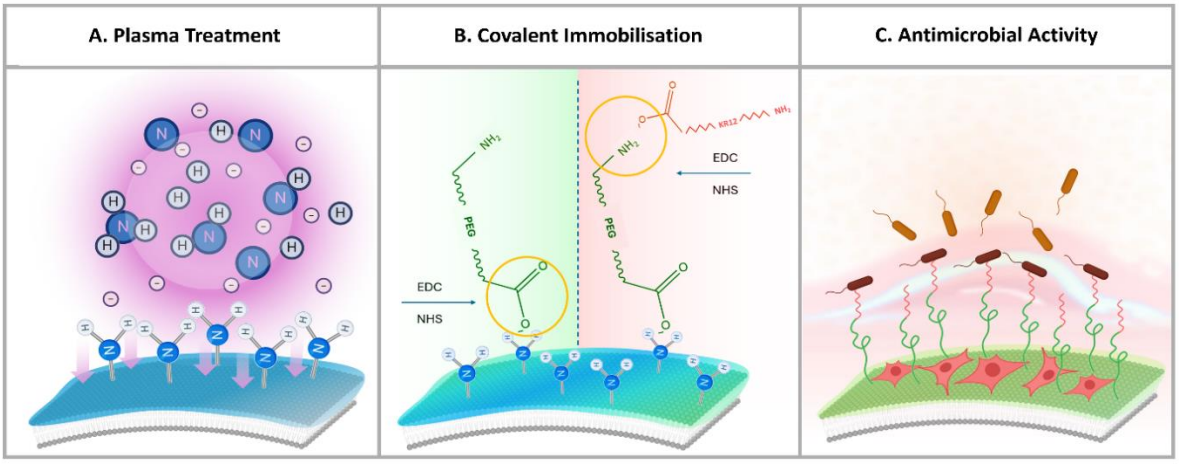


Figure 2-1. Schematic illustration of the step-by-step process of A. plasma treatment, B. PEG attachment, and KR-12 immobilisation, outlining the preparation of C. antimicrobial coating for titanium surfaces.

Table 2-1. Description of sample names corresponding to various surface modifications.

Name	**Description**
UTi	Polished titanium alloy Ti6Al4V
NH_2-Ti	Plasma-treated titanium surface
KR12-NTi	KR-12 immobilisation on the treated titanium surface

PEG-NTi	PEG attachment on the treated titanium surface
KR12-PNTi	KR-12 immobilisation on the PEG-functionalised titanium surface

2.2.2 Plasma treatment

The plasma process involves numerous adjustable parameters, including precursor pressure, applied power, frequency, time, pulse duration, and substrate location [65, 66]. Therefore, optimising a specific plasma process requires systematically studying how material properties depend on each of these parameters. In plasma treatment, various voltage supplies such as direct current (DC), radio frequency (RF), microwave (MW), Pulsed DC, and alternating current (AC) can be utilised, each tailored to specific applications and material requirements [67, 68]. Pulsed DC power supplies deliver voltage in a controlled, pulsed manner rather than continuously, reducing the thermal load and also improving process control [69, 70]. Controlling the pulse voltage, duration and repetition rate, allows better management of ion energy and plasma density, leading to more precise and uniform coatings and surface modifications [71]. This type of power supply is especially useful for applications requiring high precision and minimal substrate modification. RF power supplies are also commonly used, particularly in research to introduce functional groups on surfaces [66, 72]. Therefore, this study initially evaluated the efficacy of pulsed DC and RF power supplies in generating primary amine groups on surfaces to determine the more effective power supply. The plasma parameters for both processes were optimised to maximise the grafting extent of primary amine groups, as quantified by the N/C ratio and NH_2/N ratio using XPS. Ultimately, pulsed DC demonstrated greater efficiency compared to RF supply. Therefore, we configured our plasma equipment utilising the pulsed DC supply for further detailed investigations aimed at optimising the parameters.

Plasma treatments were conducted using a purpose-designed reactor featuring adjustable plasma parameters. The reactor employs a parallel plane, hollow disk-shaped electrode configuration within a Pyrex glass chamber (300 cm^3). The upper electrode, serving as the anode, has an inlet for injecting working gases into the chamber, while the lower electrode, serving as the cathode, includes a sample holder. This geometric setup (Figure 2-2a) ensures rotational symmetry and a uniform plasma distribution over surfaces.

Discharges were ignited between the positively driven upper electrode and the grounded lower electrode, positioned 7 cm apart. The power supply, applied for the experiments, delivers a peak voltage of 2 kV, with adjustable pulse duration and repetition rates ranging from 5 to 12 µs and 20 to 90 kHz, respectively. High-purity H_2 and N_2 gases (99.999%, air-liquid) were injected through electronic MKS mass flow controllers (MFC). The setup includes a Pfeiffer HiPace 80 turbomolecular pump and an MVP 015-2 diaphragm pump, ensuring a base pressure of less than 5 x 10^{-5} mbar. A Pfeiffer PKR 251 vacuum gauge and a gate valve were used to establish the working pressure.

Before performing the plasma treatment, the sample preparation started with polishing titanium disks (10 mm diameter, 2 mm thickness) which served as representative models for the prevalent materials found in dental and orthopaedic implants (commercially pure medical grade 5 Ti6Al4V, William Gregor LTDL.T.D., East Grinstead, UK). The polishing process started with grinding the disks consecutively with 800, 1200, and 2500 grit Struers silicon carbide/abrasive papers using Struers Metallographic equipment. Subsequently, the disks were polished to mirror-finish using a 0.05 µm particle size colloidal silica, following Bruker's protocols. After polishing, substrates were cleaned using sequential water and ethanol washes in an ultrasonic bath and then dried under a high vacuum (< 5×10^{-6} mbar). The cleaned substrates were subsequently placed in the plasma reactor, and the chamber was evacuated. This procedure ensures the removal of any unwanted organic materials from the surface before plasma treatment.

When the chamber reached the appropriate base pressure (< 5×10^{-5} mbar), the mixture of N_2 and H_2 was introduced via MFCs until steady working flow rates were achieved. Plasma ignition was achieved using a variety of pulse parameters over designated time intervals of 30 seconds, 1 minute, 5 minutes, and 10 minutes. Table 2-2 details the range of plasma parameters employed with the pulsed DC power supply.

Immediately following plasma modification, the processed substrates were stored for 12 hours before undergoing XPS analyses. This analysis quantified the extent of primary amine group grafting by measuring the N/C ratio and NH_2/N ratio on the modified titanium surfaces.

Table 2-2. Range of Plasma Parameters Investigated for Pulsed DC Power Supply.

Voltage supplier	N_2/H_2 gas ratio	Flow rate (SCCM)	Distance	Pressure (mbar)	Frequency (kHz)	Pulsed duration (µs)	Time (seconds)
Pulsed DC-2 kV	25 / 75	10 /10	Afterglow 7 cm	0.06 - 3.5	20 - 90	5 - 11	30 - 600

2.2.3 PEG attachment

In order to attach PEG as a flexible linker onto titanium surfaces a hetero-bifunctional PEG (NH_2-PEG-COOH, average M_N 2000, Catalogue number: 757545), purchased from Sigma Aldrich, was used. The procedure entailed the activation of the carboxyl group in PEG using 1-Ethyl-3-(3-dimethyl-aminopropyl) carbodiimide (EDC, supplied by Thermo Fisher Scientific, CAS number: 33472-58-9), leading to the creation of a highly reactive O-acylisourea [73]. Following this, the formed intermediate complex underwent reaction with the primary amine groups located on the titanium surface by Sulfo-NHS (N-hydroxysulfosuccinimide, supplied by Thermo Fisher Scientific) as an activating agent, as outlined in the literature [73].

The initial phase involved preparing a 1 mg/ml solution of PEG in MES (2-(N-morpholino) ethanesulfonic acid) buffer (0.1M, pH 6.0). Amino-functionalised substrates (NH_2-Ti, as detailed in Table 2-1) were then immersed in the PEG solution for 1 hour. Subsequently, a solution containing EDC (23 $mg.l^{-1}$) was added, followed by the gradual addition of Sulfo-NHS (77 $mg.l^{-1}$). The resulting grafted samples, denoted as PEG-NTi, underwent sequential washing with deionised (DI) water and ethanol using vortex agitation to eliminate non-covalently bound reactants before being dried and stored in a desiccator.

2.2.4 Covalent immobilisation of KR-12

To immobilise the KR-12 (H-KRIVQRIKDFLR-OH), supplied by BOCSCI Inc., NY, USA, on the amine groups of the grafted PEG, a similar EDC/NHS protocol was employed. The resulting samples were labelled as KR12-PNTi. The same methodology was utilised to immobilise KR-12 directly onto the plasma-treated surface of NH_2-Ti,

labelled as KR12-NTi. Following the protocol outlined in the previous section, the substrates were immersed in a 1 mg/ml solution of KR-12 in MES buffer. After 1 hour of incubation, EDC and Sulfo-NHS solutions were sequentially added dropwise to activate the carboxylic groups of the peptides and subsequently react with the primary amine groups. This systematic approach ensured a consistent process for immobilising KR-12 onto either the amine-functionalised surface of NH_2-Ti or the amine terminal of the PEG chains grafted onto the surface of PEG-NTi. To eliminate peptides not bound covalently to the samples, two washing cycles using DI water and ethanol, employing vortex agitation were conducted for thorough cleansing. To quantify the density of immobilised peptides, an Fmoc (fluorenyl methyloxy carbonyl)-labelled KR-12 (Fmoc-KRIVQRIKDFLR-OH) was employed, using the same protocol as described.

The KR-12 concentration, used for the immobilisation, was selected based on the minimum inhibitory concentration (MIC) of KR-12 as reported in previous studies [74-76]. This guaranteed that the released quantity remained below the MIC threshold while determining optimised concentrations favourable for antimicrobial properties and osteogenic differentiation and promotion.

2.2.5 Thermal and mechanical stability of plasma-treated surfaces

To assess the thermal and mechanical stability of plasma-treated surfaces, NH_2-Ti samples underwent various conditions, with subsequent re-examination of XPS analysis to quantify NH_2 content changes. For ambient stability, discs were placed in a 24-well plate at room temperature for intervals up to 14 days, with three replicates for each period. Then, the XPS analyses were conducted to measure NH_2 amount alternations.

In aqueous environments, NH_2 percentage alterations were measured after the incubation in phosphate-buffered saline (PBS) at 37°C over 14 days, with three replicates per duration. The mechanical stability was determined by subjecting discs to ultrasonication in PBS for 30 min, 1, 1.5, 2, 2.5 and 3 hours, followed by XPS analysis, with three replicates per duration.

2.2.6 Surface characterisation

X-ray Photoelectron Spectroscopy (XPS)

The surface elemental compositions of UTi and NH_2-Ti were characterised using a Thermo NEXSA XPS at Harwell XPS, Oxford. This system features a monochromated Al Kα X-

ray source (1486.7 eV), a spherical sector analyser, three multichannel resistive plates, and 128-channel delay line detectors. Data acquisition was performed at 19.2 W, with an X-ray beam measuring 400 x 200 µm. Survey scans were performed at a pass energy of 200 eV, and high-resolution scans employed a pass energy of 40 eV. To neutralise the electronic charge, a Dual-beam low-energy electron/ion source (Thermo Fisher Scientific FG-03) was used. Measurements were conducted at a pressure below 10^{-8} Torr and at a temperature of 294 K. For data analysis, CasaXPS v2.3.20PR1.0 was employed, with peak fitting performed using a Shirley background subtraction before component analysis. All binding energies were calibrated to the C 1s signal at 284.8 eV.

Atomic Force Microscopy (AFM)

The surface topography and roughness variations of PEG-attached and KR-12-attached samples were examined at room temperature using tapping mode AFM. A Bruker Multimode 8 system with Pt-coated silicon cantilevers (SCM-PIT) from Bruker was employed. Random sites were scanned in 5 µm² and the images were digitally processed with NanoScope Analysis 1.7 software to determine the R_a.

Atenuated Total Reflectance-Fourier Transform Infrared Spectroscopy (ATR-FTIR)

To validate the mechanisms of the chemical reactions, the substrates were examined using ATR-FTIR spectroscopy. This analysis was conducted before and after the reactions with a Nicolet 6700 FTIR instrument (Thermo Fisher Scientific) and processed using the Omnic 8 software suite (Thermo Fisher Scientific). The spectra covered a range from 4000 to 400 cm^{-1}, obtained from an average of 64 scans per background, with a spectral resolution of 2 cm^{-1}.

Water Contact Angle (WCA) measurements

Surface wettability, assessed through static WCA measurement, is a key determinant of a surface's hydrophilic or hydrophobic nature, influencing cell attachment. The static WCAs were measured at room temperature by examining the profile of sessile water droplets. A 5 µL droplet of DI water was placed on the sample surface using a Hamilton syringe on a Kruss DSA100 apparatus (Germany), which includes a CCD camera and an image analysis processor. The WCAs were calculated using the built-in CAM 100 software. Each test was performed in triplicate, with four droplets measured at different locations on each sample and three different samples analysed per group. A static image was taken within three seconds after droplet deposition, and the angles were measured from this image. The

reported values are the averages of these nine measurements for each surface type.

2.2.7 Concentration of immobilised KR-12

To quantify the KR-12 loading on the surface, the number of Fmoc groups was estimated by measuring the maximum ultraviolet (UV) absorption at 301 nm. This estimation enabled the calculation of the peptides, as each peptide contained one Fmoc group (Fmoc-KRIVQRIKDFLR-OH). Fmoc groups attached to the peptides were cleaved using 20% piperidine in dimethylformamide (DMF), a common reaction mechanism in solid-phase peptide synthesis utilising the Fmoc/t-Bu (Tert-Butyl) method [77]. The presence of piperidine leads to the formation of dibenzofulvene–piperidine adducts, through a Michael-type addition, which are soluble in the reaction solvents. This solubility allows for spectrophotometric measurement based on the Beer-Lambert law. A multipoint standardisation method, involving a calibration curve, was used to measure the solution's UV light absorption at a specific wavelength. Calibration points were prepared and validated on the same day as the analysis to ensure accuracy.

For the preparation of the calibration curve, Fmoc-KR12 stock solutions (1 mg/mL = 637 μM) were prepared in 20% (v/v) piperidine in DMF (99.8% purity), with both solvents supplied by Sigma Aldrich. The Fmoc removal reactions were conducted for 30 minutes at room temperature. Following this, 5.0 mL of the stock solution was diluted to 50.0 mL with 20% (v/v) piperidine in DMF. Dibenzofulvene-base solutions with varying concentrations (from 10 to 310 μM in 30 μM intervals) were prepared using a dilution technique. These solutions were prepared in triplicate and their absorbance was measured at 301 nm, where the absorption was attributed solely to the dibenzofulvene-base adduct. A calibration curve plotting dibenzofulvene-base adduct concentration against absorbance was then constructed.

For the analysis, every peptide-immobilised titanium surface (KR12-NTi and KR12-PNTi) underwent immersion in a 20% v/v piperidine solution in DMF, where Fmoc removal reactions took place over a 30-minute period at room temperature. Following this, the absorbance of each solution was measured at 301 nm (n = 3) and then correlated with the calibration curve.

2.2.8 KR-12 release rate

To simulate the release of KR-12 from the KR12-NTi and KR12-PNTi disks, the samples,

which were immobilised with Fmoc-labelled KR-12, underwent incubation in a 20 ml PBS solution at 37°C with mild shaking for 7 days.

To evaluate the rate of KR-12 release, the samples were removed from the reaction solution at predetermined intervals. Subsequently, the absorbance of each solution was measured at 301 nm (n = 3) and then correlated with the established calibration curve. The preparation of this calibration curve involved preparing varying concentrations (ranging from 10 to 310 μM in 30 μM intervals) of Fmoc-labelled KR-12 in PBS (supplied by Sigma-Aldrich) using a dilution technique. This enabled the plotting of Fmoc-labelled KR-12 concentration against absorbance.

2.2.9 Antimicrobial activity assay

Orthopaedic implant infections commonly originate from bacteria such as *Staphylococcus aureus (S. aureus), Staphylococcus epidermidis (S. epidermidis), Escherichia coli (E. coli),* and *Pseudomonas aeruginosa (P. aeruginosa)* [78-80]. Therefore, in this study the antimicrobial efficacy of the coatings was assessed against two Gram-positive bacteria, *S. aureus* (SH1000) and *S. epidermidis* (ATCC 12228), as well as two Gram-negative bacteria, *E. coli* (ATCC 25922) and *P. aeruginosa* (PAO1). To begin, the strains were grown on Mueller-Hinton (MH) agar plates (supplied by Thermo Fisher Scientific) using the Streak Plate method. Subsequently, a colony of each strain was cultured in MH broth (Thermo Fisher Scientific) at 37°C overnight with mild shaking. To count the number of colonies forming units (CFUs) in a bacterial suspension, serial dilutions of the bacterial culture were prepared in a 96-well plate and then cultured on MH agar plates based on the Miles and Misra method [81]. The bacterial suspension was diluted to a concentration of 10^5 CFU mL^{-1} in MH broth for subsequent analyses.

The titanium disks with different coatings alongside the polished titanium, as a control sample, were sterilised in 1 mL of 70% ethanol for 5 minutes at room temperature and then rinsed with sterilised DI water in a sterile environment, repeated thrice. Following that, 20 μL of the bacterial suspension was dropped onto each sample, and they were incubated for 24 hours at 37°C, using a direct contact test protocol, as described in detail in the following section. Then, bacterial growth inhibition ratio, Confocal Laser Scanning Microscopy (CLSM), and SEM were employed to characterise bacterial colonisation for each coating group. All procedures were conducted within a class II ventilated hood, and tools were autoclaved or sterilised with 70% ethanol before operation.

2.2.10 Bacterial growth inhibition

The surface antimicrobial activity was assessed against *S. aureus*, *S. epidermidis*, *E. coli*, and *P. aeruginosa* using a direct contact test (DCT) protocol. For each sample, a sterile petri dish was prepared by placing a round filter paper, saturated with PBS, inside to maintain humidity and prevent evaporation of the bacterial suspension. A sterile microscope slide was then positioned on the filter paper, and the sample (10×10 mm^2) was placed onto the slide. Next, 20 µl of the overnight bacterial suspension (containing 10^5 bacteria/ml) was pipetted onto the surface of the sample. A coverslip (20 x 20 mm^2) was gently placed on top to evenly distribute the inoculum across the entire surface of the disk. The sealed petri dishes were then incubated at 37°C for 24 hours. After the incubation period, the substrates covered by the bacterial suspension were transferred to a sterile 10-mL tube. Upon adding 5 mL of Mueller-Hinton (MH) broth, they were vortexed for 5 minutes to detach adherent bacteria. Given that titanium substrates are non-porous and non-absorbent, this 5-minute process effectively removed the adhered bacteria, as confirmed by SEM studies conducted before and after vortexing. After vortexing, 200 µL of the bacterial suspension was retrieved, and 10-fold serial dilutions were performed to quantify bacterial colonies on MH agar plates according to the Miles and Misra method. Following an incubation at 37°C for 20 hours, the number of colonies on each surface was recorded per cm^2 of the surface.

The bacterial growth inhibition was determined by comparing the CFU of the control sample, UTi (denoted as X_1), with those of each coated titanium sample (denoted as X_2), using the following equation:

Bacterial growth inhibition ratio (%)$= (X_1-X_2)/X_1\times100$ [82, 83]

The measurements were performed in triplicate for each type of sample, and the percentage of bacterial growth inhibition was calculated by averaging the values obtained from the three samples for each type.

E. coli and *S. aureus* were chosen as representative strains for live/dead assays and SEM analysis to investigate the antimicrobial behaviour of our treatment. *E. coli* represents Gram-negative bacteria, characterised by an outer membrane that can affect susceptibility to treatments, while *S. aureus* represents Gram-positive bacteria with a thick peptidoglycan layer that presents distinct interaction profiles. Preliminary tests on other

Gram-negative (*P. aeruginosa*) and Gram-positive (*S. epidermidis*) bacteria showed similar behaviour, therefore, we present E. coli and S. aureus as representative models for clarity and conciseness.

2.2.11 Bacterial morphology assay

After the incubation of each sample with 20 µl of bacterial suspension, as previously described, the samples were immersed in 2.5% EM grade glutaraldehyde in 0.1 M sodium cacodylate buffer, pH 7.3, for 10 minutes to fix the bacteria on the surface.

To facilitate gradual dehydration, the samples were then treated with ethanol solutions of increasing concentrations (20%, 30%, 40%, 50%, 60%, 70%, 90%, 95%, and 100%) for 10 minutes each. Subsequently, hexamethyldisilizane (HMDS) from Sigma-Aldrich was used to completely remove the alcohol.

Following fixation and dehydration, the samples underwent gold coating before being subjected to SEM imaging using a Zeiss MERLIN Field Emission SEM (Carl Zeiss GmbH, Oberkochen, Germany). All samples were scanned at a working distance of 9 mm and a voltage of 10 kV.

2.2.12 Confocal Laser Scanning Microscopy (CLSM)

CLSM was employed to characterise the live and dead bacteria on different coating surfaces. Following 24 hours of bacterial culture (20 µL, 10^5 bacteria/mL) with each substrate, as described, the surfaces were gently washed with PBS to remove non-adherent bacteria. The samples were then stained using the Live/Dead BacLight bacterial viability kit (Invitrogen, Paisley, UK) according to the manufacturer's instructions.

The kit included SYTO 9, a green-fluorescent nucleic acid stain, and propidium iodide, a red-fluorescent nucleic acid stain, both dissolved in Dimethyl Sulfoxide (DMSO). Equal volumes of these components were thoroughly mixed in a microfuge tube. A 5 µL aliquot of the dye mixture was then added to each sample and incubated in the dark at room temperature for 15 minutes. The excitation/emission maxima of the dyes are approximately 480/500 nm for SYTO 9 and 490/635 nm for propidium iodide. The samples were then characterised using a non-inverted confocal laser scanning microscope, the Leica TCS SP8. Viable bacteria appeared green under fluorescence, while non-viable bacteria appeared red. Image analyses were performed using ImageJ version 1.53k.

2.2.13 Cell viability and compatibility assessment

Cell culture

The human fetal osteoblast 1.19 cell line (hFOB 1.19), sourced from ATCC, was cultured in a 1:1 mixture of Ham's F12 Medium and Dulbecco's Modified Eagle's Medium (DMEM) without phenol red. This medium was supplemented with 2.5 mM L-glutamine, 15 mM Hepes, and 0.3 mg/mL G418, along with 1% Penicillin-Streptomycin and 10% Fetal Bovine Serum (FBS). The cells were incubated at 34°C until they reached confluence. At 90% confluence, the cells were washed with sterile PBS and treated with a 0.25% (w/v) Trypsin-0.53 mM EDTA solution for 10 minutes at 34°C to detach them from the culture surface. The cells were then transferred to a centrifuge tube containing culture medium and centrifuged at 125 x g for 5 minutes. Post-centrifugation, the cells were resuspended and sub-cultured at a 1:4 ratio. Cells from passage 3 were used in all experiments. All cell culture reagents and supplements were obtained from Gibco, Thermo Fisher Scientific Inc..

MTT assay to quantify cell viability

The cytotoxicity of the coated samples was evaluated using the MTT (3-(4, 5-dimethylthiazolyl-2)-2, 5-diphenyltetrazolium bromide) assay kit from Sigma Aldrich. The cells were cultured as previously described and cell viability on each sample was assessed at 1, 3, 5, and 7 days after seeding.

Before seeding the cells, titanium samples were rinsed twice with sterilised PBS, briefly soaked in ethanol, and then transferred to new 24-well plates. Cells were seeded onto the coated disks, 20,000 cells per disk, using a 20-µL drop. After the incubation for 30 minutes at 34°C, the cells were allowed to attach, after which additional medium was added to each well to reach a total volume of 500 µL for further culture. The culture medium was refreshed every two days.

A blank growth medium was used as the background control. At determined intervals of the incubation at 37°C, the medium in each well was substituted with 100 µL of MTT solution (0.5 mg/ml in supplemented DMEM) and incubated for 4 hours. Subsequently, the solution was aspirated, and the insoluble formazan crystals were dissolved in 100 µL of dimethyl sulfoxide (DMSO). After a 15-minute incubation period, the optical density (OD) was measured at a wavelength of 570 nm by an ELISA microplate reader and stated

as a percentage relative to the absorbance of the control. Due to the light sensitivity of the MTT reagent, all procedures were conducted in the dark.

Cell morphology

Following the outlined cell culture protocol, the coated samples underwent sterilisation through a process involving washing with PBS and ethanol. Subsequently, they were cultured with hFOB cells at a density of 20,000 cells /cm^2 to evaluate cell morphology after 5 days. After culturing, the surfaces were gently washed with PBS and fixed with 4% paraformaldehyde in PBS (supplied by Thermo Fisher Scientific) for 40 minutes. After fixation, the samples were subjected to sequential dehydration using ethanol solutions (from 20% to 100% v/v) for 10 minutes each. HMDS was employed to remove residual alcohol. Finally, the surfaces were sputter-coated with gold, and the cellular morphology was observed utilising a Zeiss MERLIN Field Emission SEM (Carl Zeiss GmbH).

2.2.14 Statistical analyses

The results are reported as mean ± standard deviation, with ($n \geq 3$) denoted. Statistical analysis was conducted using SPSS, employing a one-way analysis of variance with Tukey's post hoc test to assess significant differences between groups. A p-value of < 0.05 was regarded as statistically significant (*$p < 0.05$, **$p < 0.01$, ***$p < 0.001$).

2.3. Results and discussion

Plasma treatment was employed to introduce primary amine functional groups on a titanium surface, followed by the attachment of PEG and subsequent immobilisation of KR-12 on the PEG linker. Although numerous strategies for covalent bonding of biological molecules to titanium surfaces have been documented, with silane chemistry being particularly prominent, this study employed plasma treatment. This approach was chosen not only to minimise the number of chemical reaction steps but also to benefit from the enhanced biocompatibility of the plasma-treated surface.

It is important to note that immobilising peptides directly on plasma-treated surfaces can reduce their mobility and affect their orientation due to steric hindrance, consequently impairing their activity [84]. To address this, following plasma treatment, the carboxyl groups of functionalised PEG were reacted with the primary amine groups on the plasma-treated surface using an EDC/NHS activation process. This reaction primed the amine groups of PEG as anchoring points for subsequent an AMP immobilisation. In this study,

various ratios of PEG and peptide were explored. The concentrations reported here are the optimised and finalised parameters used for subsequent characterisations.

2.3.1 Optimisation of plasma parameters and stability of treated surfaces

Plasma, a quasi-neutral ionised gas, consists of photons, electrons, positive and negative ions, atoms, free radicals, and excited or non-excited molecules, all exhibiting collective behaviour [85]. Since surface reactions in a plasma environment such as etching, activation or cross-linking and the resulting surface properties are strictly dependent on plasma gas composition and process conditions, optimising these parameters is necessary to achieve the desired effects. Gaseous plasmas are ignited by applying a potential through a gas and can be generated in either low pressure or atmospheric pressure [86]. Low-pressure plasmas are widely used in biomaterials research since at these conditions, the discharge is more stable, and the plasma reactions can be more easily controlled. Low Temperature Plasma (LTP), also known as cold plasma, is generated at low pressures and power levels, resulting in low ion energies and densities [87, 88]. This results in more uniform treatment and the ion energies and densities are low enough to avoid causing unwanted defects, such as sample heating [86]. It also facilitates surface functionalisation and promotes extensive hydrophilisation [86].

Previous studies suggested that LTP treatment could increase surface energy and wettability without changing the surface topography, thereby accelerating protein adsorption and promoting the biological behaviour of cells [89, 90]. It was also demonstrated that hydrophilic surfaces obtained by plasma treatment before the surgical operation could reduce carbon contamination and prevent ageing, thereby enhancing new bone formation and osteointegration, and reducing the time of healing procedures [57, 88, 89]. LTP treatment has also been extensively studied as a method for introducing surface functional groups or free radicals. These features served as anchorage points for grafting antibacterial agents, including antibiotics, AMPs, enzymes, Ag nanoparticles [45, 66, 91-93].

Various parameters, including the composition of the gas mixture, gas flow rate, reactor chamber pressure, reaction time, and the reactor's geometry and physical dimensions, significantly influence the surface properties of the resulting product [86, 91]. Moreover, the electrical power input and treatment duration have a pronounced impact on the nature and concentration of the molecular species formed in the reactor, which in turn

significantly affect the incorporated functional groups [86]. Therefore, optimising power and time parameters was the first step of this study. Plasma conditions that promote a high concentration of functional groups are typically characterised by low power levels, which minimise precursor fragmentation and consequently reduce the degree of etching [66, 94].

Pulsed plasmas, which introduce additional parameters such as pulse duration and frequency, are often employed to mitigate the undesirable effects associated with Continuous wave (CW) plasmas. The high plasma powers required to modify inorganic materials can lead to high ion accelerating voltages, potentially resulting in sputtering of reactor materials and substrate damage [94, 95]. Pulsed plasmas help prevent these issues by limiting charge buildup and reducing ion bombardment duration, thereby minimising surface damage due to the differing lifetimes of ions and radicals during the plasma-off time [96, 97]. They also offer advantages such as higher instantaneous powers, lower substrate temperatures, improved treatment uniformity, and greater control over the specific plasma species produced. Additionally, pulsed plasmas significantly affect the gas-phase densities of both charged and neutral species within the system [95]. Previous studies have demonstrated that the densities of plasma species during pulsed plasma operation can be up to ten times higher than those observed under steady-state plasma conditions. These findings are based on time-resolved measurements of fast pulses, which allow for the resolution of temporal density profiles [98, 99].

Two distinct distances can be utilised for the LTP process: in-the-glow and after-glow distances. It has been demonstrated that, under fixed parameters and identical gas mixtures, coating homogeneity is more readily achieved in the plasma afterglow due to the inherent uniformity of species in the afterglow [100].

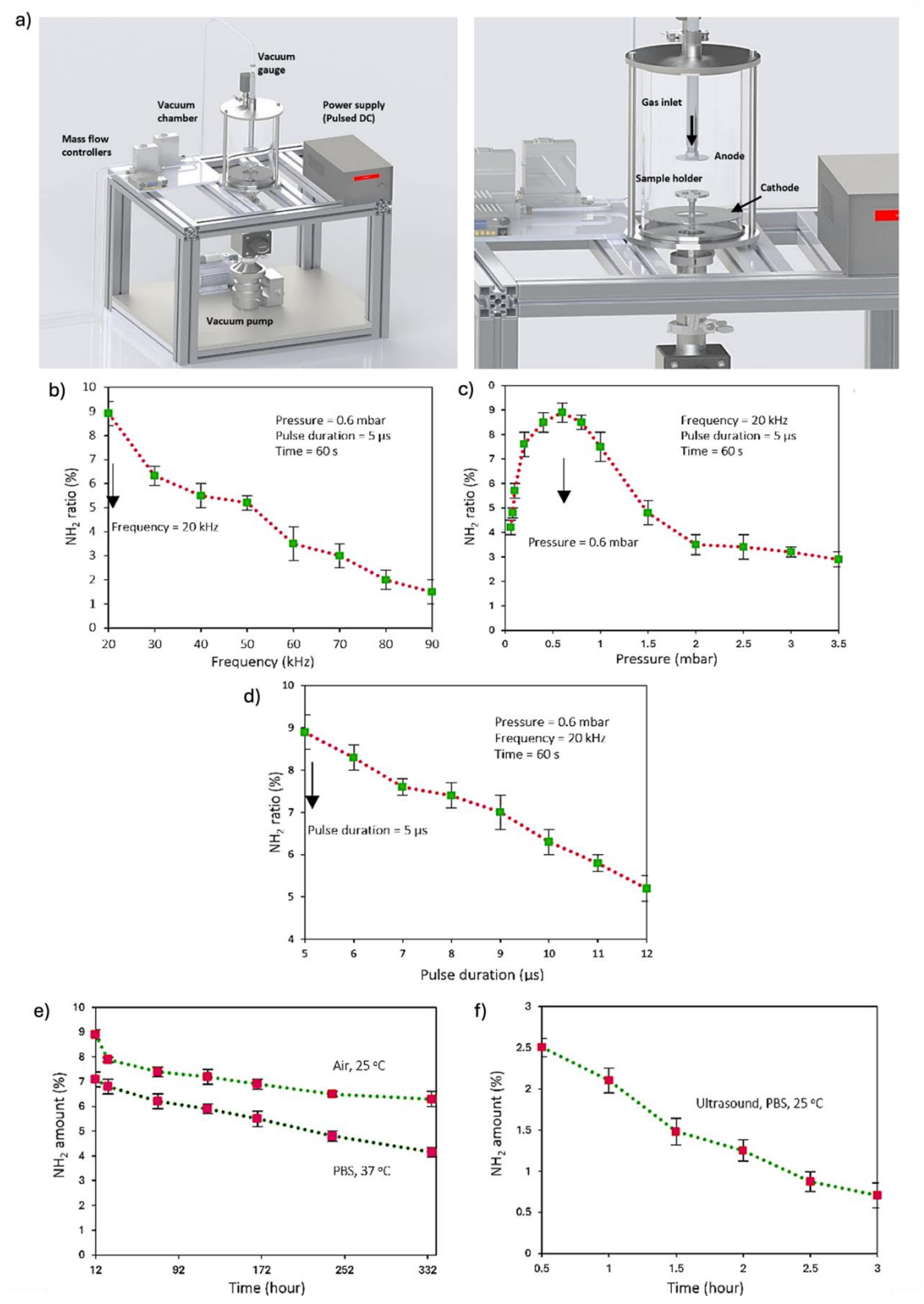


Figure 2-2. Plasma treatment evaluation: (a) Scheme of purpose-designed plasma reactor with adjustable parameters. (b-d) Concentration of primary amine groups measured by XPS as a function of varying plasma parameters to determine optimal conditions. (e) Ambient stability of primary amine groups on plasma-treated discs at room temperature

over a period of up to 14 days, with XPS analyses used to monitor changes in NH_2 concentration. (f) Mechanical stability of primary amine groups within 30 minutes of ultrasonication. Error bars represent the standard deviation from three independent experiments

Previous studies have documented over 20 reactions involved in the production of NH_2 within plasma systems using a mixture of N_2 and H_2 [101-103]. The amine functional groups formed on the surface arise from the equilibrium of these reactions in the pulsed plasma atmosphere [101-104]. To maximise the surface concentration of -NH_2 groups on titanium, the plasma equipment parameters listed in Table 2-2 were optimised. The concentration of primary amine groups for each experimental batch was then analysed using XPS.

In this study, plasma treatments were conducted using a purpose-designed reactor featuring adjustable plasma parameters, as illustrated schematically in Figure 2-2(a). Based on previous studies, to achieve stable and homogeneous functional groups on the surface, the afterglow distance was utilised [100]. The pressure was analysed within the range of 0.06 to 3.5 mbar. Frequency and pulse duration were tested between 20–90 kHz and 5–11 µs, respectively. Comparing the XPS results of various durations ranging from 30 seconds to 600 minutes in 30-second intervals, determined that the optimal treatment time was 60 seconds. Therefore, the resulting data for various parameters, with 1 minute identified as the optimal treatment duration, are presented in Figure 2.

As illustrated in Figure 2-2(b), lower frequency pulses resulted in more effective production of primary amine groups. This enhanced efficacy is attributed to phenomena occurring during the breakdown phase of the plasma, where a sufficiently strong electric field generates an electron cascade, and ignites the plasma, and also the intervals between pulses are appropriately spaced to avoid disrupting the already-formed primary amine groups [104, 105].

As depicted in Figure 2-2(c), the optimal pressure for -NH_2 production was determined to be 0.6 mbar. This pressure appears to favour the formation of primary amine groups by providing optimal conditions for particle mean free path, plasma density for the production of reactive species, and plasma sheath dynamics to ensure effective delivery of reactive species onto the titanium sample.

Lower pulse durations were directly associated with shorter residence times of reactive

species in the plasma, thereby minimising the period available for recombination or decomposition of these species. Low pulse duration also resulted in a reduced thermal load, decreasing the likelihood of desorption from the substrate surface. Furthermore, shorter plasma lifetimes ensured that primary amine groups formed in the plasma and diffused onto the sample during the plasma off-time were not subsequently bombarded by high-energy particles. Consequently, the highest percentage of primary amine groups was achieved at the shortest pulse duration (5 µs), as demonstrated in Figure 2-2(d).

To evaluate the thermal and mechanical stability of plasma-treated surfaces, the treated samples were subjected to various conditions. Figure 2-2(e) illustrates the ambient stability of primary amine groups on plasma-treated discs at room temperature over a period of up to 14 days, with XPS analyses used to monitor changes in NH_2 concentration. During the initial 24 hours of ambient storage, there was a significant decrease in NH_2 concentration, followed by a more gradual decline. After 14 days, the concentration of NH_2 groups reduced to 6.22% ± 0.24, which remained sufficient for peptide immobilisation; however, for optimal immobilisation efficiency, it is advisable to perform the reaction within 24 hours. For physiological stability, NH_2 concentration was assessed in PBS at 37°C for 14 days, resulting in a reduction to 4.15% ± 0.13. This indicates that the aqueous environment promoted instability and facilitated the removal of NH_2 groups from the surface.

Moreover, the mechanical stability was evaluated by subjecting the discs to ultrasonication in PBS for durations ranging from 30 minutes to 3 hours, as depicted in Figure 2-2(f). The graph illustrates that the mechanical stability of primary amine groups was significantly low. Most primary amine groups were depleted within 30 minutes of ultrasonication, suggesting that it may be excessively harsh for evaluating amine groups stability.

2.3.2 Surface characterisation by XPS, AFM, FTIR, and WCA

XPS measurements were performed to verify the functionalisation and grafting processes in the coating preparation by examining the chemical groups present on the titanium surface. The data were analysed using CasaXPS software with a Shirley background correction. These analyses aimed to quantify the primary amine groups on the plasma-treated titanium surface, which serve as anchoring points for subsequent immobilisation steps. The XPS survey spectra, Figure 2-3(a), of modified surfaces displayed characteristic peaks for carbon (C), oxygen (O), nitrogen (N), silicon (Si), and titanium (Ti). Also, small traces of aluminum, vanadium, sulfur, and phosphorus were detected, likely originating

from the Ti6Al4V alloy and contaminants introduced during sample preparation. Higher-resolution scans were performed to further investigate the chemical bonding on the surfaces, as shown in Figure 2-3(c) and (d).

In the XPS scan of the UTi, the titanium (Ti 2p) peak is observed at approximately 458.7 eV. The oxygen (O 1s) peak predominantly arises from the titanium oxide layer on the surface. The C 1s sharp peak is attributed to the residues from the polishing step, and the contamination from the equipment chamber, which is unavoidable in XPS measurements. This peak indicates the presence of C-C or C-H bonds, which constitutes around 10.5% of the atomic ratio on the surface.

Following the plasma treatment of the titanium sample, the elemental composition analysis of NH_2-Ti samples showed an increase in N% to 11.32% and a decrease in C% and O% to 6.75 and 49.99%, respectively. The high-resolution C 1s spectrum of the plasma-treated surface exhibited a primary peak at 285 eV attributed to C−C and C−N/C-O bonds, originating from the marginal presence of carbon contamination. Additionally, the high-resolution N 1s spectrum displayed two main peaks attributed to primary amine (NH_2) and secondary amine (NH) groups after plasma treatment. By measuring the percentage of N 1s in NH_2-Ti (11.32%) and the ratio of NH_2 to overall N on the surface (81.09%) after deconvolution of N 1s scan, the calculated percentage of primary amine groups on the surface, which act as anchoring points for further step, is 9.18%.

Upon the covalent immobilisation of the KR-12 peptide onto the NH_2-Ti surface, the NH_2 groups formed covalent binding with the carboxyl group of the KR-12. This led to a significant enhancement in the C 1s signal to 39.08%, accompanied by a reduction in the O, Ti and N signals to 33.63, 20.05, and 7.24%, respectively (Figure 2-3(b)). The C 1s signal of KR12-NTi exhibited three peaks at a binding energy of 284.9, 286.3, and 288.4 eV associated with C-C, C–O/C–N, and C=O bonds. The XPS N 1s scan of KR12-NTi revealed two peaks, one at 399.7 eV corresponding to amine bonds (-NH_2) of side chains and the one at 401.5 eV arising from amide bonds (-NHCO). This confirms the successful covalent immobilisation of KR-12 on the surface [27]. As expected, the nitrogen signal corresponding to the amide bonds, which are more prevalent than those from amines, exhibits greater intensity.

In PEG-NTi samples, reductions in the percentages of Ti, O, and N were observed, amounting to 19.11%, 30.13%, and 4.45%, respectively. This reduction is attributed to the

high carbon concentration (46.31%) in the PEG molecular chains. Upon attachment of KR-12 peptides to the PEG-NTi, the Ti content further decreased to 18.25%, while the amounts of O, N, and C showed slight increases to 30.32%, 5.04%, and 46.39%, respectively. The C 1s and N 1s scans of KR12-PNTi and KR12-NTi have similar peaks at identical binding energies, with variations in percentages, indicating no significant differences.

Quantitatively, the N/Ti atomic ratio increased from 0.04 to 0.39 following plasma treatment of the polished titanium surface. Immobilisation of the KR-12 on the NH_2-Ti subsequently reduced the N/Ti atomic ratio to 0.36, while the attachment of PEG further decreased the N/Ti ratio to 0.23 and 0.27 for PEG-NTi and KR12-PNTi, respectively. The shifts in atomic ratios of all elements after each step of surface modification are depicted in Figure 2-3(b).

The FTIR and XPS results demonstrate the successful chemical grafting of KR-12 and PEG onto the plasma-treated surfaces. However, due to unavoidable surface contamination before and after immobilisation, precise quantification of the immobilised peptide amount using XPS and FTIR proved challenging. Consequently, an alternative approach employing the Fmoc/t-Bu strategy was utilised to quantify the immobilised peptide concentration, as detailed in Experimental Methods (Section 2.4).

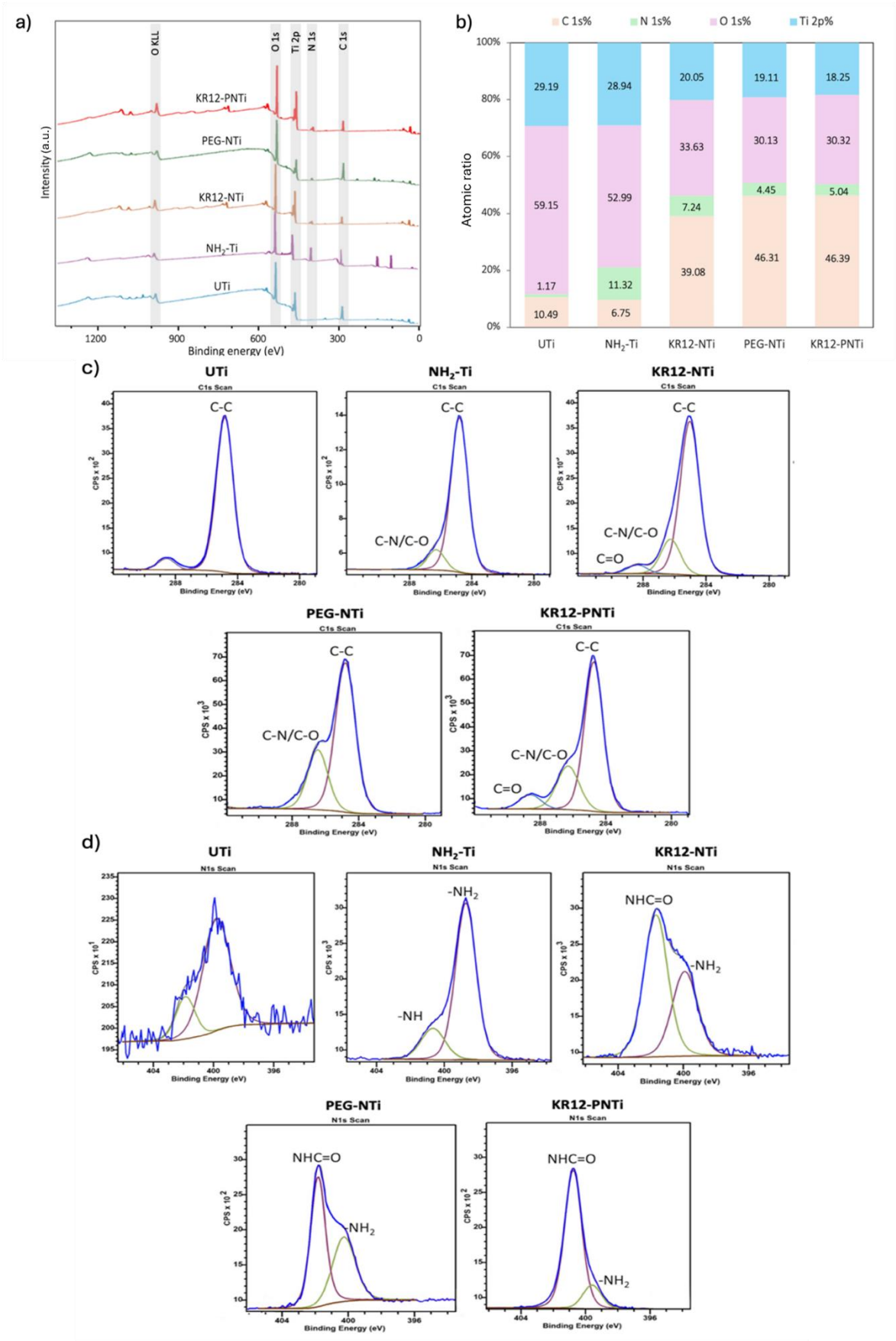


Figure 2-3. XPS results of surface elemental composition after the modification steps

during the plasma treatment, PEG attachment and KR-12 immobilisation: (a) XPS survey spectra, (b) Relative atomic ratios of chemical compositions, (c) high-resolution C1 s spectra, and (d) high-resolution N 1s spectra of different surface modifications. See Table 2.1 for abbreviations.

Surface morphology and roughness, play crucial roles in influencing cell behaviour, including adhesion, proliferation, and differentiation [106, 107]. AFM was employed to accurately analyse these surface characteristics owing to its capability to deliver high-resolution topographical data. The morphologies of surfaces were examined using AFM following each step of the coating preparation, as illustrated in Figure 2-4(a). Initially, untreated polished titanium (UTi) presented a smooth surface, although they showed barely detectable scratches remaining from the polishing step (Figure 2-4(a)). After the plasma treatment, NH_2-Ti specimens displayed a smoother surface morphology, characterised by an average roughness of 0.91 ± 0.3 nm. The direct covalent immobilisation of the KR-12 peptide (KR12-NTi samples) had no impact on surface morphology compared to NH_2-Ti, exhibiting a mean roughness (R_a) of 0.99 ± 0.3 nm. Conversely, the attachment of PEG to the surface (PEG-NTi) revealed the deposition of a polymeric layer, resulting in statistically significant increased roughness with an R_a of 5.68 ± 0.7 nm (Figure 2-4(a)). Following the introduction of KR-12 peptides after the PEG attachment, KR12-PNTi samples displayed no apparent changes compared to PEG-NTi, with a roughness of 5.81 ± 0.5 nm. This marginal alteration in morphology and roughness observed in comparison to the earlier step can be attributed to the smaller molecular chain of KR-12, as opposed to the larger molecular size of PEG. These findings allow for an evaluation of how these modifications impact surface properties and, consequently, the near-surface environment for cells. This evaluation determined that PEG attachment enhances the surface roughness, making it more conducive to promoting cell adhesion and proliferation [108].

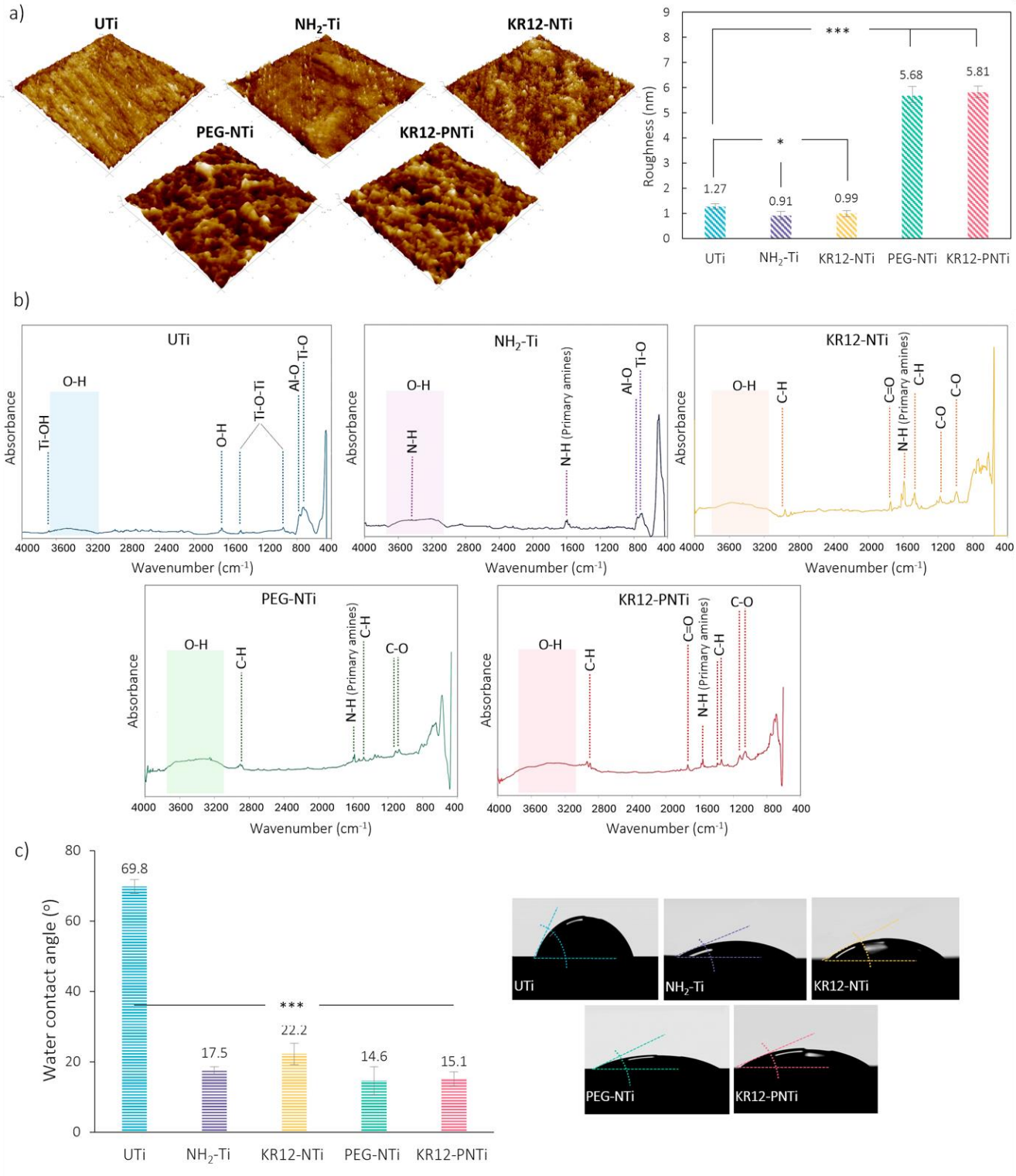


Figure 2-4. Characterisation of titanium surfaces after plasma treatment, PEG attachment and KR-12 immobilisation: (a) Surface morphology and mean roughness (Ra) analysed via AFM 3D imaging. (b) ATR-FTIR spectra of different coatings (c) Quantitative water contact angle measurements along with representative images of water droplets. Results

are presented as the mean ± standard deviation (SD) of three independent experiments performed in triplicate. Statistical significance is indicated by * for $p < 0.05$, ** for $p < 0.01$, and *** for $p < 0.001$ between UTi and all modified surfaces.

To understand the molecular composition and structural alterations during the coating preparation process, ATR-FTIR spectroscopy was utilised. The acquired IR spectrum displayed vibrational bands indicative of various chemical bonds throughout the coating development, as shown in Figure 2-4(b). The IR spectrum of UTi, identifies a prominent peak at 488 cm^{-1}, attributed to the Ti-O stretching vibration band, together with bands at 735 cm^{-1} and 786 cm^{-1} associated with the presence of Ti-O and Al-O bonds [109, 110]. The peaks at 998 cm^{-1} and 1419 cm^{-1} are associated with Ti-O-Ti stretching vibration bands [27, 111]. A broad band between 3150 and 3680 cm^{-1} corresponds to the stretching vibrations of -OH groups of adsorbed water molecules on the polished surface. Additionally, a weaker band at 1694 cm^{-1} is arising from the bending vibration of corresponding free -OH groups [111, 112].

After the plasma treatment, IR spectra exhibited broad bands corresponding to O-H bonds, albeit with elevated intensity. Notably, the plasma-treated surface, NH_2-Ti sample, demonstrates a band at 1622 cm^{-1} indicative of bending vibration of primary amines [113, 114]. Although N–H stretching vibrations of amines also appear in the 3300-3000 cm^{-1} region, they are overshadowed by the stronger O–H stretching vibrations in this area. Additionally, a band attributed to amines in the 910-665 cm^{-1} region, corresponding to N–H wag, aligns closely with titanium characteristic peaks, thus complicating their differentiation [50, 115].

Following PEG attachment, a distinct, robust band emerges at 839 cm^{-1} owing to C-C stretching vibrations. The recorded FTIR spectrum exhibits a broad signal centred at 3496 cm^{-1}, attributable to O-H stretching of terminal hydroxyl groups as well as adsorbed water molecules [116-118]. Alkane C-H stretching and bending vibration peaks are observed at 2871 cm^{-1} and 1488 cm^{-1}, respectively. PEG also displays characteristic stretching frequencies for C–O at 1081 and 1109 cm^{-1}, and a peak at 1387 cm^{-1} associated with O-H bending mode [117, 118]. The presence of these characteristic absorption peaks validates the successful grafting of PEG onto the titanium substrate.

After PEG and KR-12 immobilisation, the broadness of peaks makes it challenging to discern individual peaks. Nonetheless, peaks at 1392 and 1421 cm^{-1} coincide with CH_2

and CH_3 bending vibrations in the backbone of the immobilised KR-12 [119, 120].

The primary amine group manifests a doublet at 1611 cm^{-1} and 1648 cm^{-1} for KR12-NTi and 1605 and 1634 cm^{-1} in KR12-PNTi, indicative of N-H bending vibrations of primary amines [120]. Specific peaks at 1751 cm^{-1} and 1748 cm^{-1} related to C=O emerge solely for KR12-immobilised samples, indicating the successful immobilisation process.

The hydrophilicity of each substrate was assessed through WCA analysis. The titanium substrate exhibited a contact angle of 69.8° ± 2.7°. Subsequent plasma treatment resulted in a significantly decreased contact angle for the NH_2-Ti, measuring 17.5 ± 1.4°. This indicates increased hydrophilicity compared to the Ti substrate (Figure 2-4(c)). The covalent immobilisation of the KR-12 peptide on the titanium surface to prepare the KR12-NTi sample, slightly decreased hydrophilicity (22.2 ± 2.1°). This decrease can be attributed to the hydrophobic amino acids present in the KR-12 peptide (KRIVQRIKDFLR), such as leucine, isoleucine, and valine [121, 122]. Subsequently, the integration of PEG linkers demonstrated the lowest hydrophilicity compared to other coatings on titanium surfaces. Upon immobilising KR-12 on PEG linkers, the hydrophilicity of PEG-NTi (WCA = 14.6° ± 2.7°) increased to WCA = 15.1° ± 1.8° for KR12-PNTi.

2.3.3 Concentration of the immobilised KR-12 and release rate

The Fmoc/t-Bu method is commonly used for measuring peptide concentrations due to the beneficial UV absorption properties of the Fmoc group. Figure S1 (appendix) of the SI document shows how the Fmoc group is removed through a β-elimination reaction when treated with piperidine, as a secondary amine. This reaction produces the highly reactive dibenzyl-fluorescein (DBF) which then reacts with excess piperidine, resulting in a DBF adduct that exhibits a characteristic UV absorbance peak at 301 nm.

A calibration curve correlating the concentration of the DBF-based adduct with absorbance was prepared by measuring UV absorption over a concentration range of 10 to 310 μM. This curve demonstrated a linear relationship (molar absorption coefficient = 8.14 $L.mol^{-1}.cm^{-1}$, at λ = 301 nm) as presented in Figure S1 (appendix) of the SI document. The absorbance of each solution (n = 3) was measured at λ = 301 nm and matched against the calibration curve. The findings indicated that the quantities of Fmoc groups on surfaces, without or with the PEG linker, were 59.67 nmol and 68.03 nmol, respectively, with reaction yields of 12.2% and 10.7%.

To analyse the stability of the coating and measure the release rate, the same Fmoc-labelled KR-12 peptide was used. The UV absorption of the released peptide was measured after the immersion of KR12-NTi and KR12-PNTi in PBS for various time intervals.

As shown in Figure 2-5, the accumulated release profile can be described in two distinct stages. Initially, a significant amount of KR-12 was released from the substrates within 30 minutes of immersion in PBS at 37 °C with gentle shaking. The amounts released within this period indicate the physically adsorbed KR-12, which were 5.91 ± 0.9 µM and 13.08 ± 1.8 µM for the KR12-NTi and KR12-PNTi substrates, respectively. These results indicate that approximately 19.67% of the peptide on KR12-PNTi was physically attached, while 8.90% of the peptide on KR12-NTi was physically attached. PEG is recognised for its amphiphilic properties, enabling it to physically adsorb a higher number of peptides through hydrogen bonding and van der Waals interactions. The remaining peptides were covalently immobilised, providing longer-term stability. Taking into account the burst release of peptides as physically adsorbed, it can be concluded that 54.35 nmol and 54.64 nmol of peptides were covalently attached to the surfaces of KR12-NTi and KR12-PNTi, respectively.

Following the initial release observed within the first 30 minutes of immersion, both KR12-NTi and KR12-PNTi coatings exhibited a gradual sustained release profile after the first hour, continuing throughout the 7-day measurement period. KR12-NTi released to a concentration of 6.81 ± 0.6 µM, while KR12-PNTi released to 15.76 ± 0.8 µM. Despite the nearly identical concentrations of covalently bonded KR-12 on both coatings, KR12-PNTi showed a higher rate of peptide release. The gradual release could be attributed to the disentanglement and dissolution of PEG molecular chains as well as the slower detachment of peptides caused by the hydrolysis of amide bonds Although amide bonds are generally stable, they can undergo slow hydrolysis in aqueous environments, leading to gradual peptide release [123-125].

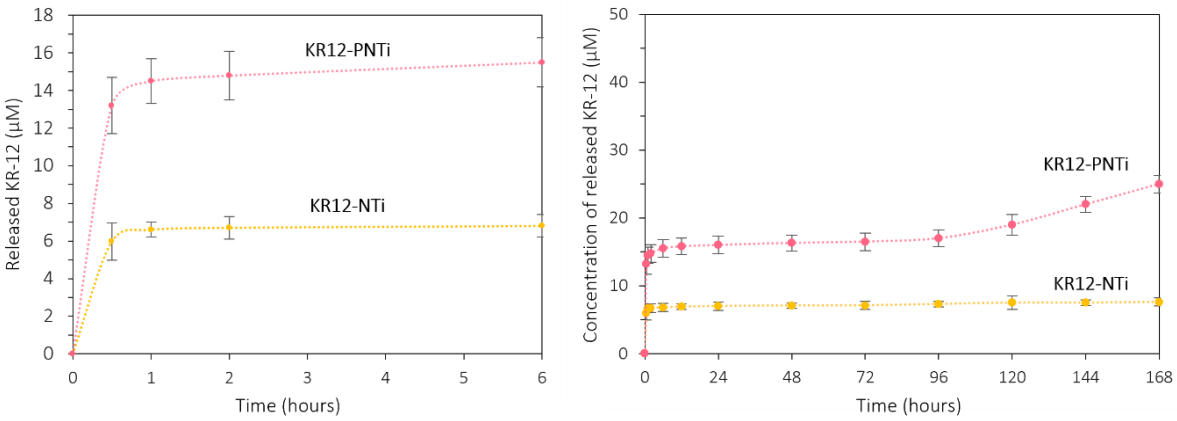


Figure 2-5. KR-12 release rates from KR12-NTi and KR12-PNTi in PBS at 37 °C for 168 hours. Results are presented as the mean ± standard deviation (SD) of independent experiments performed in triplicate.

2.3.4 Antimicrobial activity assay

S. aureus and *S. epidermidis*, Gram-positive bacteria, along with *E. coli* and *P. aeruginosa*, Gram-negative bacteria, were selected to evaluate the antimicrobial efficacy of AMP-immobilised titanium surfaces intended for orthopaedic applications.

In this study, the antibacterial activities of the substrates were assessed using a DCT as graphed in Figure 2-6(a). UTi exhibited no antibacterial activity, demonstrating 0% bacterial inhibition ratio, while NH_2-Ti displayed mild antibacterial effects, with inhibition ratio ranging from 3.49% to 4.15% for Gram-positive bacterial strains and 24.51% to 26.65% for Gram-negative bacterial strains.

This slight inhibition may be attributed to the highly positive surface charge introduced by amino-functionalised surfaces in an aqueous environment. Bacterial cell membranes are typically negatively charged, leading to electrostatic attraction between the bacteria and the surface. This interaction can disrupt the bacterial cell membrane, resulting in cell lysis [126, 127]. Gram-negative bacteria have a thinner peptidoglycan layer and possess both an inner and outer membrane [128]. This structural difference makes them more susceptible to surface interactions and membrane disruption, resulting in greater inhibition compared to Gram-positive bacteria [128]. This hypothesis is supported by SEM micrographs of *E. coli* morphologies (Figures 2-6(c)), which show shrunken and damaged membranes in some bacteria.

Upon modifying NH_2-Ti with KR-12, the KR12-NTi surfaces exhibited significant antibacterial activity ($p < 0.001$), with growth inhibition of 88.43%, 87.18%, 85.30%, and 85.45% against *E. coli*, *P. aeruginosa*, *S. aureus*, and *S. epidermidis*, respectively. The incorporation of KR-12 markedly enhanced the antibacterial properties of titanium surfaces against both Gram-positive and Gram-negative bacteria. This improvement aligns with previously reported findings on KR-12's effectiveness in killing Gram-negative and Gram-positive bacteria in solution [76, 129, 130].

PEG-NTi surfaces exhibited growth inhibition rates of 55.18%, 47.61%, 44.02%, and 49.11% against *E. coli*, *P. aeruginosa*, *S. aureus*, and *S. epidermidis*, respectively. This demonstrates greater bacterial growth inhibition compared to NH_2-Ti, which can be attributed to the antifouling properties of PEG. PEG is recognised for its capability to establish a hydrophilic and steric barrier that mitigates interactions between the surface and biomolecule. The hydrophilic properties of PEG facilitate the formation of a hydrated layer on the surface, thereby reducing nonspecific bacterial adsorption [261].

KR12-PNTi demonstrated the highest antibacterial efficacy, achieving growth inhibition of 92.30%, 94.79%, 91.29%, and 90.23% against *E. coli*, *P. aeruginosa*, *S. aureus*, and *S. epidermidis*, respectively (Figure 2-6(a)). The antibacterial mechanism of AMPs involves their interaction with bacterial cell membranes, facilitated by the peptides' positive charge, which disrupts and ultimately leads to bacterial death. AMPs attached with PEG linkers are hypothesised to exhibit enhanced interaction with bacterial membranes due to improved mobility, a phenomenon supported by previous research [31, 131]. Compared to KR12-NTi, KR12-PNTi, which incorporates flexible PEG linkers, demonstrated an average increase of 7% in antimicrobial activity across all bacterial strains. This enhancement can be attributed to the burst release of electrostatically bonded AMPs, attached to the PEG linkers which are more than twice as high compared to AMPs attached without PEG linkers. This phenomenon has been described in the previous section.

For the evaluation of bactericidal efficacy and adherence properties of various substrates, live/dead staining analysis was employed after 24 hours, as illustrated in Figures 2-6(b) and 2-6(c). In the live/dead assay, dead bacteria were visualised emitting red fluorescence, whereas live bacteria emitted green fluorescence. *S. aureus* and *E. coli* were selected as representative Gram-positive and Gram-negative bacteria, respectively, to demonstrate bacterial behaviour on different substrates. Consistent with the DCT results, live/dead

staining revealed that UTi exhibited no antimicrobial activity against both strains, since all bacteria remained viable and stained green. On the NH_2-Ti sample, both strains of bacteria appeared alive and emitted green fluorescence (Figure 2-6(b) and 2-6(c)). However, a few attached *E. coli* bacteria appeared red, possibly due to electrostatic interactions with the amine-functionalised surface and subsequent membrane disruption, resulting in mild growth inhibition. On PEG-NTi surfaces, a significantly lower number of attached bacteria were observed compared to NH_2-Ti, indicating the antifouling properties of PEG without bactericidal activity, since all adhered bacteria appeared alive in the live/dead staining (Figure 2-6(b) and 2-6(c)). In contrast, KR12-NTi and KR12-PNTi exhibited dead bacteria attached to the surface, evidence of the bactericidal property of KR-12. The number of dead attached bacteria was lower on KR12-PNTi, due to the antifouling effect of PEG.

Furthermore, SEM analyses were conducted to characterise the morphology of *S. aureus* and *E. coli* after 24 hours of culture on the surfaces, as depicted in Figure 2-6(b) and 2-6(c). On UTi and NH_2-Ti surfaces, bacteria displayed typical shapes with intact cell walls, indicating a lack of antimicrobial activity. Despite the absence of biofilm formation on UTi, numerous bacteria adhered and formed aggregates. NH_2-Ti, however, exhibited slight inhibition of bacterial colonisation compared to UTi, consistent with findings from DCT and live/dead staining results. Considering the antibacterial mechanism of amino-functionalised surfaces, it is anticipated that electrostatic interactions of NH_2-Ti with bacterial membranes played a critical role in bacterial eradication by inducing membrane damage, as observed in some *E. coli* bacteria of NH_2-Ti shown in Figure 2-6(c). The cell morphology observed on PEG-NTi resembled that of NH_2-Ti, with decreased bacterial attachment proposing PEG's role in preventing bacterial adhesion.

SEM analysis revealed distinct changes in *S. aureus* cultured on KR12-NTi and KR12-PNTi, characterised by shrunken and disrupted membranes indicative of damage. Similarly, *E. coli* on KR12-NTi and KR12-PNTi exhibited corrugated, distorted, and lysed morphology, suggesting membrane damage potentially induced by the AMPs.

The observed results in SEM analyses can be explained by the mechanism of action of AMPs, against bacterial membranes. AMPs primarily target and disrupt bacterial membranes by interacting with their lipid components. These peptides often have amphipathic structures, allowing them to bind to bacterial membranes and insert

themselves into the lipid bilayer. This interaction disrupts the membrane integrity, leading to leakage of cellular contents, structural collapse, and eventually cell death.

S. aureus cells on KR12-NTi and KR12-PNTi showed shrunken and disrupted membranes. This is likely due to KR-12 targeting the bacterial cytoplasmic membrane, forming pores or destabilizing the bilayer. This leads to osmotic imbalance and the loss of intracellular components, causing the cells to shrink and appear disrupted under SEM.

E. coli cells exhibited corrugated, distorted, and lysed morphologies. These effects reflect the destabilization of the outer membrane (specific to Gram-negative bacteria like *E. coli*) in addition to the cytoplasmic membrane. The corrugation and lysis suggest that KR-12 likely disrupts the lipid A and phospholipid regions of the outer membrane, allowing the AMP to penetrate and damage the inner cytoplasmic membrane. The loss of membrane integrity leads to cell lysis and the observed morphological distortions.

AMPs immobilised on KR12-PNTi demonstrated higher bactericidal activity. This enhancement can be attributed to This enhancement can be attributed to the burst release of electrostatically bonded AMPs, attached to the PEG linkers.

While SEM results provide valuable information, they are insufficient to fully elucidate the precise mechanism by which KR-12 interacts with cellular membranes. However, they do suggest that immobilised KR-12 can cause significant damage to bacterial membranes. Further studies using Transmission Electron Microscopy (TEM) will be essential for obtaining a more detailed understanding of this process.

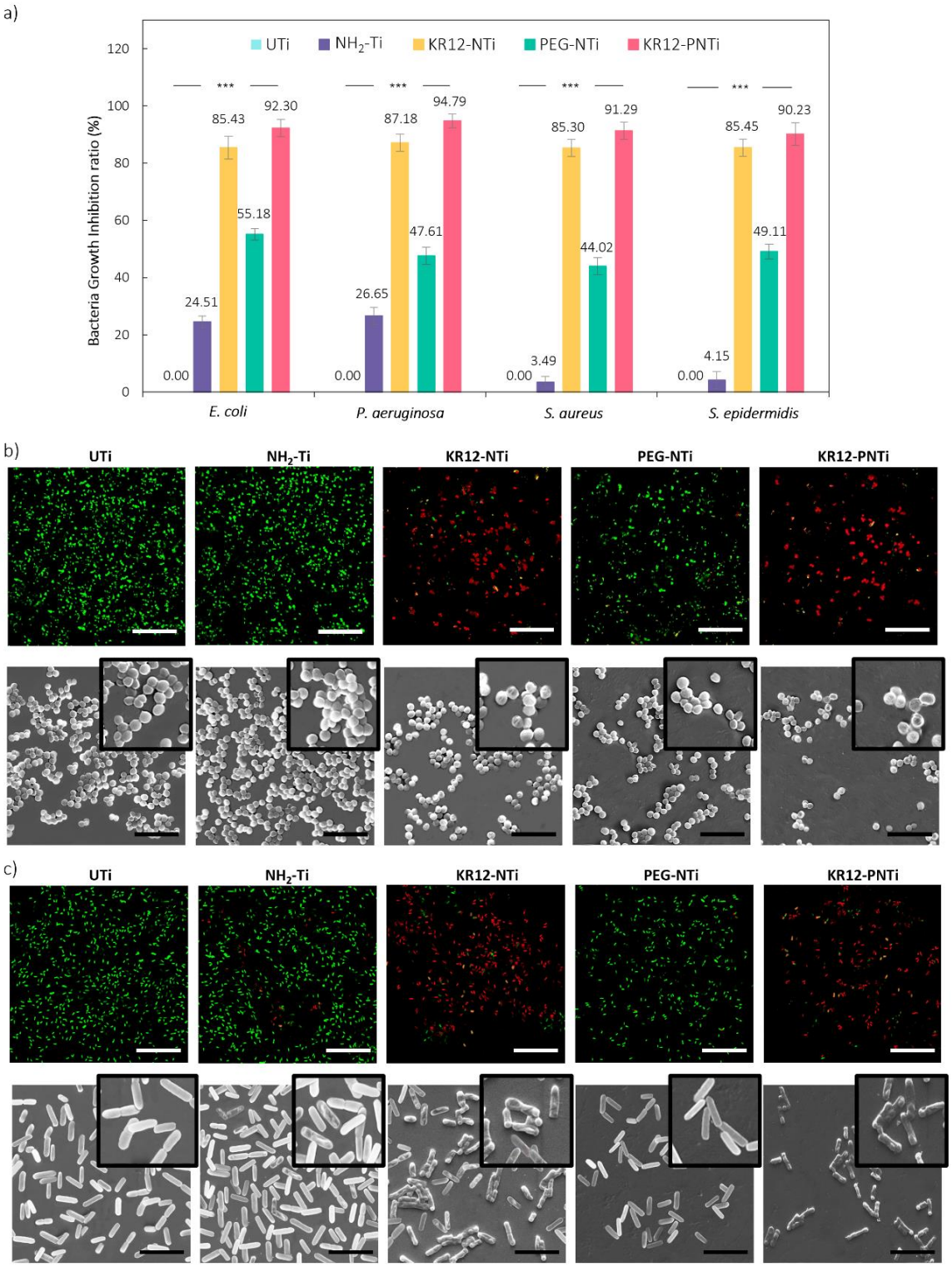


Figure 2-6. Assessment of antimicrobial activity; (a) Bacterial growth inhibition of the various surface coatings against *E. coli*, *P. aeruginosa*, *S. aureus*, and *S. epidermidis* with UTi samples serving as controls showing 0.00% inhibition. Statistical significance is denoted by * for $p < 0.05$, ** for $p < 0.01$, and *** for $p < 0.001$. Error bars represent the

standard deviation from three independent experiments, each performed in triplicate. (b) The fluorescence live/dead assay and SEM images of (b) *S. aureus* and (c) *E. coli* cultured on different coatings (Live/Dead assay scale bars = 10 µm, green bacteria: live, red bacteria: dead); (SEM images scale bars = 5 µm). All assessments were taken after 24 hours of surface incubation. Both KR12-NTi and KR12-PNTi surfaces exhibited higher bacterial affinity than NH_2-Ti and PEG-NTi. The inclusion of PEG as a linker appeared to reduce bacterial adhesion. AMPs attached to KR12-NTi and KR12-PNTi demonstrated effective bactericidal activity, disrupting the membranes of both *E. coli* and *S. aureus* bacteria.

2.3.5 Cytocompatibility and cell adhesion

The cytocompatibility of various coatings on titanium surfaces was evaluated using hFOB 1.19 cells, a human osteoblast cell line commonly used in studies of osteoporosis, bone tissue engineering, and orthopaedic biomaterials [132]. The MTT assay was used to evaluate cell viability, which indirectly measures cell proliferation through metabolic activity. This assay also provides insight into cytocompatibility by determining whether cells remain metabolically active when in contact with the materials. Previous investigations into the cytotoxicity of the KR-12 peptide in solution have shown no cytotoxic effects within a specific concentration range [19, 76, 129]. However, cell viability tends to decrease at higher concentrations of the AMP. Thus, it is critical to find an optimal balance in the loading of antibacterial agents to ensure efficacy without inducing cytotoxicity. High-loading densities of antibacterial agents can effectively kill bacteria but may also pose a risk of cytotoxicity.

In this study, cell viability percentages of different substrates relative to the control were evaluated at three intervals (3, 5, and 7 days), presented in Figure 2-7(a). Results from the MTT assay demonstrated higher proliferation rates of hFOB cells on titanium samples with different coatings compared to the control (standard TCP- Tissue Culture Plastic) at each time point which is consistent with previous findings on the cytocompatibility of PEG and the non-toxicity of the KR-12 peptide at the concentration used in this study. [19, 37].

NH_2-Ti and PEG-NTi surfaces, while exhibiting slight antimicrobial activity, showed comparable biocompatibility to UTi across all tested intervals. The biocompatibility of the plasma-treated titanium surfaces with the cell viability of 110.14%, 124.41%, and 129.44% for days 3, 5, and 7, is attributed to the introduction of amine groups. Amine-

functionalised surfaces can more effectively adsorb proteins from the biological environment, forming a protein layer that mediates cell attachment, promotes integrin binding, and activates subsequent cell signalling pathways that support cell proliferation and differentiation [133, 134]. Additionally, amine groups confer a positive charge to the surface in an aqueous environment, which can favourably interact with the negatively charged cell membranes, enhancing cell adhesion [135, 136]. KR12-NTi and KR12-PNTi samples also supported cell growth, indicating strong cell attachment despite minimal bacterial adherence. After 3 to 7 days of incubation, cell viability on all coated surfaces was significantly higher than the control, tissue culture plastic (TCP), indicating good cytocompatibility even with the grafted KR-12 and no statistically significant differences in metabolic activity were detected between the various coatings and UTi at any time point.

Cell adhesion and interaction between cells and coatings are fundamental to the successful integration of implants into native bone tissue [95, 96]. To assess the cells adhesion and their distribution on each surface, SEM analysis was conducted following a 5-day incubation period.

The SEM images in Figure 2-7(b), captured on day 5, illustrate normal attachment and growth of hFOB cells on UTi surface. Compared to UTi, cell spreading on NH_2-Ti was slightly higher on day 5, consistent with MTT results, and these cells exhibited a well-spread attachment morphology. These attached cells displayed extensive spreading after plasma treatment, highlighting the excellent biocompatibility of the amino-functionalised surfaces. Despite initial observations of suboptimal cell attachment on UTi, hFOB cells demonstrated consistent growth on KR12-NTi and KR12-PNTi surfaces with a flattened morphology and increased cell spreading, indicating viability and proliferation. The number of attached cells appeared similar across all surfaces. By day 5, the cells exhibited spread morphology with filopodia extending towards adjacent cells. This behaviour reflects active cytoskeletal remodeling, a hallmark of healthy cell attachment and intercellular communication. The similar number of attached cells across surfaces suggests that while surface modifications affect cell morphology and interaction, the overall cell viability remains high on all tested surfaces. These observations highlight the critical role of surface functionalization in modulating cell behaviour, particularly in promoting enhanced spreading and attachment, which are indicative of superior biocompatibility and suitability for biomedical applications.

Our ultimate objective was to develop a multifunctional coating that combines bone regenerative activity with antimicrobial properties. To fully realise this goal in the future, extensive in vivo investigations will be necessary to assess long-term biocompatibility, explore the molecular mechanisms underlying bone regeneration, and thoroughly examine the host immune response to the coated implants.

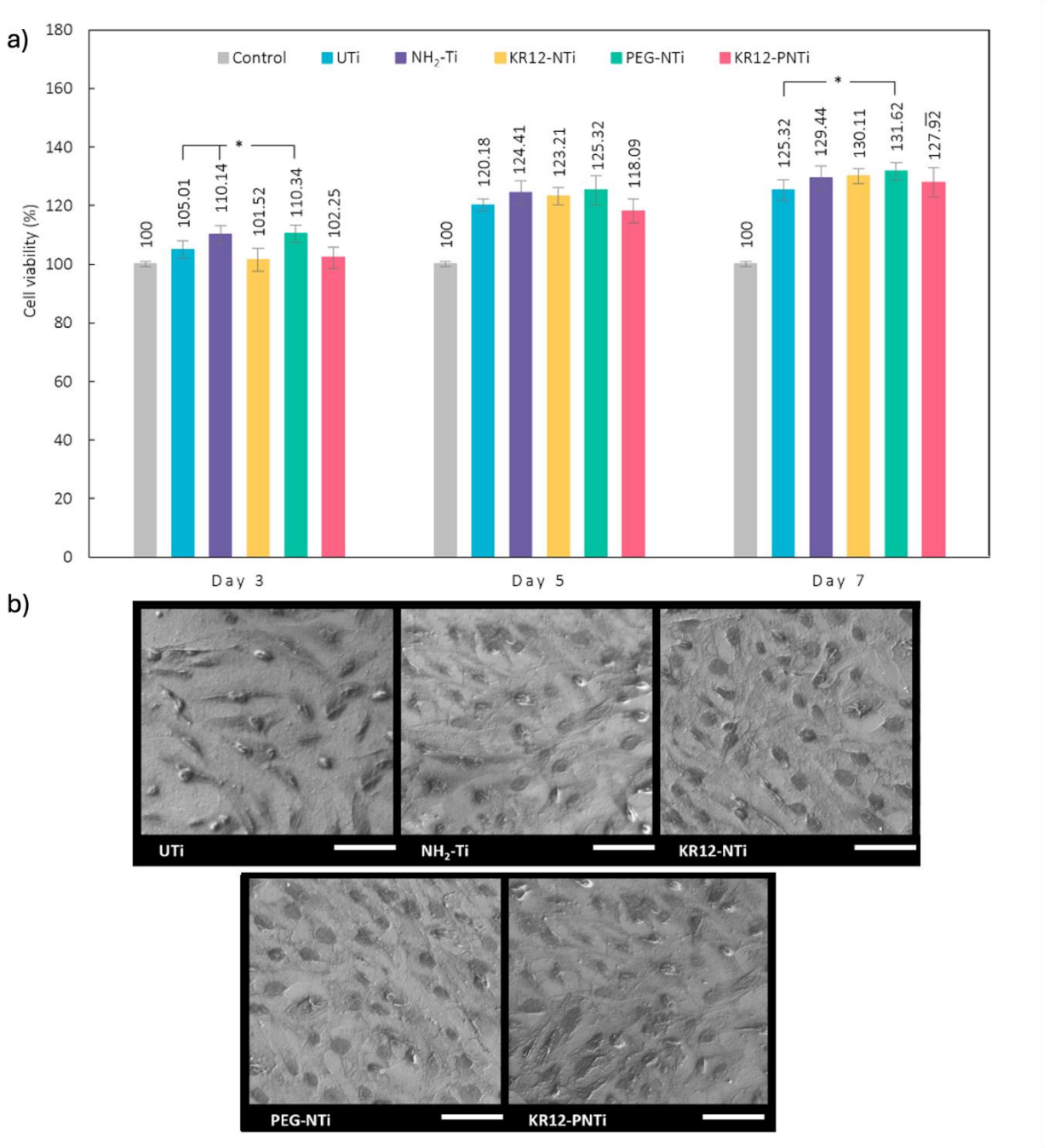


Figure 2-7. Cytocompatibility and cell morphology analyses: (a) Cell viability results from the MTT assay of hFOB cells cultured on various substrates over 3, 5, and 7 days, no significant difference was observed compared to UTi; Statistical significance is denoted

by * for $p < 0.05$. (b) SEM micrographs depicting the morphology of hFOB cells on day 5 (Scale bars = 20 μm); By day 5, cells displayed a spread morphology with filopodia extending towards neighbouring cells.

2.4. Conclusions

The prevention of bacterial adhesion and biofilm formation while promoting osteointegration remains a persistent challenge for medical implants. This study demonstrated the potential of plasma treatment to create functional groups as anchor points for peptide immobilisation, while mitigating the side effects of chemical reactions and minimising time requirements. Plasma treatment also increases surface energy and wettability without altering surface topography, thereby facilitating protein adsorption and promoting favourable cells behaviour.

The objective was to optimise plasma treatment parameters to achieve comparable levels of surface-bound amine functional groups to those achieved with chemical techniques such as silanisation. XPS analyses revealed that the distribution and density of primary amine groups could be adjusted with plasma parameters, reaching a maximum of 9.18% without altering the titanium surface morphology or bulk properties.

Following the creation of primary amine groups, PEG linkers and AMPs were immobilised on the surface to combine antifouling and bactericidal properties while promoting tissue integration, effectively inhibiting bacterial biofilm formation. Antimicrobial activity against four pathogenic bacterial strains showed more than 90% bacteria growth inhibition ratio. AMPs grafted with PEG linkers exhibited higher activity against bacteria adhesion and colonisation compared to those without linkers This can be justified by the peptide release analysis, which indicates that the burst release of electrostatically bonded peptides is approximately twice as high for samples with PEG linkers compared to AMPs attached without PEG linkers. Additionally, cell promotion and adhesion demonstrated by MTT assay and SEM micrographs underscored the potential of integrating plasma treatment with the covalent bonding of AMPs to capitalise on both the antimicrobial activity of KR-12 and the cell promotion properties of the plasma-treated titanium.

The integration of plasma treatment technology in the peptide attachment of medical implants presents a promising strategy to substitute chemical reactions. This innovative approach not only enhances the biocompatibility and functionality of implants but also

holds potential for broader applications. The versatility of plasma treatment allows for the adaptation of this technology to various types of peptides and substrates, paving the way for advancements across a range of medical applications.

Ethics Approval and Consent to Participate

Ethics approval was not required for this project.

Declarations of Interests

The authors state that they have no known competing financial interests or personal relationships that could have influenced the work reported in this paper.

Credit Authorship Contribution Statement

Mohadesh Zare: Methodology, Investigation, Formal analysis, Data curation, Writing – original draft. **Bogdan Butoi:** Conceptualisation, Investigation, Data curation. **Corneliu Porosnicu:** Conceptualisation, Investigation, Writing – reviewing & editing. **Ion N. Mihailescu:** Validation, Investigation. **David Grossin:** Investigation, Data curation, Writing – reviewing & editing. **Sarah A. Kuehne:** Supervision, Writing – reviewing & editing. **Zubair Ahmed:** Supervision, Writing – reviewing & editing; **Artemis Stamboulis:** Supervision, Writing – reviewing & editing, Project administration, Conceptualisation, Funding acquisition.

Acknowledgements

This work is part of a project that has received funding from the European Union's Horizon 2020 research and innovation program under the Marie Skłodowska-Curie Innovative Training Network AIMed grant agreement No 861138.

2.5. References

1. Bandyopadhyay, A., et al., *Improving biocompatibility for next generation of metallic implants.* Progress in Materials Science, 2023. **133**: p. 101053.
2. Campoccia, D., L. Montanaro, and C.R. Arciola, *A review of the clinical implications of anti-infective biomaterials and infection-resistant surfaces.* Biomaterials, 2013. **34**(33): p. 8018-8029.
3. von Eiff, C., et al., *Infections Associated with Medical Devices.* Drugs, 2005. **65**(2): p. 179-214.

4. Maan, A.M.C., et al., *Recent Developments and Practical Feasibility of Polymer-Based Antifouling Coatings.* Advanced Functional Materials, 2020. **30**(32): p. 2000936.
5. Wang, L.-S., et al., *Protein-Based Films as Antifouling and Drug-Eluting Antimicrobial Coatings for Medical Implants.* ACS Applied Materials & Interfaces, 2021. **13**(40): p. 48301-48307.
6. Wang, H., et al., *Preclinical performance testing of medical devices with antimicrobial effects.* Nature Reviews Bioengineering, 2023. **1**(8): p. 589-605.
7. Quinn, J., et al., *Titanium for orthopedic applications: an overview of surface modification to improve biocompatibility and prevent bacterial biofilm formation.* IScience, 2020. **23**(11).
8. Kalelkar, P.P., M. Riddick, and A.J. García, *Biomaterial-based antimicrobial therapies for the treatment of bacterial infections.* Nature Reviews Materials, 2022. **7**(1): p. 39-54.
9. Rai, A., et al., *Antimicrobial peptide-based materials: opportunities and challenges.* Journal of Materials Chemistry B, 2022. **10**(14): p. 2384-2429.
10. Wang, G., *The antimicrobial peptide database provides a platform for decoding the design principles of naturally occurring antimicrobial peptides.* Protein Science, 2020. **29**(1): p. 8-18.
11. Fjell, C.D., et al., *Designing antimicrobial peptides: form follows function.* Nature Reviews Drug Discovery, 2012. **11**(1): p. 37-51.
12. Magana, M., et al., *The value of antimicrobial peptides in the age of resistance.* The Lancet Infectious Diseases, 2020. **20**(9): p. e216-e230.
13. Mookherjee, N., et al., *Antimicrobial host defence peptides: functions and clinical potential.* Nat Rev Drug Discov, 2020. **19**(5): p. 311-332.
14. Lazzaro, B.P., M. Zasloff, and J. Rolff, *Antimicrobial peptides: Application informed by evolution.* Science, 2020. **368**(6490): p. eaau5480.
15. Engelberg, Y. and M. Landau, *The Human LL-37 (17-29) antimicrobial peptide reveals a functional supramolecular structure.* Nature communications, 2020. **11**(1): p. 3894.
16. Ajish, C., et al., *A novel hybrid peptide composed of LfcinB6 and KR-12-a4 with enhanced antimicrobial, anti-inflammatory and anti-biofilm activities.* Scientific Reports, 2022. **12**(1): p. 4365.

17. Lakshmaiah Narayana, J., et al., *Short and robust anti-infective lipopeptides engineered based on the minimal antimicrobial peptide KR12 of human LL-37.* ACS infectious diseases, 2021. **7**(6): p. 1795-1808.
18. Bechinger, B. and S.-U. Gorr, *Antimicrobial peptides: mechanisms of action and resistance.* Journal of dental research, 2017. **96**(3): p. 254-260.
19. Meng, X., et al., *KR-12 coating of polyetheretherketone (PEEK) surface via polydopamine improves osteointegration and antibacterial activity in vivo.* Journal of Materials Chemistry B, 2020. **8**(44): p. 10190-10204.
20. Ao, H., et al., *Covalent immobilization of KR-12 peptide onto a titanium surface for decreasing infection and promoting osteogenic differentiation.* Rsc Advances, 2016. **6**(52): p. 46733-46743.
21. Li, H., et al., *The antimicrobial peptide KR-12 promotes the osteogenic differentiation of human bone marrow stem cells by stimulating BMP/SMAD signaling.* RSC advances, 2018. **8**(28): p. 15547-15557.
22. Kazemzadeh-Narbat, M., et al., *Strategies for antimicrobial peptide coatings on medical devices: a review and regulatory science perspective.* Critical Reviews in Biotechnology, 2021. **41**(1): p. 94-120.
23. Holmberg, K.V., et al., *Bio-inspired stable antimicrobial peptide coatings for dental applications.* Acta Biomater, 2013. **9**(9): p. 8224-31.
24. Chen, J., et al., *Preparation of an antimicrobial surface by direct assembly of antimicrobial peptide with its surface binding activity.* Journal of materials chemistry. B, 2017. **5**(13): p. 2407-2415.
25. Fang, Z., et al., *High-throughput screening and rational design of biofunctionalized surfaces with optimized biocompatibility and antimicrobial activity.* Nature Communications, 2021. **12**(1): p. 3757.
26. Yazici, H., et al., *Self-assembling antimicrobial peptides on nanotubular titanium surfaces coated with calcium phosphate for local therapy.* Mater Sci Eng C Mater Biol Appl, 2019. **94**: p. 333-343.
27. Gevrek, T.N., et al., *Thiol-Reactive Polymers for Titanium Interfaces: Fabrication of Antimicrobial Coatings.* ACS Applied Polymer Materials, 2019. **1**(6): p. 1308-1316.
28. Costa, F., et al., *Covalent immobilization of antimicrobial peptides (AMPs) onto biomaterial surfaces.* Acta biomaterialia, 2011. **7**(4): p. 1431-1440.
29. Onaizi, S.A. and S.S.J. Leong, *Tethering antimicrobial peptides: Current status and potential challenges.* Biotechnology Advances, 2011. **29**(1): p. 67-74.

30. Wu, X., et al., *Flexible peptide linkers enhance the antimicrobial activity of surface-immobilized bacteriolytic enzymes.* ACS applied materials & interfaces, 2018. **10**(43): p. 36746-36756.
31. Shriver-Lake, L.C., G.P. Anderson, and C.R. Taitt, *Effect of linker length on cell capture by poly (ethylene glycol)-immobilized antimicrobial peptides.* Langmuir, 2017. **33**(11): p. 2878-2884.
32. Xi, D., et al., *Design, expression and characterization of the hybrid antimicrobial peptide LHP7, connected by a flexible linker, against Staphylococcus and Streptococcus.* Process biochemistry, 2013. **48**(3): p. 453-461.
33. Ortiz-Gómez, V., et al., *Antimicrobial Polymer–Peptide Conjugates Based on Maximin H5 and PEG to Prevent Biofouling of E. coli and P. aeruginosa.* ACS Applied Materials & Interfaces, 2020. **12**(41): p. 46991-47001.
34. Cui, Z., et al., *Molecular engineering of antimicrobial peptide (AMP)–polymer conjugates.* Biomaterials science, 2021. **9**(15): p. 5069-5091.
35. Berglin, M., et al., *Flexible and Biocompatible Antifouling Polyurethane Surfaces Incorporating Tethered Antimicrobial Peptides through Click Reactions.* Macromolecular Bioscience, 2024. **24**(4): p. 2300425.
36. Pandey, L.M., *Design of biocompatible and self-antibacterial titanium surfaces for biomedical applications.* Current Opinion in Biomedical Engineering, 2023. **25**: p. 100423.
37. Chen, Q., et al., *Impact of Antifouling PEG Layer on the Performance of Functional Peptides in Regulating Cell Behaviors.* Journal of the American Chemical Society, 2019. **141**(42): p. 16772-16780.
38. Horseman, T., Z. Wang, and S. Lin, *Colloidal interactions between model foulants and engineered surfaces: Interplay between roughness and surface energy.* Chemical Engineering Journal Advances, 2021. **8**: p. 100138.
39. Yagasaki, T. and N. Matubayasi, *Molecular Dynamics Study of the Antifouling Mechanism of Hydrophilic Polymer Brushes.* Langmuir, 2023. **39**(37): p. 13158-13168.
40. Liu, Y., et al., *Molecular simulations and understanding of antifouling zwitterionic polymer brushes.* Journal of materials chemistry B, 2020. **8**(17): p. 3814-3828.
41. Wang, F., et al., *Review of the research on anti-protein fouling coatings materials.* Progress in Organic Coatings, 2020. **147**: p. 105860.

42. Gao, J., et al., *Probing Interfacial Behavior and Antifouling Activity of Adsorbed Copolymers at Solid/Liquid Interfaces.* Langmuir, 2023. **39**(13): p. 4557-4570.
43. Hasan, A., et al., *Surface Design for Immobilization of an Antimicrobial Peptide Mimic for Efficient Anti-Biofouling.* Chemistry – A European Journal, 2020. **26**(26): p. 5789-5793.
44. Kostiv, U., et al., *Versatile Bioconjugation Strategies of PEG-Modified Upconversion Nanoparticles for Bioanalytical Applications.* Biomacromolecules, 2020. **21**(11): p. 4502-4513.
45. Durán, I.R., et al., *Atmospheric pressure cold plasma versus wet-chemical surface treatments for carboxyl functionalization of polylactic acid: A first step toward covalent immobilization of bioactive molecules.* Colloids and Surfaces B: Biointerfaces, 2020. **189**: p. 110847.
46. Bilek, M.M.M., et al., *Plasma treatment in air at atmospheric pressure that enables reagent-free covalent immobilization of biomolecules on polytetrafluoroethylene (PTFE).* Applied Surface Science, 2020. **518**: p. 146128.
47. Egghe, T., et al., *Silanization of Plasma-Activated Hexamethyldisiloxane-Based Plasma Polymers for Substrate-Independent Deposition of Coatings with Controlled Surface Chemistry.* ACS Applied Materials & Interfaces, 2022. **14**(3): p. 4620-4636.
48. Yang, T., et al., *From surface to bulk modification: Plasma polymerization of amine-bearing coating by synergic strategy of biomolecule grafting and nitric oxide loading.* Bioactive Materials, 2020. **5**(1): p. 17-25.
49. Anbumani, S., et al., *Oxygen plasma-enhanced covalent biomolecule immobilization on SU-8 thin films: A stable and homogenous surface biofunctionalization strategy.* Applied Surface Science, 2021. **553**: p. 149502.
50. Hu, R., et al., *Highly concentrated amino-modified biochars using a plasma: Evolution of surface composition and porosity for heavy metal capture.* Carbon, 2020. **168**: p. 515-527.
51. Boix-Lemonche, G., et al., *Covalent grafting of titanium with a cathelicidin peptide produces an osteoblast compatible surface with antistaphylococcal activity.* Colloids and Surfaces B: Biointerfaces, 2020. **185**: p. 110586.
52. Ghaisani, A.D., T.E. Saraswati, and K. Kusumandari, *A comparative amination study of TiO2/Fe3O4/carbon nanocomposites prepared in one- and two-step plasma-based methods.* Chemical Papers, 2024. **78**(2): p. 1227-1237.

53. Finke, B., et al., *Plasma processes for cell-adhesive titanium surfaces based on nitrogen-containing coatings.* Surface and Coatings Technology, 2011. **205**: p. S520-S524.
54. Strauss, L., et al., *Plasma surface modification and three-dimensional structuring of additively manufactured polyetheretherketone implants for improvement of osseointegration.* Plasma Processes and Polymers, 2024. **21**(3): p. 2300082.
55. Seemann, A., et al., *RGD-Modified Titanium as an Improved Osteoinductive Biomaterial for Use in Dental and Orthopedic Implants.* Bioconjugate Chemistry, 2022. **33**(2): p. 294-300.
56. Pulsipher, D.J. and E.R. Fisher, *NH2 and NH Surface Production in Pulsed NH3 Plasmas on TiO2: A Steady‐State Probe of Short Pulse Plasmas.* Plasma Processes and Polymers, 2013. **10**(1): p. 6-18.
57. Zheng, Z., et al., *Effects of novel non-thermal atmospheric plasma treatment of titanium on physical and biological improvements and in vivo osseointegration in rats.* Scientific Reports, 2020. **10**(1): p. 10637.
58. Shiau, D.-K., et al., *Enhancing the blood response and antibacterial adhesion of titanium surface through oxygen plasma immersion ion implantation treatment.* Surface and Coatings Technology, 2019. **365**: p. 173-178.
59. Jiang, P., et al., *Advanced surface engineering of titanium materials for biomedical applications: From static modification to dynamic responsive regulation.* Bioactive Materials, 2023. **27**: p. 15-57.
60. Alipal, J., et al., *An updated review on surface functionalisation of titanium and its alloys for implants applications.* Materials Today: Proceedings, 2021. **42**: p. 270-282.
61. Spriano, S., et al., *A critical review of multifunctional titanium surfaces: New frontiers for improving osseointegration and host response, avoiding bacteria contamination.* Acta biomaterialia, 2018. **79**: p. 1-22.
62. Wang, D., et al., *Antibiofilm peptides against biofilms on titanium and hydroxyapatite surfaces.* Bioactive Materials, 2018. **3**(4): p. 418-425.
63. Kurup, A., P. Dhatrak, and N. Khasnis, *Surface modification techniques of titanium and titanium alloys for biomedical dental applications: A review.* Materials Today: Proceedings, 2021. **39**: p. 84-90.

64. Sun, J., et al., *Bio-clickable mussel-inspired peptides improve titanium-based material osseointegration synergistically with immunopolarization-regulation.* Bioactive Materials, 2022. **9**: p. 1-14.
65. Alavi, S.K., et al., *Atmospheric Pressure Plasma Jet Treatment of Polymers Enables Reagent-Free Covalent Attachment of Biomolecules for Bioprinting.* ACS Applied Materials & Interfaces, 2020. **12**(34): p. 38730-38743.
66. Akdoğan, E. and H.T. Şirin, *Plasma surface modification strategies for the preparation of antibacterial biomaterials: A review of the recent literature.* Materials Science and Engineering: C, 2021. **131**: p. 112474.
67. Dou, S., et al., *Plasma-Assisted Synthesis and Surface Modification of Electrode Materials for Renewable Energy.* Advanced Materials, 2018. **30**(21): p. 1705850.
68. Bogaerts, A. and E.C. Neyts, *Plasma Technology: An Emerging Technology for Energy Storage.* ACS Energy Letters, 2018. **3**(4): p. 1013-1027.
69. Saleem, M., et al., *Comparative performance assessment of plasma reactors for the treatment of PFOA; reactor design, kinetics, mineralization and energy yield.* Chemical Engineering Journal, 2020. **382**: p. 123031.
70. Samizadeh Nikoo, M., et al., *Nanoplasma-enabled picosecond switches for ultrafast electronics.* Nature, 2020. **579**(7800): p. 534-539.
71. Vervloessem, E., et al., *Sustainable NOx production from air in pulsed plasma: elucidating the chemistry behind the low energy consumption.* Green Chemistry, 2022. **24**(2): p. 916-929.
72. Sun, X., et al., *Advance in Using Plasma Technology for Modification or Fabrication of Carbon-Based Materials and Their Applications in Environmental, Material, and Energy Fields.* Advanced Functional Materials, 2021. **31**(7): p. 2006287.
73. Rezvanian, P., et al., *Enhanced Biological Response of AVS-Functionalized Ti-6Al-4V Alloy through Covalent Immobilization of Collagen.* Scientific Reports, 2018. **8**(1): p. 3337.
74. Nie, B.e., et al., *Covalent immobilization of KR-12 peptide onto a titanium surface for decreasing infection and promoting osteogenic differentiation.* RSC Advances, 2016. **6**(52): p. 46733-46743.
75. Jacob, B., et al., *Short KR-12 analogs designed from human cathelicidin LL-37 possessing both antimicrobial and antiendotoxic activities without mammalian cell toxicity.* J Pept Sci, 2013. **19**(11): p. 700-7.

76. Blasi-Romero, A., et al., *KR-12 Derivatives Endow Nanocellulose with Antibacterial and Anti-Inflammatory Properties: Role of Conjugation Chemistry.* ACS Applied Materials & Interfaces, 2023. **15**(20): p. 24186-24196.
77. Al Musaimi, O., et al., *Calculating Resin Functionalization in Solid-Phase Peptide Synthesis Using a Standardized Method based on Fmoc Determination.* ACS Combinatorial Science, 2019. **21**(11): p. 717-721.
78. Oliveira, W., et al., *Staphylococcus aureus and Staphylococcus epidermidis infections on implants.* Journal of hospital infection, 2018. **98**(2): p. 111-117.
79. Jiang, N., et al., *Antibiotic loaded β-tricalcium phosphate/calcium sulfate for antimicrobial potency, prevention and killing efficacy of Pseudomonas aeruginosa and Staphylococcus aureus biofilms.* Scientific Reports, 2021. **11**(1): p. 1446.
80. Crémet, L., et al., *Orthopaedic-implant infections by Escherichia coli: Molecular and phenotypic analysis of the causative strains.* Journal of Infection, 2012. **64**(2): p. 169-175.
81. Miles, A.A., S. Misra, and J. Irwin, *The estimation of the bactericidal power of the blood.* Epidemiology & Infection, 1938. **38**(6): p. 732-749.
82. Banerjee, A., et al., *Inhibition and eradication of bacterial biofilm using polymeric materials.* Biomaterials Science, 2023. **11**(1): p. 11-36.
83. Heimhalt, M., et al., *An Inhibitor-in-Pieces Approach to DAHP Synthase Inhibition: Potent Enzyme and Bacterial Growth Inhibition.* ACS Infectious Diseases, 2021. **7**(12): p. 3292-3302.
84. Gómez-Arribas, L.N., et al., *Hierarchically Imprinted Polymer for Peptide Tag Recognition Based on an Oriented Surface Epitope Approach.* ACS Applied Materials & Interfaces, 2020. **12**(43): p. 49111-49121.
85. Tsujita, H., et al., *Effect of Plasma Treatment on Titanium Surface on the Tissue Surrounding Implant Material.* Int J Mol Sci, 2021. **22**(13).
86. Liu, P., et al., *Plasma-activated interfaces for biomedical engineering.* Bioactive Materials, 2021. **6**(7): p. 2134-2143.
87. Chiang, W.-H., et al., *Microplasmas for Advanced Materials and Devices.* Advanced Materials, 2020. **32**(18): p. 1905508.
88. Nicol, M.J., et al., *Antibacterial effects of low-temperature plasma generated by atmospheric-pressure plasma jet are mediated by reactive oxygen species.* Scientific Reports, 2020. **10**(1): p. 3066.

89. Cámara-Torres, M., et al., *Tuning Cell Behavior on 3D Scaffolds Fabricated by Atmospheric Plasma-Assisted Additive Manufacturing.* ACS Applied Materials & Interfaces, 2021. **13**(3): p. 3631-3644.
90. Ma, C., et al., *Plasma-controlled surface wettability: recent advances and future applications.* International Materials Reviews, 2023. **68**(1): p. 82-119.
91. Chen, Z., et al., *Cold atmospheric plasma delivery for biomedical applications.* Materials Today, 2022. **54**: p. 153-188.
92. Joseph, B., et al., *Insights into the biomechanical properties of plasma treated 3D printed PCL scaffolds decorated with gold nanoparticles.* Composites Science and Technology, 2021. **202**: p. 108544.
93. Bjelajac, A., et al., *Gold nanoparticles synthesis and immobilization by atmospheric pressure DBD plasma torch method.* Nanoscale Advances, 2023. **5**(9): p. 2573-2582.
94. Oehrlein, G.S., et al., *Future of plasma etching for microelectronics: Challenges and opportunities.* Journal of Vacuum Science & Technology B, 2024. **42**(4).
95. Hori, M., *Radical-controlled plasma processes.* Reviews of Modern Plasma Physics, 2022. **6**(1): p. 36.
96. Özbek, Y.Y., *Surface properties of AISI 4140 steel modified by pulse plasma technique.* Journal of Materials Research and Technology, 2020. **9**(2): p. 2176-2185.
97. Wagatsuma, K., *Characteristics of the transient signal from pulsed glow discharge plasma for atomic emission analysis.* Applied Spectroscopy Reviews, 2020. **55**(1): p. 76-86.
98. van den Bekerom, D., et al., *2D-imaging of absolute OH and H2O2 profiles in a He-H2O nanosecond pulsed dielectric barrier discharge by photo-fragmentation laser-induced fluorescence.* Plasma Sources Science and Technology, 2023. **32**(1).
99. Gao, S. and Y. Zhang, *Numerical Study on Plasma Characteristics Driven by Pulsed Voltages from Microseconds to Nanoseconds*, in *Pulsed Discharge Plasmas: Characteristics and Applications*, T. Shao and C. Zhang, Editors. 2023, Springer Nature Singapore: Singapore. p. 455-495.
100. Glosík, J., et al., *A contribution to the study of the influence of metastables in the flowing afterglow plasma.* Czechoslovak Journal of Physics B, 1987. **37**(2): p. 188-193.
101. van Helden, J.H., et al., *Production Mechanisms of NH and NH2 Radicals in N2−H2 Plasmas.* The Journal of Physical Chemistry A, 2007. **111**(45): p. 11460-11472.

102. Jonusas, M., K. Leroux, and L. Krim, *N + H surface reaction under interstellar conditions: Does the NH/NH2/NH3 distribution depend on N/H ratio?* Journal of Molecular Structure, 2020. **1220**: p. 128736.
103. Marshall, P. and P. Glarborg, *Probing High-Temperature Amine Chemistry: Is the Reaction NH3 + NH2 ⇄ N2H3 + H2 Important?* The Journal of Physical Chemistry A, 2023. **127**(11): p. 2601-2607.
104. Cabrero-Antonino, M., et al., *Plasma-Induced Defects Enhance the Visible-Light Photocatalytic Activity of MIL-125(Ti)-NH2 for Overall Water Splitting.* Chemistry – A European Journal, 2020. **26**(67): p. 15682-15689.
105. Liu, J., et al., *Self-limiting nitrogen/hydrogen plasma radical chemistry in plasma-enhanced atomic layer deposition of cobalt.* Nanoscale, 2022. **14**(12): p. 4712-4725.
106. Rabel, K., et al., *Controlling osteoblast morphology and proliferation via surface micro-topographies of implant biomaterials.* Scientific Reports, 2020. **10**(1): p. 12810.
107. Raja, I.S., et al., *The predominant factor influencing cellular behavior on electrospun nanofibrous scaffolds: Wettability or surface morphology?* Materials & Design, 2022. **216**: p. 110580.
108. Majhi, S., V.C. Peddiraju, and A. Mishra, *Effect of antimicrobial peptide (AMP)–tethered stainless steel surfaces on the bacterial membrane.* Materials Today Chemistry, 2021. **21**: p. 100541.
109. Ferraris, S., et al., *Surface modification of Ti–6Al–4V alloy for biomineralization and specific biological response: Part I, inorganic modification.* Journal of Materials Science: Materials in Medicine, 2011. **22**(3): p. 533-545.
110. Ma, L., et al., *Biomimetic Ti–6Al–4V alloy/gelatin methacrylate hybrid scaffold with enhanced osteogenic and angiogenic capabilities for large bone defect restoration.* Bioactive Materials, 2021. **6**(10): p. 3437-3448.
111. Sandomierski, M., et al., *Improving the abrasion resistance of Ti6Al4V alloy by modifying its surface with a diazonium salt and attaching of polyurethane.* Sci Rep, 2020. **10**(1): p. 19289.
112. Marsotto, M., et al., *Multifunctional Platform for Covalent Titanium Coatings: Micro-FTIR, XPS, and NEXAFS Characterizations.* Langmuir, 2023. **39**(19): p. 6837-6845.
113. Gong, X.-Y., et al., *Novel high-flux positively charged composite membrane incorporating titanium-based MOFs for heavy metal removal.* Chemical Engineering Journal, 2020. **398**: p. 125706.

114. Chan, K.V., et al., *Investigating the stability of cyclopropylamine-based plasma polymers in water.* Applied Surface Science, 2020. **517**: p. 146167.
115. Li, P., et al., *Fabricating a wettable microwells array onto a nitrogen plasma-treated ITO substrate: high-throughput fluorimetric platform for selective sensing of ammonia in blood using polymer-stabilized NH2-MIL-125.* Journal of Materials Chemistry B, 2021. **9**(30): p. 5998-6005.
116. Cheah, P., et al., *Versatile Surface Functionalization of Water-Dispersible Iron Oxide Nanoparticles with Precisely Controlled Sizes.* Langmuir, 2021. **37**(3): p. 1279-1287.
117. Sinha Ray, S., R. Dangayach, and Y.-N. Kwon, *Surface engineering for anti-wetting and antibacterial membrane for enhanced and fouling resistant membrane distillation performance.* Chemical Engineering Journal, 2021. **405**: p. 126702.
118. He, X., et al., *One-step self-assembly of biogenic Au NPs/PEG-based universal coatings for antifouling and photothermal killing of bacterial pathogens.* Chemical Engineering Journal, 2021. **421**: p. 130005.
119. Barreto, M.S.C., E.J. Elzinga, and L.R.F. Alleoni, *The molecular insights into protein adsorption on hematite surface disclosed by in-situ ATR-FTIR/2D-COS study.* Scientific Reports, 2020. **10**(1): p. 13441.
120. Liu, M., et al., *Hyaluronidase-Responsive Bactericidal Cryogel for Promoting Healing of Infected Wounds: Inflammatory Attenuation, ROS Scavenging, and Immune Regulation.* Advanced Science, 2024. **11**(17): p. 2306602.
121. Liang, Q., et al., *Development strategies and application of antimicrobial peptides as future alternatives to in-feed antibiotics.* Science of The Total Environment, 2024. **927**: p. 172150.
122. Ganesan, N., et al., *Antimicrobial Peptides and Small Molecules Targeting the Cell Membrane of Staphylococcus aureus.* Microbiology and Molecular Biology Reviews, 2023. **87**(2): p. e00037-22.
123. Tomita, S., et al., *Hydrolysis of amide bonds in dipeptides and nylon 6 over a ZrO2 catalyst.* Catalysis Science & Technology, 2024. **14**(14): p. 3898-3908.
124. Nashchekina, Y.A., et al., *The Effect of Carbodiimide on the Structural, Mechanical and Biological Properties of Collagen Films.* Cell and Tissue Biology, 2021. **15**(6): p. 586-593.
125. Nair, M., et al., *Tunable bioactivity and mechanics of collagen-based tissue engineering constructs: A comparison of EDC-NHS, genipin and TG2 crosslinkers.* Biomaterials, 2020. **254**: p. 120109.

126. Bazaka, K., et al., *Plasma-assisted surface modification of organic biopolymers to prevent bacterial attachment.* Acta Biomaterialia, 2011. **7**(5): p. 2015-2028.
127. Boden, A., *Immobilisation strategies for the tethering of polymers and antimicrobial peptides to design multifunctional surface coatings*. 2020, Swinburne.
128. Beveridge, T.J., *Structures of gram-negative cell walls and their derived membrane vesicles.* Journal of bacteriology, 1999. **181**(16): p. 4725-4733.
129. Lei, R., et al., *Turning cationic antimicrobial peptide KR-12 into self-assembled nanobiotics with potent bacterial killing and LPS neutralizing activities.* Nanoscale, 2024. **16**(2): p. 887-902.
130. Jacob, B., et al., *Short KR‐12 analogs designed from human cathelicidin LL‐37 possessing both antimicrobial and antiendotoxic activities without mammalian cell toxicity.* Journal of peptide science, 2013. **19**(11): p. 700-707.
131. Yu, K., et al., *Toward Infection-Resistant Surfaces: Achieving High Antimicrobial Peptide Potency by Modulating the Functionality of Polymer Brush and Peptide.* ACS Applied Materials & Interfaces, 2015. **7**(51): p. 28591-28605.
132. Nemcakova, I., et al., *Heat treatment dependent cytotoxicity of silicalite-1 films deposited on Ti-6Al-4V alloy evaluated by bone-derived cells.* Scientific Reports, 2020. **10**(1): p. 9456.
133. Omrani, M.M., et al., *Enhanced Protein Adsorption, Cell Attachment, and Neural Differentiation with the Help of Amine Functionalized Polycaprolactone Scaffolds.* Journal of Macromolecular Science, Part B, 2016. **55**(6): p. 617-626.
134. Chen, Q., et al., *Dual mechanism β-amino acid polymers promoting cell adhesion.* Nature Communications, 2021. **12**(1): p. 562.
135. Borah, R., et al., *Surface-Functionalized Conducting Nanofibers for Electrically Stimulated Neural Cell Function.* Biomacromolecules, 2021. **22**(2): p. 594-611.
136. Milky, B., et al., *Long-term adherence of human brain cells in vitro is enhanced by charged amine-based plasma polymer coatings.* Stem Cell Reports, 2022. **17**(3): p. 489-506.

Chapter Three:

Enzyme-Responsive Coatings Supporting Dual Functionality: Osteoblast Promotion and Antimicrobial Activity for Orthopaedic Implants

---

Mohadeseh Zare [a*], Laura Colomina Alfaro [b], Antonella Bandiera [b], Esra Mutlu [a], David Grossin [c], Fernando Albericio [d], Sarah A. Kuehne [e], Zubair Ahmed [f], Artemis Stamboulis[a*]

[a] Biomaterials Research Group, School of Metallurgy and Materials, University of Birmingham, Edgbaston, Birmingham, B15 2TT, UK

[b] Department of Life Sciences, University of Trieste, via L. Giorgieri, 1, Trieste, 34127 Italy

[c] CIRIMAT, Toulouse INP, Université Toulouse 3 Paul Sabatier, CNRS, Université de Toulouse, 4 Allée Emile Monso - BP44362, 31030 Toulouse Cedex 4, France

[d] School of Chemistry and Physics, University of KwaZulu-Natal, Durban, 4000 South Africa

[e] School of Science and Technology, Nottingham Trent University, Nottingham, NG11 8NS, UK

[f] Neuroscience and Ophthalmology, Institute of Inflammation and Ageing, College of Medical and Dental Sciences, University of Birmingham, Edgbaston, Birmingham, B15 2TT, UK

*Corresponding authors: a.stamboullis@bham.ac.uk; zare.mohadeseh@gmail.com

M.Z. developed the main conceptual framework, conducted the experiments, and analyzed the data. L.C.A. assisted in performing the experiments. E.M., A.B., F.A., and D.G. contributed to the experimental design and data interpretation. A.S. provided overall project supervision. S.A.K. and Z.A. supervised the microbiological analyses and biological assessments.

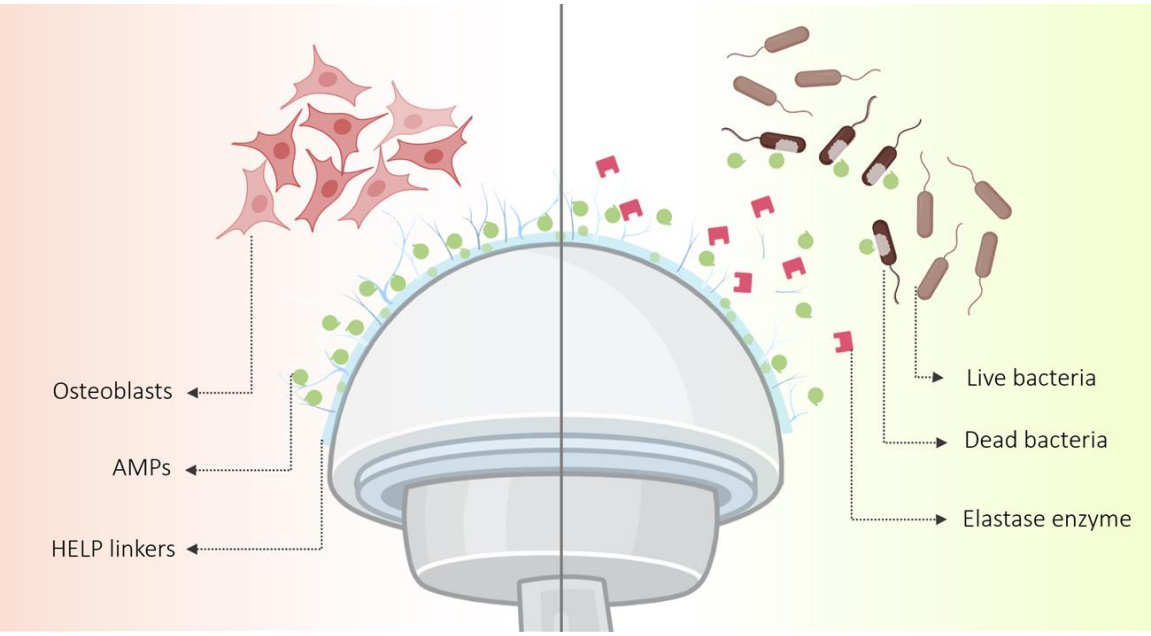
Abstract

Implant-associated infections pose significant challenges due to bacterial resistance to antibiotics. Recent research highlights the potential of immobilising antimicrobial peptides (AMPs) onto implants as an alternative to conventional antibiotics for bacterial infection prevention. While various AMP immobilisation methodologies have been investigated, they still lack responsiveness to biological cues. This study proposes an enzyme-responsive antimicrobial coating for orthopaedic devices using KR-12, an AMP derived from Cathelicidin LL-37, coupled with the human elastin-like Peptide (HELP) as a biomimetic and stimuli-responsive linker while mimicking the extracellular matrix (ECM). During implantation, these customised interfaces encounter the innate immune response, triggering elastase release. The biodegradation of HELP biopolymer by the elastase enzyme enables the controlled release of KR-12. After coupling KR-12 with HELP attached titanium surface, the antimicrobial activity against four pathogenic bacterial strains (*Staphylococcus aureus, Staphylococcus epidermidis, Escherichia coli*, and *Pseudomonas aeruginosa*) was assessed, revealing an inhibition ratio of bacterial adhesion and colonisation exceeding 92% for all tested strains. Comparing this surface with a titanium surface functionalised directly with KR-12 without the use of HELP as a linker, the antimicrobial activity was significantly higher, with an average increase of 15% against all strains. It is thought that the enhanced antimicrobial activity was due to the improved mobility of KR-12 coupled with HELP and its stimuli-responsive controlled release. Furthermore, the prepared coatings demonstrated strong adhesion and proliferation of human osteoblasts, as evidenced by MTT assay and SEM (Scanning Electron Microscopy) micrographs. By day 5, cells on modified surfaces displayed well-spread morphologies with extensive filopodia, indicating improved biocompatibility and cytoskeletal activity. These observations highlight the effectiveness of surface functionalisation in promoting cell adhesion, viability, and proliferation, making it suitable for biomedical applications.

These findings suggest extensive potential for smart coatings that combine the antimicrobial potential of AMPs with HELP's biological properties.

Keywords: Antimicrobial peptide, Human-Elastin Like Polypeptide, KR-12, Enzyme-responsive coating, Osteoblast promotion, Bacterial growth inhibition.

Graphical abstract:



3.1. Introduction

The implantation of medical devices carries a notable risk of nosocomial pathogens colonising and forming biofilms on device surfaces, subsequently leading to infections with prolonged healing periods [157, 158]. According to the concept of the "race for the surface", proposing a competition between host and bacterial cells for colonisation on the implant surface [276], the likelihood of bacterial attachment decreases if the host cells establish colonisation on the implant surface first, and vice versa [276, 277]. Upon implant placement, the surface becomes coated with a protein film, providing potential receptors for bacterial adhesive ligands, thus promoting further colonisation [278]. Biofilms, once formed, serve as effective shields for microorganisms against host immune responses and antibiotic treatments [279].

Titanium, renowned for its mechanical strength, chemical inertness, and compatibility with biological systems, remains the predominant material choice in orthopaedic, bone surgery, and dental applications, with the goal of improving human tissue healing [204, 207, 208]. However, despite its exceptional characteristics, bacterial colonisation on titanium surfaces remains a significant factor contributing to implant failure, often requiring revision surgery and introducing complexities to patient treatment and recovery processes [205, 206].

To effectively inhibit bacterial biofilm formation, it is essential to modify surfaces with

antimicrobial coatings to combine antifouling methods to deter bacterial adhesion and colonisation while enhancing biocompatibility by reducing potential toxicity to human cells [7, 280, 281]. Recent advancements in antimicrobial coatings aim to develop multifaceted structures with controllable toxicity and bioengineering capabilities. This pursuit has led to a high interest in the development of AMP based systems [166, 167]. AMPs, which are naturally found in various organisms, possess distinct structural features characterised by cationic and amphiphilic domains. These features are crucial for disrupting bacterial cell membranes. Unlike traditional antibiotics, AMPs have demonstrated a broad spectrum of activity against bacteria, fungi, and viruses, while also avoiding the induction of bacterial resistance. This resistance avoidance stems from their ability to permeate the cytoplasmic membrane without triggering typical resistance mechanisms [168, 169].

Amidst a diverse array of AMPs that have been documented, the human cathelicidin peptide LL-37 emerges as a noteworthy antimicrobial agent renowned for its multifaceted immunomodulatory capabilities [170]. One notable fragment of LL-37 is the cationic KR-12, [66]. The shorter length, reduced cytotoxicity, and cost-effectiveness of KR-12 make it an attractive option for various biomedical applications, including surface immobilisation on materials used in wound dressings, urinary catheters, and implants [171]. KR-12 interacts favorably with bacterial membranes due to its α-helical conformation and positive charge, while also minimising cytotoxic effects. Structural studies suggest that AMPs like KR-12 function by creating nanometric pores in cell membranes or inducing membrane micellisation [172]. Prior research has shown that controlled concentrations of KR-12 promote osteogenic differentiation in human bone marrow-derived mesenchymal stem cells, in addition to its antibacterial properties [38, 173, 174].

Two primary approaches, physical adsorption and covalent immobilisation, have been explored for immobilising AMPs on titanium implants [92, 175]. The simpler method, involving the physical adsorption of AMPs onto the titanium surface is less stable compared to covalent immobilisation, leading to rapid leaching of AMPs and a subsequent reduction in antimicrobial activity over time [79, 176, 177]. In contrast, covalent immobilisation establishes a chemical bond between the AMP and the titanium surface, ensuring long-term stability and preserving AMP activity on the implant surface [3, 145]. However, a drawback of this method is that it reduces the mobility of the peptide and can

cause steric hindrance [13]. To address this limitation, a flexible linker between the AMP and the titanium surface can be introduced as a solution. The linkers provide flexibility to AMPs, increasing their exposure and facilitating better mobility and penetration of bacteria, thereby enhancing antimicrobial efficacy [178-180].

Although covalent immobilisation of AMPs using linkers ensures high antimicrobial efficiency, the increased concentration of antimicrobial agents on the surface may compromise the biocompatibility, angiogenic activity, and osteogenic activity of the implant, consequently delaying sufficient osseointegration [282-284]. To address these critical issues, there is a demand to explore novel antimicrobial coatings capable of selectively targeting bacteria under pathological conditions [285, 286]. Therefore, developing statically versatile implant coatings would significantly enhance their applicability, necessitating the design of a coating capable of responding to fluctuations in pH or enzymatic activity [287-289]. The findings of recent studies emphasised the significance of biomaterial coatings that respond to pathogen microenvironments inhibiting the contact between AMPs and normal cells, thereby decreasing their toxicity [290, 291]. Such an approach was followed by Suo et al, who reported that AMP–Hyaluronic acid (AMP-HA) hybrid hydrogels exhibited excellent broad-spectrum antibacterial activity, showing on-demand release of AMPs specifically in acidic environments, expediting wound healing in infected mice. These findings suggest a promising avenue for the development of biomaterial coatings that could effectively manage chronic infected wounds by harnessing the innate properties of AMPs and responsive hydrogel systems.

The ideal antimicrobial coatings should exhibit efficacy against diverse pathogens, biocompatibility with host tissues, long-lasting activity, physiological stability, minimal cytotoxicity, resistance to biofilm formation, ease of application, and cost-effectiveness for medical deployment [11, 292]. To meet these criteria for the anticipated antimicrobial coating, an ideal linker for immobilising AMPs on titanium implants could be ECM-inspired polymers, such as HELPs [293, 294]. HELP is a well-described recombinant biopolymer comprising sequences resembling natural human tropoelastin, offering enhanced biocompatibility, improved cell adhesion, and increased anchoring sites for effective AMP immobilisation [295, 296]. Moreover, HELP can be degraded by physiological pathways, mitigating the risk of harmful byproducts [297-299]. Previous studies have assessed the proteolytic susceptibility of HELP matrices, demonstrating their

potential for enzymatic -triggered release of model compounds [300-303]. The elastolytic activity, present in both prokaryotic and eukaryotic organisms, is associated with various pathological conditions such as pulmonary emphysema, cystic fibrosis, infections, inflammation, chronic wounds, and atherosclerosis [304, 305]. Leveraging this concept, HELP polypeptides show promise as proteolytic stimuli-responsive systems for controlling the release of AMPs [297].

In this study, we developed an ECM-mimicking system based on HELPs to tether AMPs onto implanted devices. We leveraged enzyme-mediated release, taking advantage of physiologically normal inflammatory reactions or remodelling processes, which are most active during tissue healing and bone formation after surgical implantation [303]. Initially, HELP biopolymer was immobilised onto titanium disks as linkers. Subsequently, the AMP KR-12 was attached covalently at an optimised immobilisation density to maximise cell viability and antimicrobial activity. The antimicrobial activity of the coating against various pathogenic bacteria was investigated, and the cytocompatibility of the coating was assessed using human osteoblast bone cells.

3.2. Experimental methods

3.2.1 Sample preparation

The immobilisation of peptides on the titanium substrates involved a systematic three-step process. Prior to initiating the process, production and purification of HELP were carried out. To immobilise the peptides using HELP linkers on the titanium substrates, firstly, hydroxylation and silanisation were carried out, followed by the HELP linker attachment and subsequent peptide immobilisation. Each stage of this sequential procedure is precisely outlined in the following sections. The summarising processing scheme is illustrated in Figure 3-1. Table 3-1 provides the description of sample names used in the experimental work.

Table 3-1. Description of sample names indicating different surface modifications.

Sample name	Description
PTi	Polished titanium alloy Ti6Al4V
Sil-PTi	Silanised titanium surface
KR12-STi	KR-12 immobilised on Sil-PTi
HELP-STi	HELP attached on Sil-PTi

KR12-HTi	KR-12 immobilised on HELP-attached Sil-PTi

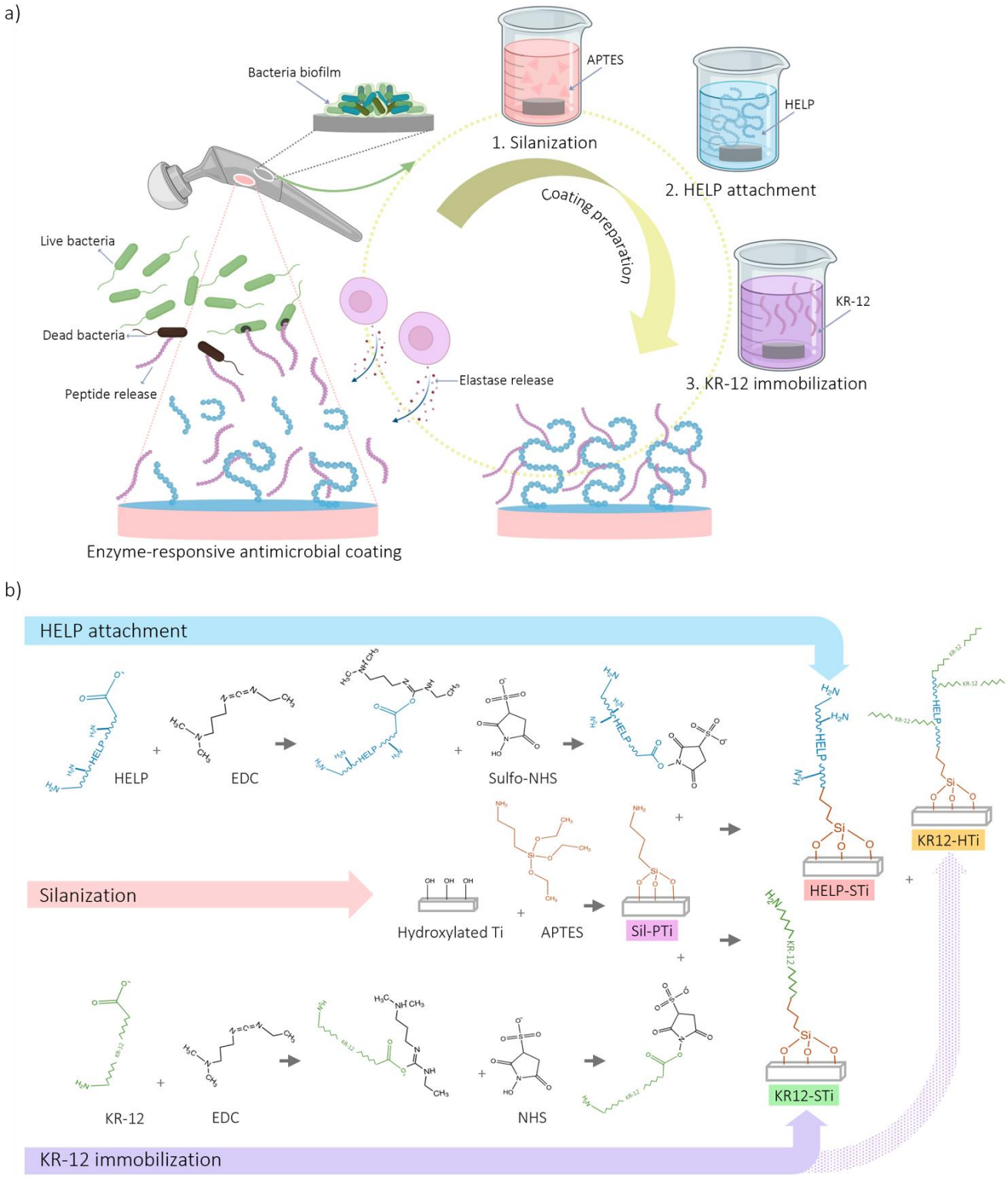


Figure 3-1. Schematic representation of (a) step-by-step procedure of silanisation, HELP

attachment, and KR-12 immobilisation to prepare enzyme-responsive antimicrobial coating for titanium implant surfaces, and (b) the chemical reactions occurred in each step at the interface of the titanium surface and the reagents. The diagram is not drawn to scale, and symbols are just utilised to elucidate the underlying concepts; APTES = (3-aminopropyl) triethoxysilane, HELP = Human elastin-like polypeptide, EDC = 1-ethyl-3-diaminopropyl carbodiimide hydrochloride, sulfo-NHS = sulfo-N-hydroxysuccinimide.

3.2.2 Silanisation of titanium substrates

Titanium disks, 10 mm in diameter and 2 mm in thickness served as representative models for the prevalent materials found in dental and orthopaedic implants (commercially pure Medical grade 5 Ti6Al4V, William Gregor LTD, East Grinstead, UK). The preparation process started with grinding the titanium disks consecutively with 800, 1200, and 2500 grit Struers silicon carbide/abrasive papers using Struers Metallographic equipment. Subsequently, the disks were polished to mirror finish using a 0.05 μm particle size colloidal silica, following Bruker's protocols. To ensure cleanliness, the polished disks were sonicated for 30 mins in ethanol followed by 30 mins sonication in deionised (DI) water. Then, the titanium disks were air-dried at room temperature and stored in a desiccator until needed.

To facilitate the silanisation process, a thorough 2-hour etching process using an oxidising solution (50:50 v/v, 98% H_2SO_4/ 30% H_2O_2) was carried out introducing hydroxyl groups on the surfaces. The etched surfaces were washed twice in DI water and ethanol with 30-minute sonication intervals. Silanisation, a common method for immobilising biomolecules on inorganic surfaces, was then performed [306]. An organic silane, 3-Aminopropyltriethoxysilane (APTES) (ThermoFisher Scientific, Birmingham UK), was used as the intermediate linker, enhancing the adhesion process. The hydroxylated (TiOH) titanium substrates, were immersed in a 10% v/v APTES solution in toluene (purity ≥ 99.5%, Sigma Aldrich, UK) at 80°C for 4 hours with a continuous mild shaking to introduce functional amino groups on the titanium surface. Following this, the surfaces were sonicated following two 10-minute sonication cycles in each one of the following solvents: pure toluene, ethanol, and water.

3.2.3 Production and purification of the HELP biopolymer

The expression and purification of the recombinant HELP biopolymer were performed in

standard conditions as described in the literature [300, 307]. The details of the HELP biopolymer sequences are provided in the appendix. Briefly, recombinant clones of *Escherichia coli* (*E. coli*) C3037I strain (New England Biolabs, Ipswich, MA, USA) transformed with the plasmid carrying the HELP DNA sequence were grown in Luria Bertani medium (LB) supplemented with 50 µg/mL of ampicillin and 70 µg/mL of chloramphenicol. An overnight starter culture was used to seed the expression culture in Terrific Broth carried on at 37 °C under shaking until a turbidity of approximately OD_{600} = 1 was reached. The expression of HELP polypeptide was induced by adding 0.1 mM isopropyl β- d-1- thiogalactopyranoside. Growth was continued for an additional 5 hours. Bacterial cells were collected by centrifugation at 8000 rpm for 20 min at 10°C using a Beckman–Coulter, J-26 XP.

The pellets were suspended in 400 mL of the extraction solution containing 50 mM Tris/HCl pH 8, 250 mM NaCl, 0,1 mM EDTA, 0,1% Triton X-100, and 1 mM PMSF and disrupted using a high-pressure homogeniser (Panda NS1001L, GEA Niro Soavi, Italy). Then, 2-mercaptoethanol was added to 20 mM and after cooling the bacterial lysate on ice, the mixture was centrifuged at 10000 rpm, for 30 minutes at 8 °C (Beckman–Coulter, J-26 XP). The cellular debris was discarded, and the supernatant was further processed to purify the HELP biopolymer following a well-established procedure known as Inverse Transition Cycling (ITC) which is based on the thermo-responsive properties of the elastin domain [308]. Briefly, the biopolymer was precipitated by adding NaCl to the supernatant to a final concentration of 1.5 M at 37 °C. The aggregated part was separated from the solution by centrifugation at 7000 rpm for 30 min at 37 °C. The pellet was re-dissolved in cold water and any non-soluble components were removed through cold centrifugation. In total, three ITC cycles were performed to ensure the desired degree of purification. The material was lyophilised for long-term storage and further use.

3.2.4 HELP attachment

To enable the attachment of HELP as a linker onto titanium surfaces, the process involved the selective activation of the carboxyl group in HELP using 1-Ethyl-3-(3-dimethyl-aminopropyl) carbodiimide (EDC, ThermoFisher Scientific), resulting in the formation of a highly reactive *O*-acylisourea. This intermediate complex subsequently reacted with the primary amine groups present on the titanium surface using NHS (ThermoFisher Scientific) as an activating agent, as described in the literature [216].

The initial step involved preparing 1 mg/ml HELP solution in MES (2-(N-morpholino) ethanesulfonic acid) buffer (0.1M, pH 6.0). Amino-functionalised substrates (Sil-PTi, see Table 3-1) were then immersed in the HELP solution for 1 hour. Following this immersion, a solution of EDC (23 mg. l^{-1}) was introduced, followed by the sequential addition of sulfo-NHS (77 mg. l^{-1}) in a dropwise manner. The grafted samples, HELP-STi, were successively washed with DI water and ethanol using a vortex to remove non-covalently bound reactants before drying and storing in a desiccator.

3.2.5 Covalent immobilisation of KR-12

Following the attachment of HELP, a similar EDC/NHS protocol was employed to immobilise the KR-12 (H-KRIVQRIKDFLR-OH), on the amine groups of HELP, labeled as KR12-HTi. The identical procedure was employed to immobilise KR-12 directly onto the silanised surface of Sil-PTi, labelled as KR12-STi. The KR-12 was supplied by BOCSCI Inc., NY, USA. To immobilise them, the carboxylic groups of the peptides were activated with EDC and subsequently reacted with the primary amine groups of the silanised surface of Sil-PTi or the HELP biopolymer on the surface of HELP-STi. Following the same protocol outlined in the previous section, the substrates were incubated in a 1 mg/ml solution of KR-12 in MES buffer. After 1 hour of incubation, EDC and sulfo-NHS solutions were added dropwise in sequence to facilitate the covalent binding of the KR-12 peptide. This step-by-step procedure ensured a consistent and effective process for the immobilisation of the KR-12 peptide on the silanised surfaces and HELP-modified surfaces. Two wash cycles with DI water and ethanol, employing a vortex for thorough cleansing, were performed to remove non-covalently bound peptides from the samples. To precisely quantify the immobilised peptides on the surfaces, an Fmoc (fluorenyl-methyloxy-carbonyl)-labelled KR-12 (Fmoc-KRIVQRIKDFLR-OH) was used, following the protocol mentioned above. The peptide percentage used for the KR-12 immobilisation was selected and evaluated based on the minimum inhibitory concentration (MIC) of KR-12 as reported in previous studies [217-219]. This approach ensured that the released amount remained below the MIC threshold, while optimised concentrations conducive to osteogenic differentiation and promotion were determined.

3.2.6 Surface characterisation

Scanning Electron Microscopy (SEM)

At each stage of sample preparation, SEM was carried out to assess the influence of individual steps on the surface morphology using a Jeol 6060 with an Oxford Inca EDS. Before the examination, the samples were Au sputter-coated using a Polaron Emitech SC7640 Sputter Coater. Each sample was then subjected to a comprehensive imaging process, capturing five images at a working distance of 9 mm and a voltage of 20 kV.

Atenuated Total Reflectance-Fourier Transform Infrared Spectroscopy (ATR-FTIR)

To confirm the chemical reaction mechanisms, the presence of functional groups was assessed through ATR-FTIR spectra analysis before and after the chemical reactions using a Nicolet 6700 FTIR machine (Thermo Scientific) and Omnic 8 software suite (Thermo Scientific) in the range from 4000 to 400 cm^{-1}. The spectra were acquired from an average of 64 scans/background at a spectral resolution of 2 cm^{-1}.

Atomic Force Microscopy (AFM)

The surface topography and roughness changes of HELP-attached and peptide-attached samples were analysed in the tapping mode at room temperature using Bruker Multimode 8 and Pt-coated silicon cantilevers provided by Bruker (SCM-PIT). Scans were taken at random sites in 20 μm^2 using a 5 mm scan head at a scan rate of 0.1 Hz for all measurements. The pictures were digitally processed by NanoScope Analysis 1.7 software and the R_a were measured.

X-Ray Photoelectron Spectroscopy (XPS)

The surface elemental compositions of PTi and Sil-PTi were measured using a Thermo NEXSA XPS equipped with a monochromated Al Kα X-ray source (1486.7 eV). The system included a spherical sector analyser, three multichannel resistive plates, and 128 channel delay line detectors. Data acquisiton occured at 19.2 W and an X-ray beam size of 400 x 200 µm. Survey scans were performed at a pass energy of 200 eV, and high-resolution scans used a pass energy of 40 eV. Electronic charge neutralisation was managed via a dual-beam low-energy electron/ion source (Thermo Scientific FG-03). Measurements were taken at a pressure below 10^{-8} Torr and a room temperature of 294 K. Data processing was completed using CasaXPS v2.3.20PR1.0 with peak fitted done using Shirley background subtraction prior to component analysis. Binding energies were calibrated with the C 1s signal at 284.8 eV and minimum of three different samples were analysed for each group.

Water Contact Angle (WCA) measurments

Surface wettability, determined through static WCA measurements, is a strong indicator of surface's hydrophilic/hydrophobic properties that influence the cells attachment. Static water contact angles were measured at room temperature, analysing the profile of sessile drops. A 5 µL droplet of DI water was deposited on the sample surface using a Hamilton syringe set on a Kruss DSA100 apparatus (Germany) equipped with a CCD camera and an image analysis processor. The WCAs were calculated using the built-in CAM 100 software. The test was performed in triplicate. Four droplets were measured on different locations on each sample, and three different samples in each group. A static picture was taken within three seconds after droplet deposition, and angles were measured on the static picture. The reported values are the averages of these 9 measurements for each type of surface.

3.2.7 Concentration of immobilised KR-12

The quantification of KR-12 loading on the surface involved estimating the number of Fmoc groups by measuring the maximum ultraviolet (UV) absorption at 301 nm. The determination of Fmoc groups loading at the surface enabled the calculation of the peptides as each peptide contained one Fmoc (Fmoc-KRIVQRIKDFLR-OH). Fmoc groups attached to the peptides were readily cleaved using 20% piperidine in dimethylformamide (DMF), a common reaction mechanism during solid-phase peptide synthesis employing

the Fmoc/t-Bu (Tert-Butyl) method. The presence of piperidine induces the formation of dibenzofulvene–piperidine adducts via a Michael-type addition, which are soluble in reaction solvents, enabling the spectrophotometric measurement based on the Beer–Lambert law [220]. A multipoint standardisation method (calibration curve) was established to measure the solution's UV light absorption ability at a specific wavelength. The calibration points were prepared and validated on the same day as the analysis to ensure accuracy.

For the calibration curve preparation, Fmoc-KR12 stock solutions (1 mg/mL = 637 μM) were prepared in 20% (v/v) piperidine in DMF. Both solvents were provided by Sigma Aldrich. Fmoc removal reactions were carried out for 30 min at room temperature. Subsequently, 5.0 mL of the stock solution was diluted to 50.0 mL with 20% (v/v) piperidine in DMF. Dibenzofulvene-base solutions of varying concentrations (ranging from 10 to 310 μM in 30 μM intervals) were prepared using a dilution technique. These solutions were prepared in triplicate and measured at 301 nm, where absorption was solely due to the dibenzofulvene-base adduct. Then, a calibration curve of dibenzofulvene-base adduct concentration versus absorbance was constructed.

For analysis, each peptide-immobilised titanium surface was immersed in 20% v/v piperidine solution in DMF, and Fmoc removal reactions were conducted for 30 min at room temperature. Subsequently, the absorbance of each solution was measured at 301 nm (n = 3) and correlated to the calibration curve.

3.2.8 KR-12 release triggered by elastase degradation of HELP

As described in previous studies, the HELP moiety has been reported to be susceptible to degradation in the presence of elastase [300]. Elastase is a serine protease with a broad specificity, as it cleaves proteins at the carboxyl side of small hydrophobic amino acids. It also hydrolyses amides and esters without an activator. For the release of KR-12 from the KR12-HTi and KR12-STi disks, the samples were soaked in 50 mM Tris/HCl pH 7.5, 1 mM $CaCl_2$ buffer, and 50 µl solution of the elastase enzyme from porcine pancreas (Sigma Aldrich, #E7885) was added (50 µg/mL final concentration). Then, they were incubated with the elastase solution at 37^{o}C for specific time points of 2, 4, 6, 12, and 24 hours in a final reaction volume of 500 µl. In parallel, the same conditions were adopted to set up control reactions for KR12-HTi and KR12-STi without adding the enzyme. To assess the remaining KR-12 after elastase-mediated degradation, the samples were removed from the

reaction solution and washed gently with DMF at fixed times. Then, piperidine/ DMF cleavage was utilised by the protocol described above. The remaining amount subtracting the measured immobilised peptides amount provided the released amount of peptide during the enzyme degradation.

3.2.9 Antimicrobial activity assay

Orthopaedic implant infections are caused most often by *Staphylococcus aureus (S. aureus)* and *Staphylococcus epidermidis (S. epidermidis)*, *Escherichia coli (E. coli)*, and *Pseudomonas aeruginosa (P. aeruginosa)* which can be acquired during surgery or subsequently through a hematogenous route [221-223].

To assay the antimicrobial activities of the prepared coatings, two Gram-positive bacteria, *S. aureus* (SH1000) and *S. epidermidis* (ATCC 12228), and two Gram-negative bacteria, *E. coli* (ATCC 25922) and *P. aeruginosa* (PAO1) were grown on Mueller-Hinton (MH) agar plates using the Streak Plate method. Then, a colony of each strain was cultured in MH broth at 37 ^{o}C, overnight. To count the number of colony forming units (CFU) in a bacterial suspension, serial dilutions of the bacterial culture were prepared in a 96-well plate and cultured on MH agar plates based on the Miles and Misra method [224]. The bacterial suspension was adjusted to a concentration of 10^5 CFU mL^{-1} in MH broth for further analysis.

The coated titanium samples and polished substrate (control sample) were sterilised in 1 mL of 70% ethanol for 5 min at room temperature and then washed with sterilised DI water in a sterile environment. This process was repeated three times. Then, 20 μL of the bacterial suspension was added to the samples followed by incubation for 24 h at 37 ^{o}C. Bacterial growth inhibition ratio, CLSM, and SEM were used to characterise the bacterial colonisation for each group of coatings. All work was carried out in a class II ventilated hood, and the tools were autoclaved or sterilised with 70% ethanol before use.

3.2.10 Bacterial growth inhibition

The surface antimicrobial activity was tested against *S. aureus*, *S. epidermidis*, *E. coli*, and *P. aeruginosa* by a modified DCT protocol. For each sample, a sterile petri dish was prepared with a round filter paper saturated with phosphate-buffered saline (PBS) to maintain humidity and avoid evaporation of the bacterial suspension. A sterile microscope slide was positioned on the filter paper, and the sample (10 × 10 mm^2) was kept on the

slide. Then, 20 µl of the overnight bacterial suspension (containing 10^5 bacteria/ml) was pipetted onto the sample surface. A coverslip (20 x 20 mm^2) was carefully positioned on top to spread the inoculum over the entire disk surface. Then, closed petri dishes were incubated at 37 °C for 24 hours.

After incubation, the substrates covered with the bacterial suspension were moved to a 10-mL sterile tube, and after the addition of 5 ml of MH, were vortexed for 5 min to detach adherent bacteria. Since the titanium substrates are non-porous and non-absorbent, the 5-minute process was efficient in removing the adhered bacteria. This has been attested by SEM studies before and after vertexing. 200 µL of the bacterial suspension was collected, and 10-fold serial dilutions of the suspension were prepared to count the bacterial colonies on MH agar plates using the Miles and Misra method. After incubation at 37 ^oC for 20 h, the number of colonies on each sample was counted.

The bacterial growth inhibition ratio was calculated by measuring the CFU of the control sample, PTi, (denoted as B1) and each coated titanium (denoted as B2) using the following equation.

$$\text{Bacterial growth inhibition ratio (\%)} = (B_1-B_2)/B_1 * 100.$$

The measurements were conducted in triplicate for each type of sample, and the percentage of bacterial growth inhibition was averaged over the three samples.

For the SEM analysis and live/dead assays, *E. coli* and *S. aureus* were chosen as representative strains to assess the antimicrobial activity of the coatings. *E. coli* was selected to represent Gram-negative bacteria due to its characteristic outer membrane, which can influence susceptibility. At the same time, *S. aureus* was chosen as a model for Gram-positive bacteria, given its thick peptidoglycan layer and distinct interaction properties. The Gram-negative *P. aeruginosa* and the Gram-positive *S. epidermidis* displayed similar results. Therefore, we focused on *E. coli* and *S. aureus* to streamline the analysis and clearly illustrate the findings.

3.2.11 Bacterial morphology assay

After incubation with 20 µl of bacterial suspension (as described in 2.5.1.), the samples were immersed in 2.5% EM grade glutaraldehyde in 0.1 M sodium cacodylate buffer, pH 7.3, for 10 minutes to fix the bacteria on the surface. To remove water slowly, the samples were dehydrated for 10 min in ethanol solutions of increasing concentrations of 20, 30,

40, 50, 60, 70, 90, 95, and 100%. After dehydration, hexamethyldisilizane, HMDS (Sigma-Aldrich), was used to remove the alcohol. After fixation and dehydration, the samples were coated with gold before SEM imaging by a Zeiss MERLIN Field Emission SEM (Carl Zeiss GmbH, Oberkochen, Germany). All samples were scanned at a voltage of 10 kV and a working distance of 9 mm.

3.2.12 Confocal Laser Scanning Microscopy (CLSM)

CLSM was applied to characterise the live or dead bacteria on various coating surfaces. Briefly, after 24 h of bacteria culture (20 µl, 10^5 bacteria/ml) with each substrate (as described in 2.5.1.), the surfaces were gently washed with PBS to remove non-adherent bacteria. Then, the samples were stained with the Live/Dead BacLight bacterial viability kit (Invitrogen, Paisley, UK) according to the manufacturer's instructions. The kit included a solution of SYTO 9, the green-fluorescent nucleic acid stain, and propidium iodide, the red-fluorescent nucleic acid stain, in Dimethyl Sulfoxide (DMSO). Equal volumes of the components were mixed thoroughly in a microfuge tube. 5 µL of the dye mixture was added to each sample and incubated in the dark at room temperature for 15 minutes. The excitation/emission maxima of the dyes are about 480/500 nm for SYTO 9 stain and 490/635 nm for propidium iodide. The samples were characterised by non-inverted CLSM using a Leica TCS SP8 microscope. The viable bacteria appeared fluorescent green, while the non-viable bacteria appeared fluorescent red.

3.2.13 Cell viability and compatibility assessment

Cell culture

The human fetal osteoblast cell line, hFOB 1.19, obtained from ATCC, was cultured in a 1:1 mixture of Ham's F12 Medium and Dulbecco's Modified Eagle's Medium (DMEM) without phenol red, supplemented with 2.5 mM L-glutamine, 15 mM Hepes, and 0.3 mg/ml G418. This medium was further completed with 1% Penicillin-Streptomycin and 10% fetal bovine serum (FBS). The cells were incubated at 34°C until reaching confluence. Upon 90% confluence, the cells were rinsed with sterile PBS and treated with 0.25% (w/v) Trypsin-0.53 mM EDTA solution for 10 minutes at 34°C to detach them from the tissue culture polystyrene. Subsequently, the cells were transferred to a centrifuge tube containing the culture medium and centrifuged at approximately 125 x g for 5 minutes. The centrifuged cells were then diluted and subcultured at a ratio of 1:4. Cells from passage 3 were utilised in all experiments. The culture medium supplements and all reagents for

cell culture were purchased from Gibco, ThermoFisher Scientific Inc..

3.2.13 Quantification of cell viability using MTT assay

The cytotoxicity of coated titanium surfaces was assessed using the MTT (3-(4, 5-dimethylthiazolyl-2)-2, 5-diphenyltetrazolium bromide) assay supplied by Sigma Aldrich. The cell viability on each titanium sample was measured at 1, 3, 5, and 7 days post-seeding. The cells were cultured as described above, and titanium samples were washed twice with PBS and briefly soaked in ethanol before transfer to new 24-well plates. The cells were then seeded onto the coated disks (10 mm diameter), previously positioned in 24-well plates, at a density of 20,000 cells per disk, using a 20 μL drop. Following a 30-minute incubation at 37°C to facilitate cell attachment, additional medium was added to reach a total volume of 500 μL for further culture. The culture media were refreshed every 48 hours.

A blank growth medium served as the background control. At specific intervals during the incubation at 34°C, the medium in each well was substituted with 100 μL of MTT solution (0.5 mg ml^{-1} in supplemented DMEM) and incubated for 4 hours. Subsequently, the solution was aspirated, and the insoluble formazan crystals were dissolved in 100 μL of DMSO. After a 15-minute incubation period, the OD_{600} was measured at a wavelength of 570 nm using an ELISA microplate reader and expressed as a percentage relative to the absorbance of the non-toxic control. Due to the light sensitivity of the MTT reagent, all procedures were conducted in the dark.

Cell morphology

Following a similar cell culture procedure, the prepared samples were cultured with hFOB (20,000 cells cm^{-2}) to observe cell morphology after 3 and 7 days. After culturing, the surfaces were gently washed with PBS and then fixed with 4% paraformaldehyde in PBS (supplied by ThermoFisher Scientific) for 40 minutes. Following fixation, the samples were sequentially dehydrated with ethanol solutions (30, 50, 70, 80, 90, and 100% v/v) for 10 minutes each. HMDS was used to remove the alcohol. Finally, the surfaces were sputter-coated with gold, and the morphology of the cells was examined using a Zeiss MERLIN Field Emission SEM (Carl Zeiss GmbH).

3.2.14 Statistical analyses

The results are presented as mean ± standard deviation, with ($n \geq 3$) indicated. The

statistical analysis was performed using SPSS, a one-way analysis of variance, Tukey post hoc method, to evaluate significant differences between groups. A p-value of < 0.05 was considered statistically significant (*$p < 0.05$, **$p < 0.01$, ***$p < 0.001$).

3.3 Results and discussion

This study aimed to develop a biomimetic enzyme-responsive antimicrobial coating by exploiting the elastolytic degradation potential of the recombinant HELP biopolymer. A stepwise procedure was employed to initially functionalise a silanised titanium surface with HELP biopolymer, followed by the immobilisation of KR-12 on the HELP linker. Various strategies for the covalent bonding of biological molecules to titanium surfaces have been documented, with silane chemistry particularly prominent [309]. Among these approaches, APTES stands out due to its bifunctional nature. APTES possesses three alkoxy groups capable of forming siloxane bonds with titanium hydroxyl groups, while its nucleophilic amine groups serve as anchoring sites for the further attachment of bioactive compounds via crosslinking methods [48]. However, it should be noted that the siloxane bond in an APTES coating exhibits hydrolytic instability in aqueous environments, resulting in a gradual loss of covalently attached silane molecules over time. Moreover, the silanisation process yields a multimolecular layer, which may impact the alignment of peptides and introduce challenges in predicting their orientation [227].

Following silanisation, the carboxyl groups of HELP reacted with primary amine groups of APTES on the surface via an EDC/NHS activating process. As a result, the amine groups of HELP were primed as anchoring points for subsequent AMP immobilisation. In this study, various ratios of HELP and peptide were explored, and the reported concentrations represent the optimised and finalised parameters, which have been utilised for subsequent characterisations.

3.3.1 Surface characterisation by SEM, FTIR, AFM, XPS and WCA

The morphological characteristics of the surfaces were examined using SEM subsequent to each phase of surface functionalisation as depicted in Figure 3-2. Initially, untreated polished titanium (PTi) specimens displayed a smooth surface, albeit exhibiting scarcely detectible scratches attributed to experimental manipulation (Figure 3-2(a)). Following the silanisation initialised by hydroxylation through etching, a remarkable alteration in surface topography was observed ($p < 0.001$). Sil-PTi specimens subjected to the silanisation

process exhibited a roughened surface morphology characterised by a distinct ridge-like microstructure.

Direct covalent immobilisation of the KR-12 peptide (KR12-STi samples) elicited no observable impact on surface morphology compared to Sil-PTi. In contrast, the HELP attachment on the surface (HELP-STi) revealed the deposition of an opaque polymeric layer discernible on the rough titanium surface (Figure 3-2(a)). Furthermore, upon introducing KR-12 peptides after the HELP attachment, KR12-HTi samples showed no apparent changes, except for the micro-structured titanium surface becoming nearly entirely covered by a thin, blurred layer. This occurrence can be ascribed to the disentanglement of the HELP biopolymer during the peptide immobilisation process.

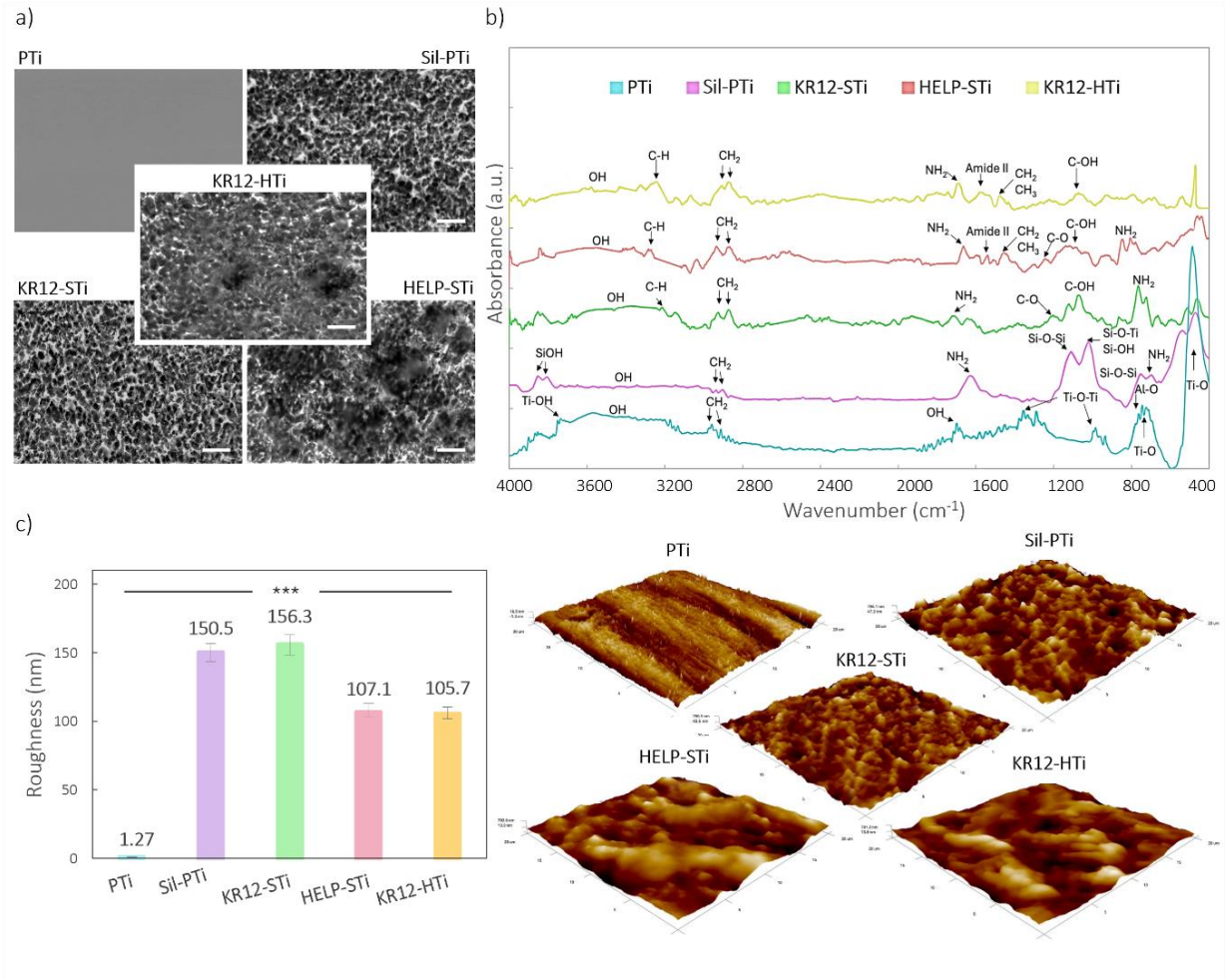


Figure 3-2. Surface characterisation of coated titanium surfaces; (a) SEM micrographs depicting the surface morphology, with a scale bar of 10 μm, (b) ATR-FTIR spectra, and (c) mean roughness (Ra) and morphology analysed by AFM 3D imaging. *** denotes statistical significance ($p < 0.001$) between the polished titanium (PTi) and all modified

surfaces.

Utilising ATR-FTIR spectroscopy provided an essential understanding of the molecular composition and structural changes throughout the coating preparation process. The obtained IR spectrum exhibited vibration bands characteristic of different stages of coating. The distinctive bonds associated with each peak are marked in the spectra, shown in Figure 3-2(b). For PTi, a prominent peak at 488 cm^{-1} is attributed to the Ti-O stretching band, characteristic of Ti6Al4V, along with bands at 735 cm^{-1} and 786 cm^{-1} corresponding to the Ti-O and Al-O bonds [250, 251]. Peaks at 998 cm^{-1} and 1413 cm^{-1} are attributed to Ti-O-Ti stretching vibration bands [145, 252]. A broad vibration band between 3150 and 3680 cm^{-1} arises from the stretching vibrations of O-H groups of physisorbed water molecules on the polished surface, while a weaker band at 1694 cm^{-1} is associated to the bending vibration of corresponding free -OH groups. Peaks at 2905 and 2943 cm^{-1}, falling between 3000 and 2800 cm^{-1}, indicate C-H absorption bands, possibly due to equipment contamination and air adsorption [252, 253].

Following silanisation with APTES, the IR spectra still show broad bands corresponding to O-H bending, albeit with decreased intensity, indicating interaction between TiO_2 and APTES molecules. The silanised surface exhibits a band at 1612 cm^{-1} corresponding to the deforming vibrations of primary amino groups and a band at 998 cm^{-1} specific to stretching vibrations in the Si-O bond of silanol groups (Si-OH) and Si-O-Ti, demonstrating APTES immobilisation through hydroxyl groups [310]. Additionally, the presence of a band at 1136 cm^{-1}, specific to Si-O-Si, suggests binding between multiple APTES molecules via ether bridges, enhancing material stability and the immobilisation process [311]. Sharp bands at 3797 and 3822 cm^{-1} indicate free silanol groups from organosilane compounds on the sample surface [310]. Furthermore, symmetric and asymmetric stretching vibrations characteristic of methylene groups from APTES are observed at 2911 and 2844 cm^{-1}, respectively [312].

After the HELP and KR-12 immobilisation, the broadness of the peak makes it challenging to distinguish individual peaks. However, characteristic peaks affirm the effectiveness of the grafting process. Sharp peaks at 2911 and 2948 cm^{-1} represent CH and CH_2 stretching and bending vibrations, while larger peaks between 1548 and 1620 cm^{-1} correspond to amide II [253, 310]. Moreover, stretching vibrations of C-H bonds are detected at 3231, 3289, and 3273 cm^{-1} in KR12-STi, HELP-STi, and KR12-HTi samples, respectively. A

peak at 1489 cm^{-1} coincides with CH_2 and CH_3 bending vibrations in the backbone of the grafted HELP biopolymer. Additional strong peaks at 1309 and 1261 cm^{-1} correspond to the C-O stretch, suggesting the presence of ester and acid [313, 314]. The primary amine group exhibits a doublet at 804 and 747 cm^{-1} for KR12-STi and 883 and 811 cm^{-1} in HELP-STi, indicating deformation vibration, while the C-O bond shows stretching vibrations at 1083 cm^{-1} and 1018 cm^{-1} [253, 315]. The broad absorption between 3650 and 3050 cm^{-1}, representing the -OH stretching region, cannot solely be attributed to -OH peaks from the carboxylic acid groups of peptides and HELP biopolymer but also to the presence of physisorbed water molecules.

Surface properties, including morphology and roughness, are critical factors affecting cell behaviour, such as adhesion, proliferation, and differentiation. AFM was employed to precisely evaluate these surface characteristics due to its ability to provide high-resolution topographical information. The surface topography was assessed after each step of the surface coating. Before the reaction, the titanium substrate exhibited a smooth morphology with very low roughness (1.2 ± 0.2 nm) due to mirror-finish polishing (Figure 3-2(b)). After silanisation, the Sil-PTi sample displayed notable alterations in surface morphology and roughness, consistent with the SEM micrographs showing a similar microstructure pattern for Sil-PTi (Figure 3-2(a)). The silanised surface exhibited a statistically significant increase in roughness (150.5 ± 8.1 nm) due to the surface pre-treatment with the etching solution. Conversely, the immobilisation of KR-12 onto the silanised surface, denoted as the KR12-STi sample, exhibited negligible alterations in both morphology and roughness. This observation suggests that the influence of the short KR-12 molecules on these surface characteristics was minimal.

The HELP integration resulted in an evident ridge-like structure (Figure 3-2(c)), demonstrating the successful assembly of HELP biopolymer onto the titanium surface. The HELP-attached surfaces exhibited reduced mean roughness values (R_a) of 107.1 ± 11.4 nm compared to Sil-PTi. This reduction suggests that the high molecular weight biopolymer of HELP serves as a covering layer for surface pores, effectively concealing sharp and large edges and imparting a smoother appearance. Following the KR-12 peptide integration for KR12-HTi, the surface morphology did not change significantly, with bulk morphology still observable. The minimal change in the morphology and roughness observed compared to the previous step is likely due to the superior coverage provided by HELP, attributed to its larger molecular size (about 30 fold). This resulted in visible

aggregation of HELP on all silanised surfaces, while the impact of the shorter molecules of KR-12 was negligible. By immobilising HELP and KR-12 on titanium surfaces and subsequently examining them with AFM, we were able to assess how these modifications influenced the surface properties and, by extension, the near-surface environment for cells. This allowed us to determine the suitability of the modified surfaces for promoting cell adhesion, and proliferation.

XPS measurements were conducted to validate the successful functionalisation and grafting at each stage of sample coating by assessing the chemical groups present on the surface. The data were analysed using CasaXPS software, employing Shirley background. These measurements aimed to determine the quantity of primary amine groups present on the silanised surface, serving as attachment points for the subsequent immobilisation steps. The XPS survey spectra (Figure S2, appendix) for each modification stage exhibited characteristic peaks corresponding to carbon (C), oxygen (O), nitrogen (N), silicon (Si), and titanium (Ti). Additionally, minimal traces of aluminium, vanadium, sulfur, and phosphorus were detected, likely originating from the Ti6Al4V alloy and contaminants introduced during sample preparation. Higher-resolution scans were conducted to further investigate the chemical bonding on the surfaces, as presented in Figure 3-3.

In the XPS region of PTi surface, the titanium (Ti 2p) peak is typically identified at around 458.7 eV. The oxygen (O 1s) peak predominantly originates from the titanium oxide layer on the surface. Additionally, the C 1s scan reveals a sharp peak attributed to residues from the polishing step, as well as the presence of carbon contamination from the equipment chamber, which is unavoidable in XPS measurements. This peak indicates the presence of C-C or C-H bonds, constituting approximately 10.49% of the atomic ratio on the surface.

Following the silanisation of titanium surfaces, the XPS survey in Figure S2, appendix revealed noticeable Si 2s and Si 2p signals in Sil-PTi compared to PTi, indicating successful grafting of APTES onto the titanium surface. The elemental composition analysis of silanised titanium samples showed an increase in N% and C% to 5.58% and 27.28%, respectively, and a decrease in O% to 42.08%. The high-resolution C 1s spectrum of the silanised surface exhibited a primary peak at 285 eV attributed to C−C and C−H bonds, originating from the presence of the propyl chain. Moreover, the high-resolution N 1s spectrum displayed two main peaks attributed to protonated and non-protonated amine groups in APTES. By measuring the percentage of N 1s in Sil-PTi (5.58%) and the ratio

of NH_2 to overall N on the surface (83.6%) after deconvolution of N 1s scan, the calculated percentage of primary amine groups on the surface, which act as anchoring points for further step, is 4.67%.

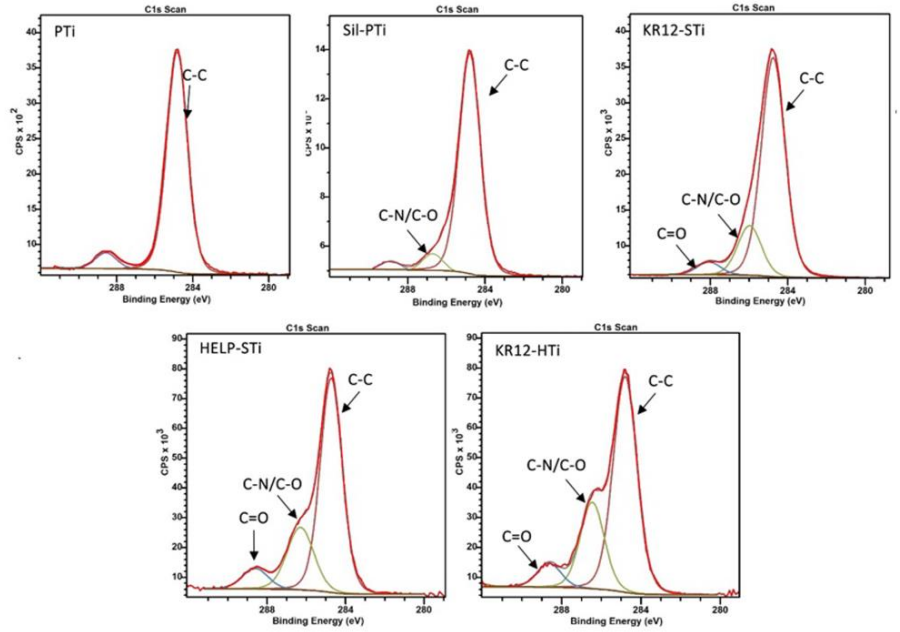
Upon the covalent immobilisation of the KR-12 peptide onto the silanised titanium surface, the amine groups on the surface formed covalent bonds with the carboxyl group of the KR-12 peptide. This led to a notable increase in the C 1s and N 1s signals, accompanied by a decrease in O and Ti signals (Figure S2, appendix). Additionally, the signals corresponding to Si 1s and Si 2p became nearly absent. Deconvolutions of the C 1s and N 1s peaks from high-resolution XPS spectra are presented in Figure 3-3. The C 1s signal of KR12-STi exhibited three peaks: one at a binding energy of 284.9 eV associated with C-C bonds, another at 286.2 eV related to C–O/C–N bonds, and a third at 288.3 eV for C=O bonds. The XPS N 1s scan of KR12-STi revealed two peaks: one at 399.8 eV corresponding to amine bonds (-NH_2) of side chains, and the one at 401.6 eV arising from amide bonds (-NHCO) confirms the covalent immobilisation of KR-12 on the surface [145]. Consequently, the nitrogen signal from the amide bonds, which are more abundant than the amines, appears more intense, as anticipated.

A subsequent increase in the nitrogen percentage, totalling 6.25 and 8.45, was noted for KR12-STi and HELP-STi, respectively, attributed to the presence of amine and amide groups within the KR-12 and HELP molecular chains. Quantitatively, the N/Ti atomic ratio rose from 0.24 to 0.31 following the immobilisation of the KR-12 peptide on the silanised surface, and from 0.68 to 0.73 for the HELP-STi and KR12-HTi. Overall, higher N/Ti and C/Ti atomic ratios were evident for the HELP-STi compared to the KR12-STi surfaces, as anticipated due to the larger molecular weight of the HELP polymers relative to the AMP KR-12. The alterations in atomic ratios of all elements were presented in Figures 3-3(c) and 3-3(d). The C 1s and N 1s scans of KR12-HTi and KR12-STi have similar peaks at identical binding energies, with variations in percentages, indicating no significant differences.

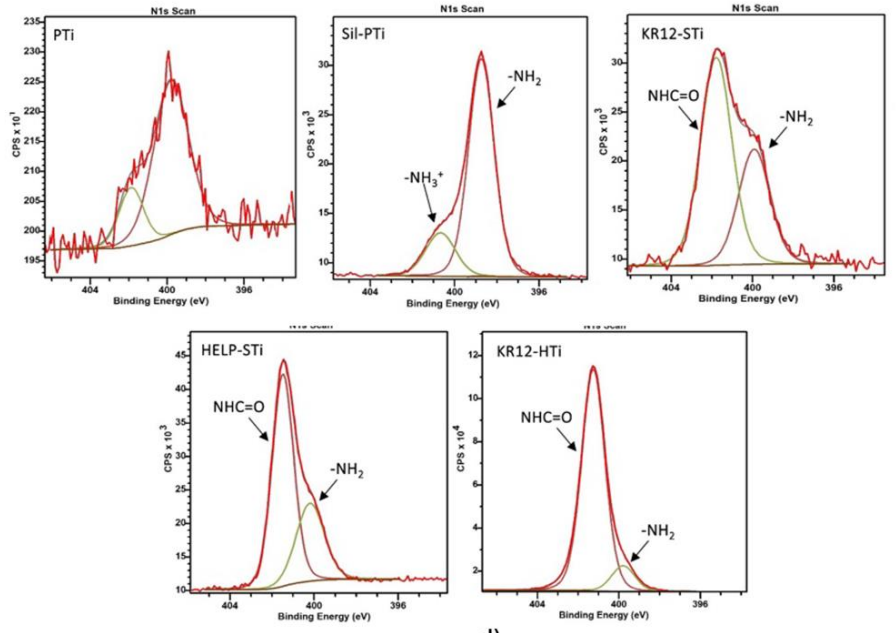
The FTIR and XPS findings illustrate the successful chemical grafting of KR-12 and HELP onto the silanised surfaces. However, due to the molecular structure resemblance between KR-12 and HELP, both composed of amino acids, precise differentiation and quantification of the immobilised peptide amount utilising XPS and FTIR poses challenges. Hence, an alternative technique using Fmoc/t-Bu strategy has been employed

to quantify the immobilised peptide content, as described in Experimental Methods (section 3.2.3.).

a)



b)



c)

	C 1s%	N 1s%	O 1s%	Si 2p%	Ti 2p%
PTi	10.49	1.17	59.15	0	29.19
Sil-PTi	27.28	5.58	42.68	1.42	23.04
KR12-STi	50.28	6.25	23.16	0.26	20.05
HELP-STi	68.61	8.45	10.41	0.12	12.41
KR12-HTi	70.28	9.04	8.32	0.11	12.25

d)

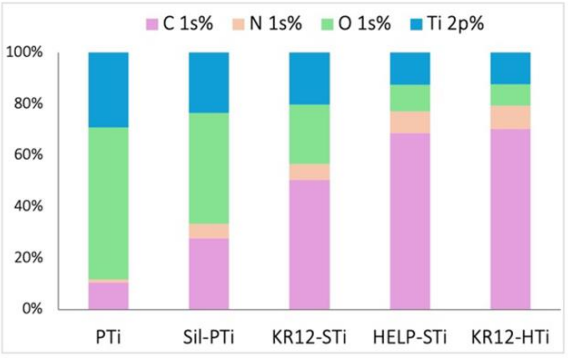


Figure 3-3. XPS analysis results for characterisation of surface elemental composition after the modification steps during the silanisation, HELP attachment and KR-12 immobilisation; (a) high-resolution C1 s spectra and (b) N 1s spectra of PTi, Sil-PTi, KR12-STi, HELP-STi, and KR12-HTi, (c) relative atomic ratios of chemical compositions, and d) ratios of different elements to Ti 2p% for all samples.

The hydrophilicity of each substrate was assessed through the WCA analysis presented in Figure 3-4. The titanium substrate exhibited a contact angle of 69.8° ± 4.7°. Subsequent silanisation resulted in a decreased contact angle for the Sil-PTi, measuring 53.6 ± 8.3°, indicating increased hydrophilicity compared to the PTi substrate (Figure 3-4). Despite the expectation of increased WCA due to the presence of the propyl chain in APTES, the hydroxyl groups and rough surface morphology led to a final reduction in WCA and a consequent increase in hydrophilicity. The covalent immobilisation of the KR-12 peptide on the titanium surface slightly decreased hydrophilicity (55.1 ± 6.2°). This reduction can be attributed to the hydrophobic amino acids present in the KR-12 peptide, such as leucine, isoleucine, and valine. Moreover, when the peptide is tethered via its C-terminal, the lysine in KR-12 becomes exposed on the surface. Lysine is a positively charged amino acid, housing a primary amine group. Although the amine group has the potential to engage in hydrogen bonding with water, it typically exhibits lower hydrophilicity in comparison to other polar functional groups such as hydroxyl (-OH) or carboxyl (-COOH). Consequently, this feature may lead to a slight increase in the overall hydrophobicity of the immobilised peptide. Nonetheless, KR12-STi can still be categorised as a hydrophilic surface due to its low WCA. It should be noted that there is no straightforward explanation relating the properties of the AMP or its orientation to the resulting WCA of the grafted surface.

The integration of HELP linkers notably increased the hydrophilicity of the titanium surface. According to the previous observations [316], the amphipathic nature of elastin-like domains enables them to reconfigure at the solid/water interface in response to the interactions with water molecules. This explains the significant reduction in WCA observed for HELP-STi surfaces (39.5° ± 7.7°). The negligible difference in hydrophilicity between HELP-STi and KR12-HTi (42.4° ± 6.9°), where the KR-12 is absent and present, respectively, suggests that the interaction with water is mainly driven by the exposure of the HELP biopolymer. This is likely due to the longer chains of HELP, which results in a higher surface coverage compared to KR-12. As indicated, incorporating the HELP linker

enhances surface hydrophilicity, potentially promoting the interaction with the biological system.

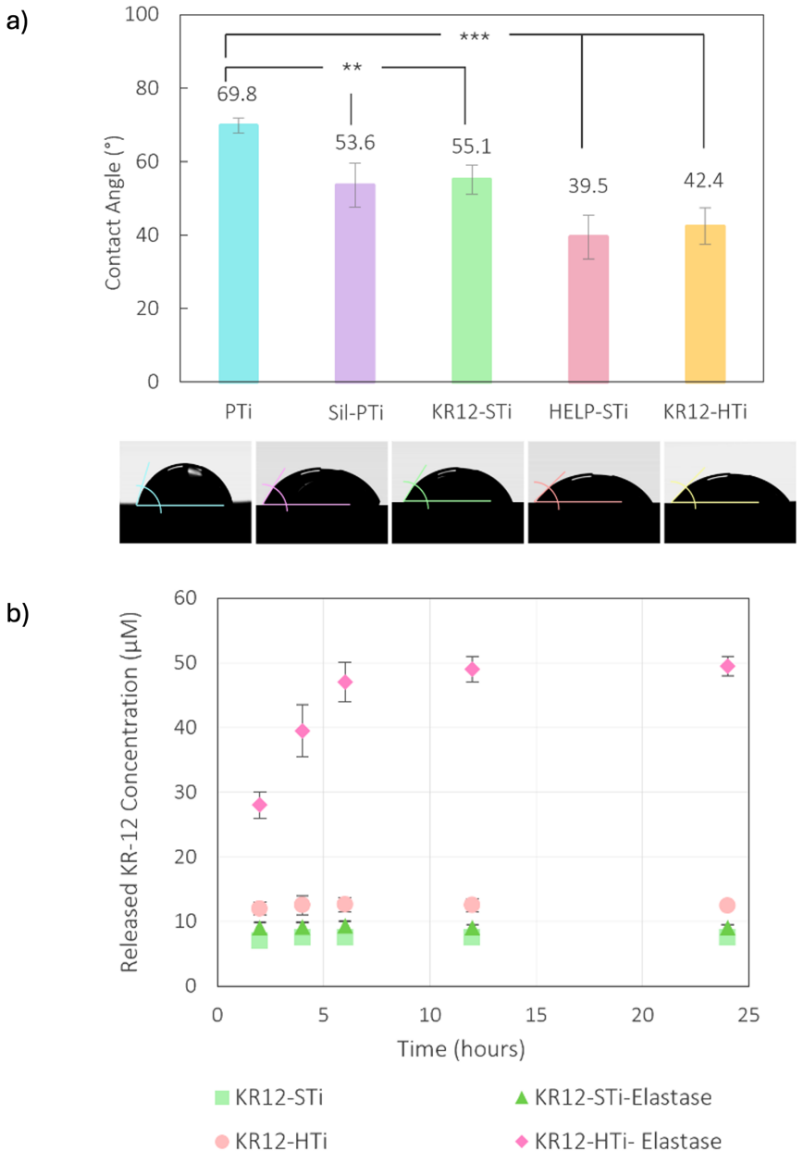


Figure 3-4. The quantitative measurement of (a) the water contact angle of each titanium substrate (**P < 0.01, ***P < 0.001) and representative images of the water drops on the different coatings, and (b) KR-12 release from coating in the absence and presence of elastase. Reactions were carried out at 37 °C for 24 hours. Following incubation, the proteolytic activities were detected by absorbance readings at 585 nm. Results were the mean ± standard deviation (SD) of three independent experiments performed in triplicate.

3.3.2 Calculation of the peptide density

The utilisation of the Fmoc/t-Bu strategy has become prevalent due to the advantageous properties of the Fmoc moiety, which exhibits absorption in the UV region. Figure S1, appendix illustrates the removal of the Fmoc group via a β-elimination reaction induced by treatment with a secondary amine, piperidine. This reaction yields the highly reactive DBF, which subsequently reacts with excess piperidine to form the DBF adduct, characterised by a distinctive UV absorbance peak at 301 nm. A calibration curve relating the concentration of the DBF-based adduct to absorbance was established by measuring UV absorption across a range of concentrations (10 to 310 μM). This curve exhibited a linear relationship with molar absorption coefficient of 8.141 $L \times mol^{-1} \times cm^{-1}$ at $\lambda = 301$ nm. Both the calibration curve and the reaction scheme are provided in Figure S1 of the appendix. The absorbance of each solution (n = 3) was assessed at $\lambda = 301$ nm and correlated with the established calibration curve. The results revealed that the quantities of Fmoc groups present on surfaces, in the presence or the absence of the HELP linker, were 61.34 nmol and 256.52 nmol, respectively, with reaction yields of 11% and 46%. KR12-HTi displayed a threefold rise in KR-12 loading compared to KR12-STi. This increase can be attributed to the higher concentration of primary amine groups in the side chains of the HELP linker acting as anchors.

3.3.3 KR-12 release triggered by elastase

This work aimed to explore the potential of HELP-based coating as a delivery system capable of releasing the antimicrobial agent under an enzymatic stimulus from the environment. As shown in Figure 3-4, a high release of KR-12 from KR12-HTi substrates was detected after incubation with elastase for 6 hours, corresponding with the high elastolytic degradation potential of HELP. It is well-known that this enzyme efficiently degrades stretches of alanines [297], like those presented in the hydrophilic domains of the HELP.

As expected, elastase exhibited very high elastolytic activity since it was able to degrade the HELP linkers on the KR12-HTi samples, detected by higher peptide release from substrates than samples without added enzyme. Both the KR12-STi with and without elastase, under similar conditions, could have slight release of 7 – 13.1 μM in 24 hours, which means that elastase was almost inactive on KR-12.

After 24 hours, 71.2 µM of the peptides were released from the KR12-HTi sample, lower than the overall amount of immobilised peptides, proving that, the grafted HELP macromolecules are less sensitive to the proteolytic activity with respect to the free form of the HELP protein in solution. In addition, a more pronounced rise in peptide release could be expected at a higher elastase concentration. Our results suggest that a substantial part of the immobilised Fmoc-labelled KR-12 was effectively released under the proteolytic stimulus.

3.3.4 Antimicrobial activity assay

S. aureus and *S. epidermidis*, as Gram-positive bacteria, and *E. coli* and *P. aeruginosa*, as Gram-negative bacteria, were specifically chosen for this study to assess the antimicrobial effectiveness of AMP-immobilised surfaces for orthopaedic applications. The antibacterial activity of the substrates was evaluated through a direct contact test, where 10^5 CFU/ml of each bacterial strain was added onto the surfaces and then incubated for 24 hours. The antimicrobial efficacy of the substrates was quantified and expressed as a percentage of bacterial killing compared to a reference (PTi) after 24 hours. The bacterial growth inhibition ratio was calculated by subtracting the colony numbers of each sample from the colony numbers of PTi and then dividing by the colony numbers of PTi, as reported in Figure 3-5(a).

PTi exhibited no antibacterial activity, while Sil-PTi showed mild antibacterial effects, with inhibition ratios ranging from 25% to 29% across all bacterial strains. This modest growth inhibition could be attributed to the rough morphology of the silanised surface, which possesses sharp edges that hinder bacterial attachment. This hypothesis was further supported by Live/Dead staining assays and SEM micrographs (Figures 3-6(b), 3-6(c)). Following modification of Sil-PTi with KR-12, KR12-STi exhibited substantial antibacterial effects, with inhibition ratios of 83.74%, 79.68%, 77.95%, and 90.81% against *E. coli*, *P. aeruginosa*, *S. aureus*, and S. *epidermidis*, respectively. Overall, the introduction of KR-12 significantly endowed titanium surfaces with antibacterial efficacy against Gram-positive and Gram-negative bacteria ($p < 0.001$), consistent with its demonstrated killing efficiency against Gram-negative bacteria in solution, reported in previous findings [40, 219, 269].

KR12-HTi demonstrated the highest antibacterial activity, with inhibition ratios of 93.74%, 99.71%, 91.86%, and 95.79% against *E. coli*, *P. aeruginosa*, *S. aureus*, and *S.*

epidermidis, respectively (Figure 3-5(a)). The antibacterial mechanism of AMPs involves the insertion of positively charged peptides into bacterial cell membranes, leading to disruption and eventual death of bacteria. AMPs with HELP biopolymer as linkers are hypothesised to interact with bacterial cell membranes more easily, thereby exhibiting superior antibacterial properties as supported by previous studies [179, 270]. Compared to KR12-STi, the KR12-HTi, supporting flexible HELP linkers increased the antimicrobial activity by an average of 14.6 % across all bacterial strains, attributed to a higher AMP density as well as to an enhanced mobility for effective bacterial interaction.

AMPs primarily exerted antibacterial effects through electrostatic interference and destabilisation of bacterial membranes. In the absence of a linker, KR12-STi destabilised bacterial membranes, increasing susceptibility to physical puncture. It has been reported that the rough surfaces, similar to that induced by silanisation process, could play a crucial role in physically puncturing destabilised bacteria, particularly effective against Gram-negative bacteria due to their thinner cell walls [268]. KR12-HTi demonstrated superior bactericidal activity against *P. aeruginosa* (the inhibition ratio of 99.71%), which is notably higher than observed for other strains. This higher inhibition ratio could be attributed to the elastase production capacity of *P. aeruginosa* [317], stimulating AMP release.To assess various substrates' bactericidal efficacy and adherence properties, we employed live/dead staining analysis, as depicted in Figures 3-6(b) and 3-6(c). In the live/dead assay, dead bacteria emitted red fluorescence, while live bacteria emitted green fluorescence. *S. aureus* and *E. coli* were selected as model bacteria of Gram-positive and Gram-negative bacteria to present the concept of bacterial behaviour on different substrates. Consistent with DCT results, live/dead staining revealed that PTi exhibited no antimicrobial activity against *S. aureus* and *E. coli*, with all bacterial colonies remaining viable and stained green.

Live/dead assay of Sil-PTi indicated that the attached bacteria were alive and green (Figure 3-5(b) and 3-6(c)). However, the number of attached bacteria was reduced with respect to the control sample, PTi, possibly due to the surface roughness, resulting in mild growth inhibition. Despite their rough morphology, both HELP-STi and KR12-HTi surfaces demonstrated greater bacterial attraction compared to Sil-PTi. The presence of HELP moiety seemed to attract the microorganisms. However, most of adhered bacteria on KR12-HTi were dead (Figure 3-5(b) and 3-5(c)).

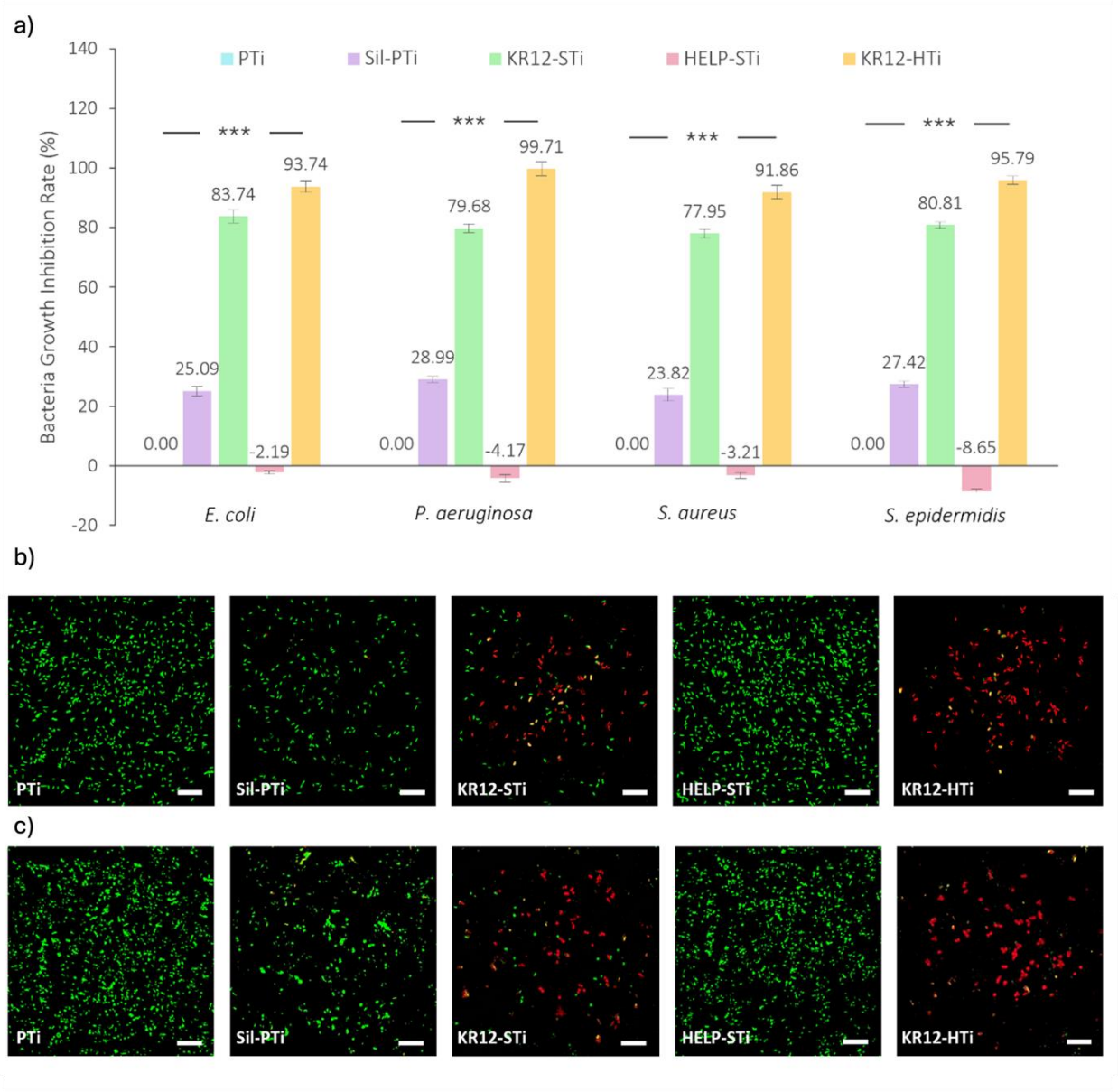


Figure 3-5. Assessment of antimicrobial activity; (a) bacterial growth inhibition ratio of the indicated surface coatings against *E. coli*, *P. aeruginosa*, *S. aureus*, and *S. epidermidis*, PTi samples were considered as controls showing 0.00% inhibition ratio. * Denotes $p < 0.05$, ** denotes $p < 0.01$, *** denotes $p < 0.001$ (all error bars denote the standard deviations over triplicate measurements), and fluorescence live/dead assay images of (b) *E. coli* and (c) *S. aureus* cultured on different coatings (Scale bars = 6 μm, green bacteria: live, red bacteria: dead). Both HELP-STi and KR12-HTi surfaces exhibited higher bacterial affinity than Sil-PTi. The inclusion of HELP as a linker appeared to amplify bacterial adhesion. However, a significant portion of bacteria that adhered to KR12-HTi were found to be deceased.

Further, we conducted SEM analyses to characterise the morphology of *E. coli* and *S. aureus* after 24 hours of the culture on the surfaces, as represented in Figure 3-6. On PTi and Sil-PTi surfaces, bacteria exhibited typical shapes with intact cell walls, suggesting a lack of antimicrobial activity. Despite the absence of biofilm formation on PTi, many bacteria adhered and aggregated. Sil-PTi, however, slightly inhibited bacterial colonisation compared to PTi, consistent with DCT and live/dead staining results. Similar cell morphology to Sil-PTi was observed for HELP-STi, coupled with increased bacterial attachment, suggesting HELP's supportive role in facilitating bacterial adhesion without detrimental effects. SEM images revealed that compared to PTi and Sil-PTi, *S. aureus* cultured on KR12-STi and KR12-HTi showed distinct morphological changes characterised by shrunken and disrupted membranes, indicative of damage. Similarly, *E. coli* on KR12-HTi and KR12-STi exhibited corrugated, distorted, and lysed morphology, suggesting membrane damage possibly induced by the AMP. It can be assumed that AMPs immobilised on KR12-HTi provided sufficient mobility to permeate the bacterial membrane, leading to bactericidal activity. On the other hand, the positively charged surfaces of KR12-STi facilitated electrostatic interactions with bacteria, thereby enhancing the efficacy of AMP action.

While SEM data alone cannot ascertain the precise mechanism of KR-12 action on cellular membranes, they strongly suggest the significant damage can be inflicted by the immobilised KR-12. Future studies employing transmission electron microscopy will provide further insights.

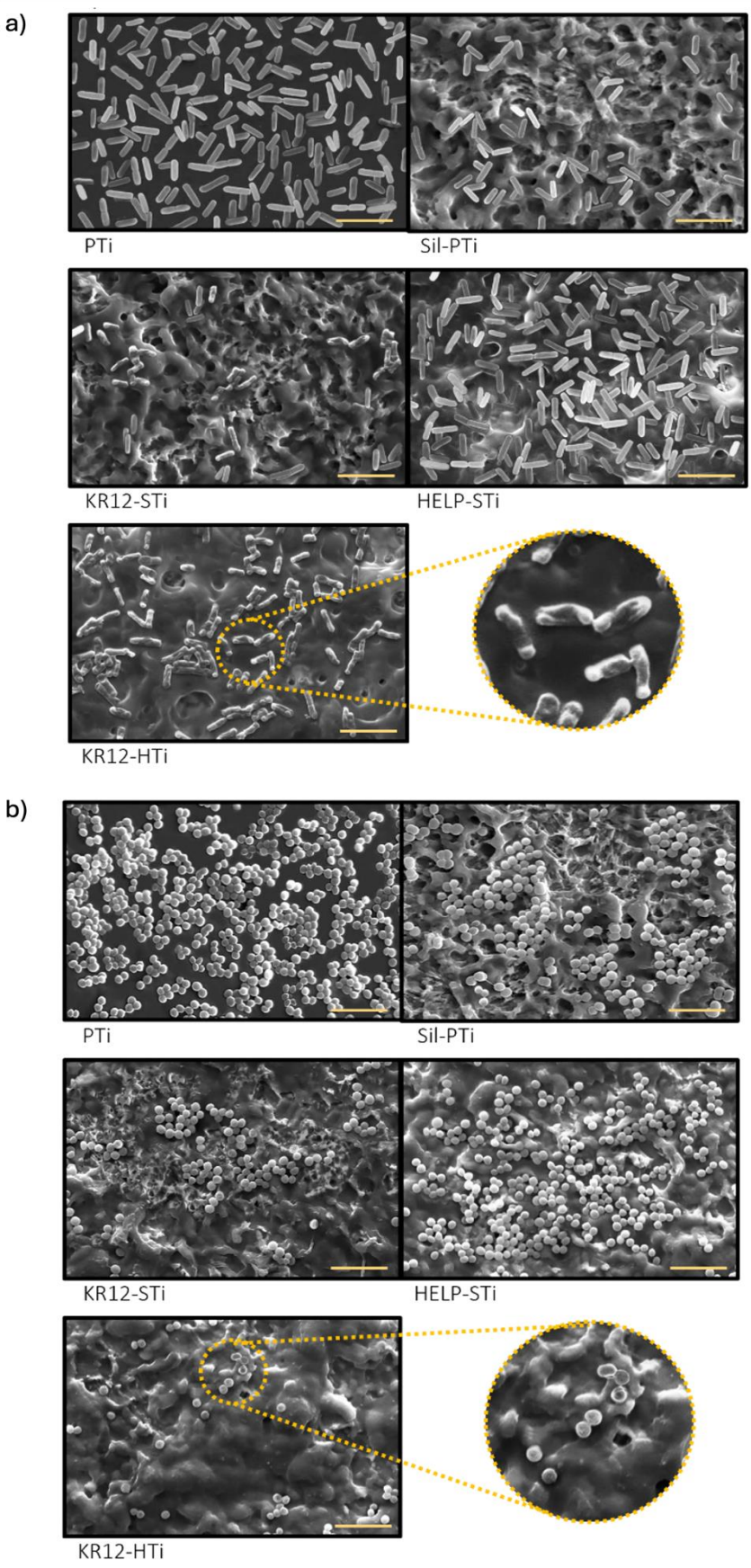


Figure 3-6. SEM characterisation of bacterial growth of substrates. SEM images of (a) *E.*

coli and (b) *S. aureus* on indicated substrates. All results were taken after 24 hours of incubation with the surface. Scale bars = 5 µm. AMPs attached to KR12-HTi and KR12-STi showed adequate bactericidal activity to disrupt the membranes of both *E. coli* and *S. aureus* bacteria.

3.3.5 Cytocompatibility and cell adhesion

The cytocompatibility of the modified titanium surfaces was evaluated using hFOB 1.19 cells, an osteoblast cell line of human origin frequently employed in studies of osteoporosis, bone tissue engineering, and orthopaedic biomaterials [271]. Cell viability was assessed via the MTT assay, which indirectly measures cell proliferation by assessing metabolic activity. It also provides a measure of cytocompatibility by determining if cells remain metabolically active when exposed to materials. Previous studies have investigated the cytotoxicity of KR-12 peptide in solution, revealing no cytotoxic effects within a specific concentration range [173, 219, 269]. However, at higher AMP concentrations, cell viability decreases. It is crucial to find a balance in loading antibacterial agents to optimise efficiency while mitigating the potential cytotoxicity. Although a high loading density of antibacterial agents can effectively eradicate bacteria, it also poses the risk of cytotoxicity.

In this study, cell viability percentages relative to control were measured at three time points (3, 5, 7 days). MTT assay results indicated higher proliferation rates of hFOB cells on titanium disks with different coatings compared to the control, standard tissue culture plastic (TCP) across all time points. This aligns with previous findings on the cytocompatibility of HELP and the low toxicity of KR-12 peptide [173, 301]. Despite exhibiting potent antimicrobial activity, KR12-HTi showed comparable biocompatibility to PTi and higher than KR12-STi surfaces. Sil-PTi and KR12-STi samples also demonstrated to support cell growth, indicating strong cell attachment despite minimal bacterial adherence, attributed to the rough morphology of the surfaces. Osteoblast cells, being larger and more resilient than bacteria, were less affected by surface roughness, thereby indicating the inherent cytocompatibility of silanised surfaces.

After 3 to 7 days of incubation, cell viability was significantly higher on HELP-STi and KR12-HTi compared to PTi, indicating good cytocompatibility even in the presence of the grafted KR-12. This excellent cell adhesion-promoting activity, attributed to HELP, aligns with the results of recent studies on its biological interactions at the molecular level [318]. These studies specifically worked on the fusion of HELP with AMPs to enhance cellular

attachment by facilitating integrin binding and interacting with ECM components. However, slightly lower viability was observed on KR12-HTi, possibly due to the release of KR-12 into the media, stemming from the destabilisation of the silanised surface [319]. In contrast to KR12-HTi, statistically significant variations ($p < 0.05$) in metabolic activity were detected between KR12-STi and PTi across all time points.

Cell adhesion and the interaction between cells and coatings play a pivotal role in successfully integrating implants into native bone tissue [203, 320]. The evaluation of cell distribution and adhesion on each surface after 3 and 7 days of incubation was performed using SEM.

The SEM images in Figure 3-7, captured on days 3 and 7, depict normal attachment and growth of hFOB cells on untreated PTi surfaces. Compared to PTi, the extent of cell spreading on Sil-PTi and KR12-STi surfaces was slightly lower on day 3, consistent with MTT results, and these cells exhibited a contracted and disjointed attachment morphology. Despite initial observations of improper cell attachment on day 3, hFOB cells showed consistent growth on Sil-PTi and KR12-STi surfaces by day 7, with flattened morphology and increased cell spreading over time, indicating viability and proliferation. The number of attached cells on HELP-STi and KR12-HTi surfaces was notably higher than Sil-PTi and KR12-STi on day 3. These attached cells displayed extensive spreading by day 7, indicative of excellent biocompatibility of the coating layer. By day 7, surfaces of HELP-STi and KR12-HTi were fully covered by a thick layer of cells with spread and flattened morphology and the formation of mineralised nodules suggesting cell-secreted mineralisation and osteoblast differentiation.

Overall, normal cell attachment and proliferation on all surfaces highlight the excellent biocompatibility of both unmodified and modified titanium alloy surfaces. By Day 7, the cells displayed spread morphology with filopodia extending towards adjacent cells, alongside the formation of mineralised deposits on KR-STi, HELP-STi, and KR-HTi surfaces (depicted by arrows in Figure 3-7(b)). Our ultimate objective was to develop multifunctional coatings integrating enhanced bone regenerative activity with stimuli responsive antimicrobialcapabilities. Achieving this goal in future requires comprehensive *in vivo* studies to assess long-term biocompatibility, detailed investigation of the molecular mechanisms underlying bone regeneration, and comprehensive examination of the host immune response to the coated implants.

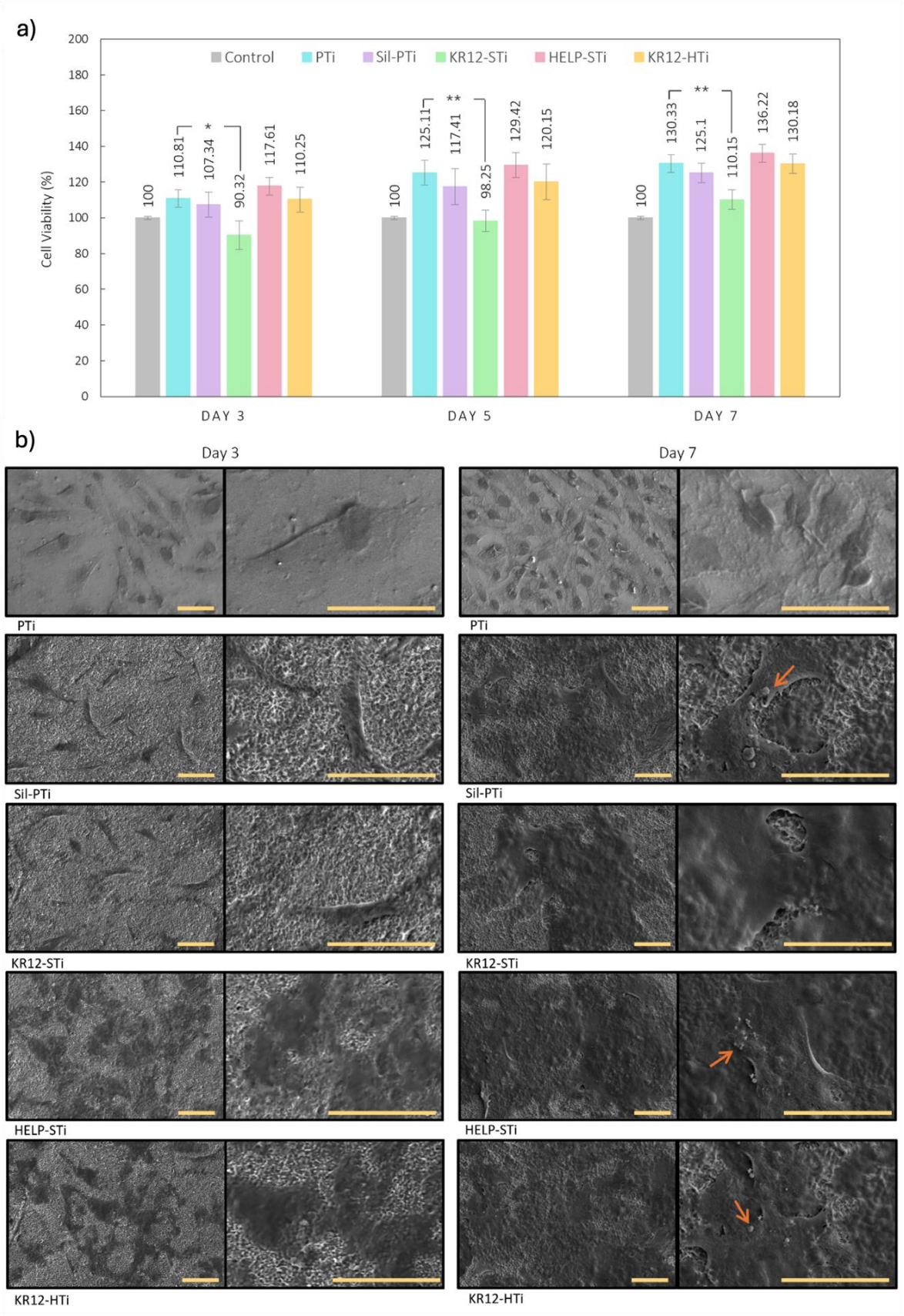


Figure 3-7. Cytocompatibility and cell morphology study; (a) cell viability results of MTT test of hFOB cells cultured on different substrates after 3, 5, and 7 days of culturing, *

denotes significant differences ($p < 0.05$) compared with PTi, and (b) SEM micrographs showing the morphology of the seeded hFOB cells on day 3 and 7. Scale bars = 20μm. By Day 7, the cells exhibited a spread morphology with filopodia extending towards adjacent cells, accompanied by the formation of mineralised deposits (depicted by arrows) on KR-STi, HELP-STi, and KR-HTi surfaces.

3.4 Conclusions

Preventing bacterial adhesion and biofilm formation while promoting osteointegration in medical implants is a significant challenge. This study explored a novel approach utilising enzyme-responsive peptide-based coatings to address this issue. By harnessing enzyme-response mechanisms, a proof of concept is presented for the development of coatings with potent antibacterial properties, improved functionalities, and enhanced cytocompatibility. Specifically, the study investigated the potential of HELP-based matrices as delivery systems triggered by enzymatic activity in the surrounding environment. During implantation, the customised interfaces encounter the innate immune response, triggering elastase release. The biodegradation of HELP biopolymer by elastase enzyme enables the controlled release of AMPs.

Through experimentation, it was demonstrated that the AMP KR-12 can be effectively immobilised onto HELP-attached titanium surfaces, named KR12-HTi, at desired densities with high reaction yields. This coating exhibited excellent antimicrobial activity against clinically significant bacteria, including *S. aureus, S. epidermidis, E. coli,* and *P. aeruginosa*. Notably, this surface displayed significant release of KR-12 upon exposure to elastase, indicating the high elastolytic degradation potential of HELP. Unlike traditional direct covalent immobilisation methods, this coating was statically versatile, offering biocompatibility and cell adhesion without external stimuli.

The study highlighted the importance of intrinsic structural factors, such as linkers, surface density, and exposure orientation, in modulating the antibacterial activity of AMPs. The utilisation of HELP as a linker resulted in a threefold increase in KR-12 loading. This enhancement can be attributed to the ability of the HELP linker to augment the number of anchors available for immobilisation, thereby increasing the density of KR-12. Surfaces grafted with HELP exhibited higher antimicrobial activity against adhered bacteria, owing not only to the increase in loading density but also to the enhanced mobility and flexibility of KR-12 due to the elongated and flexible molecular structure of HELP.

The study highlighted the potential of stimuli-responsive peptide-based coatings to reduce side effects against osteoblast cells. The release of KR-12 in response to increased elastase concentration in the surrounding environment offers a promising strategy for mitigating inflammation or infection. Finally, it is envisaged that the concourse of HELP as a linker could be implemented in new materials for a range of medical applications when drug release is required due to its double function to carry and then deliver the drug by the action of elastase enzymes.

Ethics approval and consent to participate

Ethics approval was not required for this project.

Declarations of Interests

The authors state that they have no known competing financial interests or personal relationships that could have influenced the work reported in this paper.

Credit authorship contribution statement

Mohadesh Zare: Methodology, Investigation, Formal analysis, Data curation, Writing – original draft. **Laura Colomina Alfaro:** Conceptualisation, Investigation, Data curation. **Antonella Bandiera:** Conceptualisation, Investigation, Writing – reviewing & editing. **Esra Mutlu:** Validation, Investigation. **David Grossin:** Investigation, Data curation, Writing – reviewing & editing. **Fernando Albericio:** Conceptualisation, Writing – reviewing & editing. **Sarah A. Kuehne:** Supervision, Writing – reviewing & editing. **Zubair Ahmed:** Supervision, Writing – reviewing & editing; **Artemis Stamboulis:** Supervision, Writing – reviewing & editing, Project administration, Conceptualisation, Funding acquisition.

Acknowledgements

This work is part of a project that has received funding from the European Union's Horizon 2020 research and innovation program under the Marie Skłodowska-Curie Innovative Training Network AIMed grant agreement No 861138.

3.5 References

1. Campoccia, D., L. Montanaro, and C.R. Arciola, *A review of the clinical implications of anti-infective biomaterials and infection-resistant surfaces.* Biomaterials, 2013. **34**(33): p. 8018-8029.

2. von Eiff, C., et al., *Infections Associated with Medical Devices.* Drugs, 2005. **65**(2): p. 179-214.
3. Gristina, A.G., P. Naylor, and Q. Myrvik, *Infections from biomaterials and implants: a race for the surface.* Med Prog Technol, 1988. **14**(3-4): p. 205-24.
4. Amin Yavari, S., et al., *Combating Implant Infections: Shifting Focus from Bacteria to Host.* Advanced Materials, 2020. **32**(43): p. 2002962.
5. Arciola, C.R., D. Campoccia, and L. Montanaro, *Implant infections: adhesion, biofilm formation and immune evasion.* Nature reviews microbiology, 2018. **16**(7): p. 397-409.
6. Veerachamy, S., et al., *Bacterial adherence and biofilm formation on medical implants: a review.* Proceedings of the Institution of Mechanical Engineers, Part H: Journal of Engineering in Medicine, 2014. **228**(10): p. 1083-1099.
7. Kurup, A., P. Dhatrak, and N. Khasnis, *Surface modification techniques of titanium and titanium alloys for biomedical dental applications: A review.* Materials Today: Proceedings, 2021. **39**: p. 84-90.
8. Alipal, J., et al., *An updated review on surface functionalisation of titanium and its alloys for implants applications.* Materials Today: Proceedings, 2021. **42**: p. 270-282.
9. Sun, J., et al., *Bio-clickable mussel-inspired peptides improve titanium-based material osseointegration synergistically with immunopolarization-regulation.* Bioactive Materials, 2022. **9**: p. 1-14.
10. Spriano, S., et al., *A critical review of multifunctional titanium surfaces: New frontiers for improving osseointegration and host response, avoiding bacteria contamination.* Acta biomaterialia, 2018. **79**: p. 1-22.
11. Wang, D., et al., *Antibiofilm peptides against biofilms on titanium and hydroxyapatite surfaces.* Bioactive Materials, 2018. **3**(4): p. 418-425.
12. Salwiczek, M., et al., *Emerging rules for effective antimicrobial coatings.* Trends Biotechnol, 2014. **32**(2): p. 82-90.
13. Xi, W., et al., *Point-of-care antimicrobial coating protects orthopaedic implants from bacterial challenge.* Nature Communications, 2021. **12**(1): p. 5473.
14. Cloutier, M., D. Mantovani, and F. Rosei, *Antibacterial coatings: challenges, perspectives, and opportunities.* Trends in biotechnology, 2015. **33**(11): p. 637-652.
15. Fjell, C.D., et al., *Designing antimicrobial peptides: form follows function.* Nature Reviews Drug Discovery, 2012. **11**(1): p. 37-51.

16. Magana, M., et al., *The value of antimicrobial peptides in the age of resistance.* The Lancet Infectious Diseases, 2020. **20**(9): p. e216-e230.
17. Mookherjee, N., et al., *Antimicrobial host defence peptides: functions and clinical potential.* Nat Rev Drug Discov, 2020. **19**(5): p. 311-332.
18. Lazzaro, B.P., M. Zasloff, and J. Rolff, *Antimicrobial peptides: Application informed by evolution.* Science, 2020. **368**(6490): p. eaau5480.
19. Engelberg, Y. and M. Landau, *The Human LL-37 (17-29) antimicrobial peptide reveals a functional supramolecular structure.* Nature communications, 2020. **11**(1): p. 3894.
20. Ajish, C., et al., *A novel hybrid peptide composed of LfcinB6 and KR-12-a4 with enhanced antimicrobial, anti-inflammatory and anti-biofilm activities.* Scientific Reports, 2022. **12**(1): p. 4365.
21. Lakshmaiah Narayana, J., et al., *Short and robust anti-infective lipopeptides engineered based on the minimal antimicrobial peptide KR12 of human LL-37.* ACS infectious diseases, 2021. **7**(6): p. 1795-1808.
22. Bechinger, B. and S.-U. Gorr, *Antimicrobial peptides: mechanisms of action and resistance.* Journal of dental research, 2017. **96**(3): p. 254-260.
23. Meng, X., et al., *KR-12 coating of polyetheretherketone (PEEK) surface via polydopamine improves osteointegration and antibacterial activity in vivo.* Journal of Materials Chemistry B, 2020. **8**(44): p. 10190-10204.
24. Ao, H., et al., *Covalent immobilization of KR-12 peptide onto a titanium surface for decreasing infection and promoting osteogenic differentiation.* Rsc Advances, 2016. **6**(52): p. 46733-46743.
25. Li, H., et al., *The antimicrobial peptide KR-12 promotes the osteogenic differentiation of human bone marrow stem cells by stimulating BMP/SMAD signaling.* RSC advances, 2018. **8**(28): p. 15547-15557.
26. Kazemzadeh-Narbat, M., et al., *Strategies for antimicrobial peptide coatings on medical devices: a review and regulatory science perspective.* Critical Reviews in Biotechnology, 2021. **41**(1): p. 94-120.
27. Holmberg, K.V., et al., *Bio-inspired stable antimicrobial peptide coatings for dental applications.* Acta Biomater, 2013. **9**(9): p. 8224-31.
28. Chen, J., et al., *Preparation of an antimicrobial surface by direct assembly of antimicrobial peptide with its surface binding activity.* Journal of materials chemistry. B, 2017. **5**(13): p. 2407-2415.

29. Fang, Z., et al., *High-throughput screening and rational design of biofunctionalized surfaces with optimized biocompatibility and antimicrobial activity.* Nature Communications, 2021. **12**(1): p. 3757.
30. Yazici, H., et al., *Self-assembling antimicrobial peptides on nanotubular titanium surfaces coated with calcium phosphate for local therapy.* Mater Sci Eng C Mater Biol Appl, 2019. **94**: p. 333-343.
31. Gevrek, T.N., et al., *Thiol-Reactive Polymers for Titanium Interfaces: Fabrication of Antimicrobial Coatings.* ACS Applied Polymer Materials, 2019. **1**(6): p. 1308-1316.
32. Costa, F., et al., *Covalent immobilization of antimicrobial peptides (AMPs) onto biomaterial surfaces.* Acta biomaterialia, 2011. **7**(4): p. 1431-1440.
33. Onaizi, S.A. and S.S.J. Leong, *Tethering antimicrobial peptides: Current status and potential challenges.* Biotechnology Advances, 2011. **29**(1): p. 67-74.
34. Wu, X., et al., *Flexible peptide linkers enhance the antimicrobial activity of surface-immobilized bacteriolytic enzymes.* ACS applied materials & interfaces, 2018. **10**(43): p. 36746-36756.
35. Shriver-Lake, L.C., G.P. Anderson, and C.R. Taitt, *Effect of linker length on cell capture by poly (ethylene glycol)-immobilized antimicrobial peptides.* Langmuir, 2017. **33**(11): p. 2878-2884.
36. Xi, D., et al., *Design, expression and characterization of the hybrid antimicrobial peptide LHP7, connected by a flexible linker, against Staphylococcus and Streptococcus.* Process biochemistry, 2013. **48**(3): p. 453-461.
37. Xin, H., et al., *One-step preparation of the engineered titanium implant by rationally designed linear fusion peptides with spacer-dependent antimicrobial, anti-inflammatory and osteogenic activities.* Chemical Engineering Journal, 2021. **424**: p. 130380.
38. Chen, J., et al., *Fusion peptide engineered "statically-versatile" titanium implant simultaneously enhancing anti-infection, vascularization and osseointegration.* Biomaterials, 2021. **264**: p. 120446.
39. Chen, X., et al., *In vivo osseointegration of dental implants with an antimicrobial peptide coating.* Journal of Materials Science: Materials in Medicine, 2017. **28**: p. 1-9.
40. Xu, L., et al., *Conversion of broad-spectrum antimicrobial peptides into species-specific antimicrobials capable of precisely targeting pathogenic bacteria.* Scientific Reports, 2020. **10**(1): p. 944.

41. Devnarain, N., et al., *Intrinsic stimuli-responsive nanocarriers for smart drug delivery of antibacterial agents—An in-depth review of the last two decades.* Wiley Interdisciplinary Reviews: Nanomedicine and Nanobiotechnology, 2021. **13**(1): p. e1664.
42. Zuo, Y.-M., et al., *Enzyme-Responsive Ag Nanoparticle Assemblies in Targeting Antibacterial against Methicillin-Resistant Staphylococcus Aureus.* ACS Applied Materials & Interfaces, 2020. **12**(4): p. 4333-4342.
43. Sun, Y., et al., *An enzyme-responsive and transformable PD-L1 blocking peptide-photosensitizer conjugate enables efficient photothermal immunotherapy for breast cancer.* Bioactive Materials, 2023. **22**: p. 47-59.
44. Jiang, L., et al., *Light-triggered nitric oxide release and structure transformation of peptide for enhanced intratumoral retention and sensitized photodynamic therapy.* Bioactive Materials, 2022. **12**: p. 303-313.
45. Suo, H., et al., *Injectable and pH-sensitive hyaluronic acid-based hydrogels with on-demand release of antimicrobial peptides for infected wound healing.* Biomacromolecules, 2021. **22**(7): p. 3049-3059.
46. Tan, P., et al., *pH-Triggered Size-transformable and Bioactivity-switchable Self-assembling Chimeric Peptide Nano-assemblies for Combating Drug-Resistant Bacteria and Biofilms.* Advanced Materials, 2023: p. 2210766.
47. Freitas, E.D., et al., *Antimicrobial peptides and their potential application in antiviral coating agents.* Colloids and Surfaces B: Biointerfaces, 2022. **217**: p. 112693.
48. Asif, F., et al., *Antimicrobial peptides as therapeutics: Confronting delivery challenges to optimize efficacy.* The Microbe, 2024. **2**: p. 100051.
49. van Strien, J., et al., *Elastin-like polypeptide-based micelles as a promising platform in nanomedicine.* Journal of Controlled Release, 2023. **353**: p. 713-726.
50. Bandiera, A., et al., *Human elastin-like polypeptides as a versatile platform for exploitation of ultrasensitive bilirubin detection by UnaG.* Biotechnology and Bioengineering, 2020. **117**(2): p. 354-361.
51. Sarangthem, V., et al., *Application of elastin-like polypeptide (ELP) containing extra-cellular matrix (ECM) binding ligands in regenerative medicine.* International Journal of Biological Macromolecules, 2022. **207**: p. 443-453.

52. Colomina – Alfaro, L., et al., *A Versatile Elastin-Like Carrier for Bioactive Antimicrobial Peptide Production and Delivery.* Macromolecular Bioscience. **n/a**(n/a): p. 2300236.
53. Bandiera, A., et al., *Stimuli-Induced Release of Compounds from Elastin Biomimetic Matrix.* Biomacromolecules, 2014. **15**(1): p. 416-422.
54. Guo, Z., et al., *Design of functional hydrogels using smart polymer based on elastin-like polypeptides.* Chemical Engineering Journal, 2022. **435**: p. 135155.
55. Colomina-Alfaro, L., et al., *Smart tools for antimicrobial peptides expression and application: The elastic perspective.* Biotechnology and Bioengineering, 2023. **120**(2): p. 323-332.
56. Corich, L., et al., *Evaluation of a biomimetic 3D substrate based on the Human Elastin-like Polypeptides (HELPs) model system for elastolytic activity detection.* Journal of Biotechnology, 2017. **255**: p. 57-65.
57. Bandiera, A., et al., *3D-printed scaffold composites for the stimuli-induced local delivery of bioactive adjuncts.* Biotechnology and Applied Biochemistry, 2022. **69**(5): p. 1793-1804.
58. Bandiera, A., *Elastin-like polypeptides: the power of design for smart cell encapsulation.* Expert Opinion on Drug Delivery, 2017. **14**(1): p. 37-48.
59. Fischer, N.G., et al., *Antimicrobial and enzyme-responsive multi-peptide surfaces for bone-anchored devices.* Materials Science and Engineering: C, 2021. **125**: p. 112108.
60. Heinz, A., *Elastases and elastokines: elastin degradation and its significance in health and disease.* Critical reviews in biochemistry and molecular biology, 2020. **55**(3): p. 252-273.
61. Hancock, R.E.W. and H.-G. Sahl, *Antimicrobial and host-defense peptides as new anti-infective therapeutic strategies.* Nature Biotechnology, 2006. **24**(12): p. 1551-1557.
62. Nie, B., et al., *Covalent immobilization of enoxacin on titanium surface by APTES silanization for anti-bacteria and in vivo prophylaxis of MRSA infection.* Journal of Orthopaedic Translation, 2016. **7**: p. 78-79.
63. Bandiera, A., et al., *Expression and characterization of human-elastin-repeat-based temperature-responsive protein polymers for biotechnological purposes.* Biotechnology and Applied Biochemistry, 2005. **42**(3): p. 247-256.

64. Meyer, D.E. and A. Chilkoti, *Purification of recombinant proteins by fusion with thermally-responsive polypeptides.* Nature Biotechnology, 1999. **17**(11): p. 1112-1115.
65. Rezvanian, P., et al., *Enhanced Biological Response of AVS-Functionalized Ti-6Al-4V Alloy through Covalent Immobilization of Collagen.* Scientific Reports, 2018. **8**(1): p. 3337.
66. Nie, B.e., et al., *Covalent immobilization of KR-12 peptide onto a titanium surface for decreasing infection and promoting osteogenic differentiation.* RSC Advances, 2016. **6**(52): p. 46733-46743.
67. Jacob, B., et al., *Short KR-12 analogs designed from human cathelicidin LL-37 possessing both antimicrobial and antiendotoxic activities without mammalian cell toxicity.* J Pept Sci, 2013. **19**(11): p. 700-7.
68. Blasi-Romero, A., et al., *KR-12 Derivatives Endow Nanocellulose with Antibacterial and Anti-Inflammatory Properties: Role of Conjugation Chemistry.* ACS Applied Materials & Interfaces, 2023. **15**(20): p. 24186-24196.
69. Al Musaimi, O., et al., *Calculating Resin Functionalization in Solid-Phase Peptide Synthesis Using a Standardized Method based on Fmoc Determination.* ACS Combinatorial Science, 2019. **21**(11): p. 717-721.
70. Oliveira, W., et al., *Staphylococcus aureus and Staphylococcus epidermidis infections on implants.* Journal of hospital infection, 2018. **98**(2): p. 111-117.
71. Jiang, N., et al., *Antibiotic loaded β-tricalcium phosphate/calcium sulfate for antimicrobial potency, prevention and killing efficacy of Pseudomonas aeruginosa and Staphylococcus aureus biofilms.* Scientific Reports, 2021. **11**(1): p. 1446.
72. Crémet, L., et al., *Orthopaedic-implant infections by Escherichia coli: Molecular and phenotypic analysis of the causative strains.* Journal of Infection, 2012. **64**(2): p. 169-175.
73. Miles, A.A., S. Misra, and J. Irwin, *The estimation of the bactericidal power of the blood.* Epidemiology & Infection, 1938. **38**(6): p. 732-749.
74. Chouirfa, H., et al., *Review of titanium surface modification techniques and coatings for antibacterial applications.* Acta Biomater, 2019. **83**: p. 37-54.
75. Godoy-Gallardo, M., et al., *Antibacterial Properties of hLf1–11 Peptide onto Titanium Surfaces: A Comparison Study Between Silanization and Surface Initiated Polymerization.* Biomacromolecules, 2015. **16**(2): p. 483-496.

76. Gómez-Arribas, L.N., et al., *Hierarchically Imprinted Polymer for Peptide Tag Recognition Based on an Oriented Surface Epitope Approach.* ACS Applied Materials & Interfaces, 2020. **12**(43): p. 49111-49121.
77. Ferraris, S., et al., *Surface modification of Ti–6Al–4V alloy for biomineralization and specific biological response: Part I, inorganic modification.* Journal of Materials Science: Materials in Medicine, 2011. **22**(3): p. 533-545.
78. Ma, L., et al., *Biomimetic Ti–6Al–4V alloy/gelatin methacrylate hybrid scaffold with enhanced osteogenic and angiogenic capabilities for large bone defect restoration.* Bioactive Materials, 2021. **6**(10): p. 3437-3448.
79. Sandomierski, M., et al., *Improving the abrasion resistance of Ti6Al4V alloy by modifying its surface with a diazonium salt and attaching of polyurethane.* Sci Rep, 2020. **10**(1): p. 19289.
80. Marsotto, M., et al., *Multifunctional Platform for Covalent Titanium Coatings: Micro-FTIR, XPS, and NEXAFS Characterizations.* Langmuir, 2023. **39**(19): p. 6837-6845.
81. Ranjit, E., S. Hamlet, and R.M. Love, *Keratin coated titanium as an aid to osseointegration: Physicochemical and mechanical properties.* Surface and Coatings Technology, 2023. **462**: p. 129457.
82. Ataabadi, M.R. and M. Jamshidi, *Silane modification of TiO2 nanoparticles and usage in acrylic film for effective photocatalytic degradation of methylene blue under visible light.* Scientific Reports, 2023. **13**(1): p. 7383.
83. Wang, L., et al., *Rational design of honeycomb-like APTES-TiO2/COF heterostructures: Promoted intramolecular charge transfer for visible-light-driven catalytic CO2 reduction.* Chemical Engineering Journal, 2023. **456**: p. 140990.
84. Massoumi, H., et al., *Nitric Oxide Release and Antibacterial Efficacy Analyses of S-Nitroso-N-Acetyl-Penicillamine Conjugated to Titanium Dioxide Nanoparticles.* ACS Applied Bio Materials, 2022. **5**(5): p. 2285-2295.
85. Eliaz, D., et al., *Micro and nano-scale compartments guide the structural transition of silk protein monomers into silk fibers.* Nature communications, 2022. **13**(1): p. 7856.
86. He, Z., et al., *Investigation of the chemical changes and mechanism of the epoxy-amine system by in situ infrared spectroscopy and two-dimensional correlation analysis.* Polymer Journal, 2022. **54**(12): p. 1445-1452.
87. Çelebi, B., et al., *Human Elastin-Based Recombinant Biopolymers Improve Mesenchymal Stem Cell Differentiation.* Macromolecular Bioscience, 2012. **12**(11): p. 1546-1554.

88. Lei, R., et al., *Turning cationic antimicrobial peptide KR-12 into self-assembled nanobiotics with potent bacterial killing and LPS neutralizing activities.* Nanoscale, 2024. **16**(2): p. 887-902.
89. Jacob, B., et al., *Short KR-12 analogs designed from human cathelicidin LL-37 possessing both antimicrobial and antiendotoxic activities without mammalian cell toxicity.* Journal of peptide science, 2013. **19**(11): p. 700-707.
90. Yu, K., et al., *Toward Infection-Resistant Surfaces: Achieving High Antimicrobial Peptide Potency by Modulating the Functionality of Polymer Brush and Peptide.* ACS Applied Materials & Interfaces, 2015. **7**(51): p. 28591-28605.
91. Beveridge, T.J., *Structures of gram-negative cell walls and their derived membrane vesicles.* Journal of bacteriology, 1999. **181**(16): p. 4725-4733.
92. van der Plas, M.J.A., et al., *Pseudomonas aeruginosa elastase cleaves a C-terminal peptide from human thrombin that inhibits host inflammatory responses.* Nature Communications, 2016. **7**(1): p. 11567.
93. Nemcakova, I., et al., *Heat treatment dependent cytotoxicity of silicalite-1 films deposited on Ti-6Al-4V alloy evaluated by bone-derived cells.* Scientific Reports, 2020. **10**(1): p. 9456.
94. Colomina-Alfaro, L., et al., *Materials derived from the human elastin-like polypeptide fusion with an antimicrobial peptide strongly promote cell adhesion.* Journal of Materials Chemistry B, 2024. **12**(36): p. 8966-8976.
95. Wanag, A., et al., *Influence of modification of titanium dioxide by silane coupling agents on the photocatalytic activity and stability.* Journal of Environmental Chemical Engineering, 2020. **8**(4): p. 103917.
96. Jiang, P., et al., *Advanced surface engineering of titanium materials for biomedical applications: From static modification to dynamic responsive regulation.* Bioactive Materials, 2023. **27**: p. 15-57.
97. Huang, X., et al., *Biomaterial scaffolds in maxillofacial bone tissue engineering: A review of recent advances.* Bioactive Materials, 2024. **33**: p. 129-156.

Chapter Four:

General Discussion

4.1. Research steps and objectives

Biomedical implants, while effective in forming functional interfaces with living tissues, are vulnerable to bacterial infections, which can frequently result in implant failure [1, 2]. To address this, various strategies have been developed, including the use of bactericidal agents to inhibit bacterial attachment and antifouling agents that cause bacterial cell death by either disrupting cell membranes or penetrating them. However, the effectiveness of some bactericidal agents, such as antibiotics, is diminished due to the rise of bacterial resistance [3, 4]. Consequently, recent studies have identified antimicrobial peptides (AMPs) as a promising alternative to conventional antimicrobial agents [5, 6].

This thesis focused on identifying the optimal strategy for the immobilisation of AMPs taking into account the surface material, peptide structure, and the functional groups available for attachment. A key challenge in peptide immobilisation is ensuring that AMPs retain sufficient flexibility and freedom to interact effectively with bacterial cells [7]. Additionally, it is crucial to immobilise an optimised concentration of AMPs on the surface to achieve effective antimicrobial activity [8].

To achieve long-term stability, AMPs must be covalently immobilised, necessitating chemical reactions between the peptides and the surface. Polymeric surfaces are generally more straightforward to work with than metal surfaces, as metals require prior functionalisation to introduce reactive groups that can engage in subsequent chemical reactions with the AMPs.

4.2. Phase one:

To effectively prevent bacterial biofilm formation, it is essential to integrate both antifouling and bactericidal properties while supporting tissue integration. Our strategy utilises the immobilisation of the KR-12 peptide, a bactericidal agent, onto titanium implant surfaces. This is achieved through the use of polyethylene-glycol (PEG) as a linker, which not only imparts antifouling characteristics but also enhances the mobility of the peptide, thereby increasing its antimicrobial effectiveness [9].

There are several techniques available for grafting PEG and peptide molecules onto titanium surfaces, including wet chemical methods and low-pressure plasma processes [10-14]. Firstly, our research emphasises plasma treatment due to its advantages in introducing functional groups, streamlining chemical reactions, and reducing processing

time. [15-18]. Plasma treatment also enhances surface energy and wettability, which aids in protein adsorption and encourages desirable cellular responses without altering the surface's topography [18, 19]. The primary amine groups generated during plasma treatment can strongly bond to titanium surfaces, serving as robust anchors for bioactive agents and positively influencing cell adhesion and signaling. However, despite being a well-established method for covalent binding, plasma treatment has been less successful in immobilising antimicrobial agents compared to wet chemical approaches, largely due to its relatively low efficiency in generating functional groups.

The initial objective in the first phase of this study was to optimise the plasma treatment parameters to produce surface-bound amine groups at levels comparable to those achieved through chemical methods such as silanisation. Following plasma treatment, the antimicrobial coating was prepared by introducing primary amine groups, followed by attaching PEG molecular chains as a linker and chemically bonding the AMP KR-12 to the surface using the EDC/NHS coupling reaction.

This approach resulted in a trifunctional coating that integrates: (i) the cell adhesion properties of plasma-treated surfaces, (ii) the antifouling characteristics of PEG, and (iii) the antimicrobial activity of the KR-12 peptide.

This approach was selected not only to reduce the number of chemical reaction steps but also to take advantage of the improved biocompatibility offered by the plasma-treated surface.

In this study, plasma treatments were conducted using a purpose-designed reactor featuring adjustable plasma parameters. Surface reactions in a plasma environment, such as etching, activation, or cross-linking, depend on the plasma gas composition and process conditions, which makes the optimisation crucial for achieving the desired effects [20].

Low temperature plasma (LTP) treatments are preferred in biomaterials research due to their stable discharge and better control over plasma reactions [21, 22]. This produces more uniform treatment, minimises unwanted defects like sample heating, and enhances surface functionalisation and hydrophilicity [20]. The optimised plasma parameters obtained in this study to maximise the primary amine groups are presented in Table 4-1.

Table 4-1. Optimised plasma parameters to maximise the primary amine groups.

Voltage supplier	N_2/H_2 gas ratio	Flow rate (SCCM)	Distance	Pressure (mbar)	Frequency (kHz)	Pulsed duration (µs)	Time (seconds)
Pulsed DC-2 kV	25 / 75	10 /10	Afterglow 7 cm	0.6	20	5	60

After optimising the plasma treatment conditions, it was able to immobilise the AMPs directly on the treated surface. But, directly immobilising peptides onto plasma-treated surfaces can restrict their mobility and affect their orientation due to steric hindrance, which may decrease their effectiveness. To address this, carboxyl groups on functionalised PEG were reacted with primary amine groups on the plasma-treated surface using an EDC/NHS activation process after plasma treatment. This kept the amine groups on the PEG free that acted as anchors for the attachment of AMPs. This study explored various PEG-to-peptide ratios, with the reported concentrations representing the optimised parameters for further characterisation.

XPS measurements were conducted to validate the functionalisation and grafting processes during coating preparation by analysing the chemical groups present on the surface. After deconvolution of the N 1s scan, it was determined that the percentage of N 1s in NH_2-Ti and the NH_2-to-total-N ratio on the surface resulted in 9.18% of the surface being composed of primary amine groups, essential for further steps.

4.3. Phase two:

Although numerous methods for immobilising AMPs have been explored, they often fail to respond dynamically to biological signals. This study introduces an enzyme-responsive antimicrobial coating for orthopaedic devices that utilises the AMP KR-12 along with Human Elastin-Like Polypeptide (HELP) as a biomimetic, stimuli-responsive linker designed to mimic extracellular matrix (ECM) components. Upon implantation, these specialised coatings interact with the innate immune response, leading to the release of elastase. The elastase enzyme then biodegrades the HELP biopolymer, facilitating the controlled release of KR-12.

A systematic procedure was used to develop an enzyme-responsive antimicrobial coating, beginning with the polishing and silanisation of the titanium surface using 3-Aminopropyltriethoxysilane (APTES) to introduce primary amine groups. This was followed by attaching the HELP biopolymer as an enzyme-responsive linker between the

surface and the antimicrobial peptide (AMP) KR-12, utilizing the EDC/NHS coupling reaction. Finally, the process involved a chemical reaction between the AMP KR-12 and the HELP linker using the same EDC/NHS reaction to complete the immobilisation.

Silane-based methods for covalently bonding biological molecules to titanium surfaces have been widely studied, with silane chemistry being a prominent technique [297]. Among these, APTES is notable for its dual functionality. APTES has three alkoxy groups that form siloxane bonds with titanium hydroxyl groups and nucleophilic amine groups that serve as sites for further bioactive compound attachment via crosslinking [44]. Different ratios of HELP to KR-12 were evaluated, and the concentrations presented in this study were the optimised conditions used for further characterisation.

XPS measurements were conducted to quantify the primary amine groups on the silanised surface, which serve as attachment sites for subsequent immobilisation steps. After silanising the titanium surfaces, the high-resolution N 1s spectrum showed two main peaks, corresponding to protonated and non-protonated amine groups in APTES. By analysing the N 1s signal and calculating the ratio of NH_2 to total nitrogen after deconvolution, it was determined that 4.67% of the surface comprised primary amine groups, which are critical for further functionalisation.

The potential of a HELP-based coating as a delivery system was investigated for the controlled release of antimicrobial agents in response to an enzymatic stimulus from the environment. A significant release of KR-12 peptides from the substrates was observed following a 6-hour incubation with elastase, which is consistent with the high elastolytic degradation capability of HELP. Elastase is well-known for efficiently breaking down alanine-rich sequences, which are prevalent in the hydrophilic domains of HELP [23]. As anticipated, elastase demonstrated robust elastolytic activity by degrading the HELP linkers on the samples, leading to a higher release of peptides compared to samples without the enzyme. In contrast, samples lacking the HELP linker showed minimal release of KR-12 over 24 hours, indicating that elastase had little impact on KR-12 in the absence of the linker. After 24 hours, a substantial amount of peptides (71.2 μM) was released from the samples containing the HELP linker, though this was less than the total immobilised peptide amount. This suggests that the grafted HELP macromolecules are less susceptible to proteolytic degradation compared to the free HELP protein in solution. The findings indicate that a significant portion of the immobilised Fmoc-labelled KR-12 was

successfully released in response to the proteolytic stimulus.

4.5. Overall comparison of findings

In this study, to develop advanced antimicrobial coatings for titanium implant surfaces using AMPs, two methods—plasma treatment and silanisation—were employed in separate phases of this study. Titanium implants were functionalised with the KR-12 peptide using these techniques to introduce amine groups on the surface, facilitating subsequent reactions with KR-12. Additionally, the study investigated the influence of different linkers on the antimicrobial efficacy of the peptides through surface characterisations, biological assays, and antimicrobial evaluations.

The plasma treatment method introduced 9.18% primary amine groups on the surface, compared to 4.67% for the silanisation technique. Despite this higher percentage of primary amine groups on plasma-treated surfaces, the peptide immobilisation results were almost similar: 59.67% for plasma-treated surfaces and 61.34% for silanised surfaces. Although plasma treatment provided a higher concentration of primary amine groups, the peptide immobilisation levels were comparable between the two methods. This discrepancy may be attributed to the fact that the primary amine groups on plasma-treated surfaces, while more numerous, are less stable than those on silanised surfaces. Consequently, some amine groups on the plasma-treated surfaces may have been lost during the peptide immobilisation process.

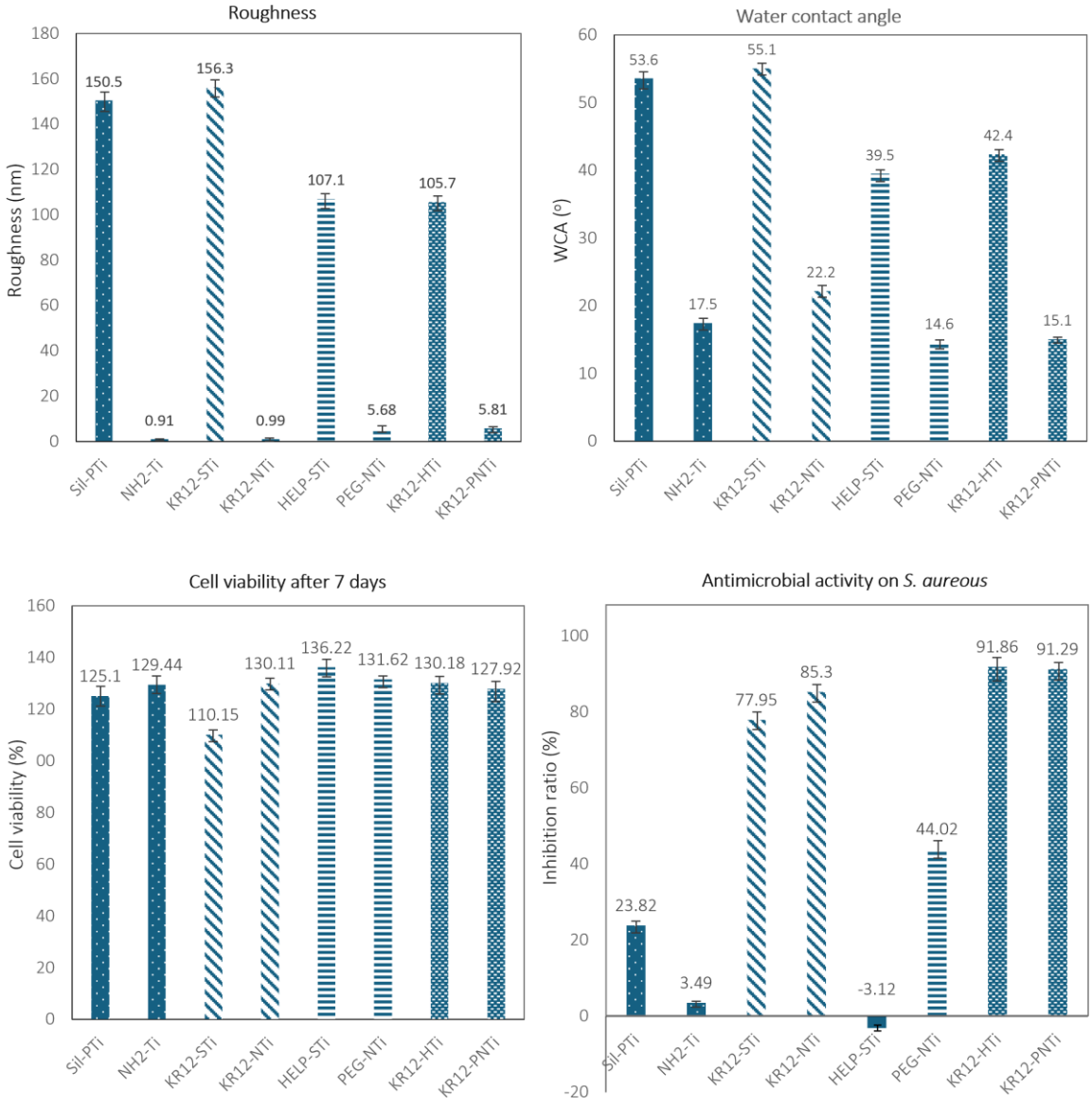


Figure 4-1. Comparison of two methods for functionalising surfaces—silanisation and plasma treatment— the results of surface roughness, water contact angle, cell viability, and bacteria inhibition ratio for prepared samples from both phases of the study.

To compare two methods for functionalising surfaces—silanisation and plasma treatment— the results of various analyses are presented in Figure 4-1, which includes data on surface roughness, water contact angle, cell viability, and bacteria inhibition ratio for samples from both phases of the study. As depicted in Figure 4-1, the silanisation technique used in phase one to create amine groups resulted in significantly higher surface roughness (150.5 nm), approximately 100 times greater than that achieved by plasma treatment (0.91 nm), which is beneficial for cell adhesion and proliferation. The optimal

surface roughness for orthopaedic implants is crucial for promoting osseointegration and ensuring implant stability. Research indicates that intermediately rough surfaces, with roughness values between 1 to 2 µm, are particularly effective in enhancing bone integration [24-26]. This range has been associated with improved cell adhesion and proliferation, leading to better clinical outcomes. It's important to note that the ideal roughness may vary depending on the specific application and implant location. The SEM images also proved that silanisation created a rough, ridge-like structure that encouraged cell adhesion, while KR-12 immobilisation minimally affects surface morphology. The effects of silanisation on the surface morphology are consistent with previous studies, which reported similar roughness and morphology after analysing SEM images [24, 25]. Regarding the effect of plasma treatment on roughness and morphology, Zhang et al. reported reduced roughness and a smoother surface after plasma treatment, which aligns with the findings of our study [26].

In terms of wettability, plasma-treated samples exhibited significantly greater hydrophilicity, with a WCA of 17.5°, which is more than double the hydrophilicity compared to silanised samples that had a WCA of 53.6°. This increase in hydrophilicity is consistent with findings from previous studies. For instance, Boonrawd et al. reported a similar enhancement in surface wettability following plasma treatment, where plasma-modified surfaces showed a drastic reduction in WCA, indicating improved hydrophilicity [27]. Similarly, studies by Ma et al. and Jo et al. demonstrated that plasma treatments effectively alter surface properties by removing contaminants and introducing polar functional groups, which contribute to higher hydrophilicity [28, 29].These results align with the findings in our study, confirming that plasma treatment leads to a notable decrease in WCA, thus improving the interaction between the surface and aqueous environments. On the other hand, silanisation treatments, while increasing hydrophilicity to some extent, do not achieve the same level of enhancement. This is due to the partial presence of hydrophobic silane chains, which limit the overall reduction in WCA [24]. Therefore, plasma treatment proves to be a more effective method for promoting hydrophilicity compared to silanisation, as demonstrated in both our study and those in the literature.

Despite these differences in surface characterisation, cell viability after 7 days was similar across all samples prepared by both methods in phases one and two, and all samples exhibited no cytotoxicity. This suggests that, although plasma treatment and silanisation can significantly alter surface properties such as wettability, roughness, and morphology,

these modifications do not negatively impact the biological compatibility of the materials. Similar observations have been reported in previous studies where surface modifications using plasma treatment or silanisation did not compromise cell viability or induce cytotoxic responses. For instance, studies by Civantos et al. and Kulkarni et al. showed that while surface chemistry changes can influence cell attachment and proliferation, they do not necessarily translate into differences in long-term cell viability [30, 31]. Moreover, it has been consistently demonstrated that both plasma-treated and silanised surfaces maintain their biocompatibility, making them suitable for biomedical applications such as implant coatings [24, 29, 32, 33]. The results of our study further support these findings, indicating that both surface modification techniques are safe for use in medical applications, as they preserve the viability of cells over extended periods without triggering cytotoxic effects.

To compare the antimicrobial activity, the data of *S. aureus* analysis were used as a representative since in orthopaedic applications, *S. aureus* is generally considered the most important and clinically relevant bacterium [34]. When comparing the inhibition ratios against *S. aureus*, the silanised samples demonstrated a mild antimicrobial effect without the addition of peptides, whereas plasma-treated surfaces did not show any antimicrobial activity on their own. However, after directly attaching KR-12 to the functionalised surfaces, plasma-treated samples exhibited an approximately 8% higher inhibition ratio than those prepared by silanisation. Additionally, attaching PEG as a linker without KR-12 resulted in a significant inhibition ratio of 44%, likely due to PEG's antifouling properties, whereas HELP linkers did not exhibit this effect. This also indicated that the choice of linker plays a crucial role in determining the baseline antimicrobial performance of the surface before AMP immobilisation. After immobilising KR-12 on the linker-attached surfaces, all samples, regardless of whether they were prepared by silanisation or plasma treatment, demonstrated similar antimicrobial activity. This suggests that once KR-12 was immobilised on the surface, its antimicrobial properties dominate, and the differences introduced by the initial surface treatments become less significant. These findings align with previous studies that have shown the critical role of AMP immobilisation in achieving effective bacterial inhibition, regardless of the underlying surface chemistry [35, 36]. Thus, while the choice of surface modification technique can influence the baseline antimicrobial properties, the attachment of AMPs like KR-12 remains a key factor in ensuring potent antimicrobial activity.

Based on these comparisons, it can be concluded that plasma treatment is as effective as the commonly used silanisation technique for functionalising surfaces for peptide immobilisation. Both methods yielded similar levels of antimicrobial activity after peptides were attached, demonstrating that plasma treatment can achieve comparable results in terms of surface functionality. However, plasma treatment offers several distinct advantages that make it a more attractive option than silanisation for certain applications. For instance, plasma treatment is a much faster process, as it does not require multiple steps of chemical reactions or lengthy preparation times. Unlike silanisation, which often involves the use of various solvents and reagents, plasma treatment reduces the risk of introducing toxic residues or by-products, which can be crucial for biomedical applications.

Moreover, this simplification translates into a reduction in overall costs, both in terms of materials and process time, making plasma treatment a more cost-efficient alternative. Additionally, the elimination of harsh chemicals in the plasma treatment process also minimises environmental impact and the need for extensive safety precautions, further reducing operational complexities. These factors make plasma treatment not only an effective but also a more sustainable and streamlined approach for functionalising surfaces for peptide immobilisation, especially in industrial or clinical settings where time, cost, and safety are key considerations.

Future work will focus on developing multifunctional coatings that combine bone regeneration with antimicrobial properties. Extensive *in vivo* studies will be conducted to assess the long-term biocompatibility of these coatings, their ability to enhance bone regeneration through interactions with bone cells, and their antimicrobial efficacy over extended periods. Additionally, immune responses to the coated implants will be closely monitored to ensure that the coatings do not trigger adverse reactions or chronic inflammation. The ultimate goal is to create a durable, safe, and effective coating for use in orthopaedic implants.

The antimicrobial activity of AMPs can be influenced by various factors in the in-vivo environment, potentially reducing their effectiveness. Biological fluids such as blood, interstitial fluid, and mucus contain proteolytic enzymes that can degrade AMPs, limiting their stability and antimicrobial action [37-39]. Additionally, the presence of salts and proteins in these fluids can neutralise the electrostatic interactions between AMPs and

bacterial membranes, diminishing their ability to disrupt bacterial cells [39]. Host immune responses may also affect AMP function by either sequestering them or altering their activity through interactions with immune cells and signaling molecules. [40]. Furthermore, the complex and dynamic nature of the in vivo environment, including variations in pH, oxidative stress, and interactions with host tissues, can impact AMP structure and activity [37, 41]. These factors highlight the need for strategies to enhance AMP stability and efficacy in clinical applications, such as encapsulation, chemical modifications, or combination therapies to overcome in vivo challenges [42].

From an industrial perspective, developing antimicrobial coatings for implants requires a balance between efficacy, scalability, cost, and regulatory compliance. Plasma treatment and silanisation both offer viable strategies, each with unique advantages and challenges. Plasma treatment stands out for its rapid processing, reduced chemical usage, and ability to enhance surface properties without altering implant morphology, making it a cost-effective and scalable option. However, its reliance on specialised vacuum equipment may present a barrier to widespread adoption. In contrast, silanisation is more accessible, using conventional chemical processes, but involves multiple reaction steps, organic solvents, and longer processing times, increasing overall costs and complexity. Additionally, regulatory approval remains a critical challenge, as both methods must undergo rigorous biocompatibility and stability testing to meet medical device standards. For successful technology transfer, manufacturers must carefully evaluate the trade-offs between process efficiency, regulatory hurdles, and commercial feasibility to integrate these antimicrobial surfaces into next-generation implant solutions.

4.6. References

1. Kalelkar, P.P., M. Riddick, and A.J. García, *Biomaterial-based antimicrobial therapies for the treatment of bacterial infections.* Nature Reviews Materials, 2022. **7**(1): p. 39-54.
2. Rai, A., et al., *Antimicrobial peptide-based materials: opportunities and challenges.* Journal of Materials Chemistry B, 2022. **10**(14): p. 2384-2429.
3. Fjell, C.D., et al., *Designing antimicrobial peptides: form follows function.* Nature Reviews Drug Discovery, 2012. **11**(1): p. 37-51.
4. Magana, M., et al., *The value of antimicrobial peptides in the age of resistance.* The Lancet Infectious Diseases, 2020. **20**(9): p. e216-e230.

5. Mookherjee, N., et al., *Antimicrobial host defence peptides: functions and clinical potential.* Nat Rev Drug Discov, 2020. **19**(5): p. 311-332.
6. Lazzaro, B.P., M. Zasloff, and J. Rolff, *Antimicrobial peptides: Application informed by evolution.* Science, 2020. **368**(6490): p. eaau5480.
7. Onaizi, S.A. and S.S.J. Leong, *Tethering antimicrobial peptides: Current status and potential challenges.* Biotechnology Advances, 2011. **29**(1): p. 67-74.
8. Mauchauffé, R., et al., *Robust bio-inspired antibacterial surfaces based on the covalent binding of peptides on functional atmospheric plasma thin films.* Journal of Materials Chemistry B, 2014. **2**(32): p. 5168-5177.
9. Chen, Q., et al., *Impact of Antifouling PEG Layer on the Performance of Functional Peptides in Regulating Cell Behaviors.* Journal of the American Chemical Society, 2019. **141**(42): p. 16772-16780.
10. Kostiv, U., et al., *Versatile Bioconjugation Strategies of PEG-Modified Upconversion Nanoparticles for Bioanalytical Applications.* Biomacromolecules, 2020. **21**(11): p. 4502-4513.
11. Hasan, A., et al., *Surface Design for Immobilization of an Antimicrobial Peptide Mimic for Efficient Anti-Biofouling.* Chemistry – A European Journal, 2020. **26**(26): p. 5789-5793.
12. Durán, I.R., et al., *Atmospheric pressure cold plasma versus wet-chemical surface treatments for carboxyl functionalization of polylactic acid: A first step toward covalent immobilization of bioactive molecules.* Colloids and Surfaces B: Biointerfaces, 2020. **189**: p. 110847.
13. Bilek, M.M.M., et al., *Plasma treatment in air at atmospheric pressure that enables reagent-free covalent immobilization of biomolecules on polytetrafluoroethylene (PTFE).* Applied Surface Science, 2020. **518**: p. 146128.
14. Egghe, T., et al., *Silanization of Plasma-Activated Hexamethyldisiloxane-Based Plasma Polymers for Substrate-Independent Deposition of Coatings with Controlled Surface Chemistry.* ACS Applied Materials & Interfaces, 2022. **14**(3): p. 4620-4636.
15. Boix-Lemonche, G., et al., *Covalent grafting of titanium with a cathelicidin peptide produces an osteoblast compatible surface with antistaphylococcal activity.* Colloids and Surfaces B: Biointerfaces, 2020. **185**: p. 110586.
16. Ghaisani, A.D., T.E. Saraswati, and K. Kusumandari, *A comparative amination study of TiO2/Fe3O4/carbon nanocomposites prepared in one- and two-step plasma-based methods.* Chemical Papers, 2024. **78**(2): p. 1227-1237.

17. Finke, B., et al., *Plasma processes for cell-adhesive titanium surfaces based on nitrogen-containing coatings.* Surface and Coatings Technology, 2011. **205**: p. S520-S524.
18. Strauss, L., et al., *Plasma surface modification and three-dimensional structuring of additively manufactured polyetheretherketone implants for improvement of osseointegration.* Plasma Processes and Polymers, 2024. **21**(3): p. 2300082.
19. Seemann, A., et al., *RGD-Modified Titanium as an Improved Osteoinductive Biomaterial for Use in Dental and Orthopedic Implants.* Bioconjugate Chemistry, 2022. **33**(2): p. 294-300.
20. Liu, P., et al., *Plasma-activated interfaces for biomedical engineering.* Bioactive Materials, 2021. **6**(7): p. 2134-2143.
21. Chiang, W.-H., et al., *Microplasmas for Advanced Materials and Devices.* Advanced Materials, 2020. **32**(18): p. 1905508.
22. Nicol, M.J., et al., *Antibacterial effects of low-temperature plasma generated by atmospheric-pressure plasma jet are mediated by reactive oxygen species.* Scientific Reports, 2020. **10**(1): p. 3066.
23. Bandiera, A., et al., *Stimuli-Induced Release of Compounds from Elastin Biomimetic Matrix.* Biomacromolecules, 2014. **15**(1): p. 416-422.
24. Zhao, Y., et al., *Biocompatible silane adhesion layer on titanium implants improves angiogenesis and osteogenesis.* Biomaterials Advances, 2022. **139**: p. 213033.
25. Marín-Pareja, N., et al., *Different organization of type I collagen immobilized on silanized and nonsilanized titanium surfaces affects fibroblast adhesion and fibronectin secretion.* ACS applied materials & interfaces, 2015. **7**(37): p. 20667-20677.
26. Zhang, L.-C., L.-Y. Chen, and L. Wang, *Surface Modification of Titanium and Titanium Alloys: Technologies, Developments, and Future Interests.* Advanced Engineering Materials, 2020. **22**(5): p. 1901258.
27. Boonrawd, W., et al., *Wettability and in-vitro study of titanium surface profiling prepared by electrolytic plasma processing.* Surface and Coatings Technology, 2021. **414**: p. 127119.
28. Ma, C., et al., *Plasma-controlled surface wettability: recent advances and future applications.* International Materials Reviews, 2023. **68**(1): p. 82-119.

29. Jo, W.-L., et al., *Non-thermal atmospheric pressure plasma treatment increases hydrophilicity and promotes cell growth on titanium alloys in vitro.* Scientific Reports, 2023. **13**(1): p. 14792.
30. Civantos, A., et al., *Titanium coatings and surface modifications: toward clinically useful bioactive implants.* ACS Biomaterials Science & Engineering, 2017. **3**(7): p. 1245-1261.
31. Kulkarni, M., et al., *Biomaterial surface modification of titanium and titanium alloys for medical applications.* Nanomedicine, 2014. **111**(615): p. 111.
32. Álvarez-López, A., et al., *Improved cell adhesion to activated vapor silanization-biofunctionalized Ti-6Al-4V surfaces with ECM-derived oligopeptides.* Biomaterials Advances, 2022. **133**: p. 112614.
33. Tsujita, H., et al., *Effect of Plasma Treatment on Titanium Surface on the Tissue Surrounding Implant Material.* Int J Mol Sci, 2021. **22**(13).
34. Pietrocola, G., et al., *Colonization and infection of indwelling medical devices by Staphylococcus aureus with an emphasis on orthopedic implants.* International journal of molecular sciences, 2022. **23**(11): p. 5958.
35. Lei, R., et al., *Turning cationic antimicrobial peptide KR-12 into self-assembled nanobiotics with potent bacterial killing and LPS neutralizing activities.* Nanoscale, 2024. **16**(2): p. 887-902.
36. Diosa, J., et al., *Formation mechanisms of chitosan-silica hybrid materials and its performance as solid support for KR-12 peptide adsorption: Impact on KR-12 antimicrobial activity and proteolytic stability.* Journal of Materials Research and Technology, 2020. **9**(1): p. 890-901.
37. Asif, F., et al., *Antimicrobial peptides as therapeutics: Confronting delivery challenges to optimize efficacy.* The Microbe, 2024. **2**: p. 100051.
38. Andersson, D.I., D. Hughes, and J.Z. Kubicek-Sutherland, *Mechanisms and consequences of bacterial resistance to antimicrobial peptides.* Drug Resistance Updates, 2016. **26**: p. 43-57.
39. Sandhu, A.K., Y. Yang, and W.-W. Li, *In Vivo Antibacterial Efficacy of Antimicrobial Peptides Modified Metallic Implants─Systematic Review and Meta-Analysis.* ACS Biomaterials Science & Engineering, 2022. **8**(5): p. 1749-1762.
40. Zhang, W., et al., *Regulators and signalling in insect antimicrobial innate immunity: Functional molecules and cellular pathways.* Cellular Signalling, 2021. **83**: p. 110003.

41. Yao, L., et al., *Development and challenges of antimicrobial peptide delivery strategies in bacterial therapy: A review.* International Journal of Biological Macromolecules, 2023. **253**: p. 126819.
42. Wang, C., et al., *Antimicrobial peptides towards clinical application: Delivery and formulation.* Advanced drug delivery reviews, 2021. **175**: p. 113818.

Chapter Five:

Conclusions and Future Perspective

5.1. Conclusions

This study focused on addressing peri-implant infections through the use of AMPs due to their broad-spectrum activity against various pathogens and their low potential for inducing bacterial resistance. To enhance the functionality of surfaces for peptide immobilisation, two methods were evaluated: plasma treatment and silanisation. Moreover, a key concern in peptide immobilisation is that AMPs require full flexibility and freedom to effectively interact with bacteria. Therefore, this study also addressed this concern by incorporating linkers like PEG during chemical immobilisation to enhance the flexibility of the AMPs.

Plasma treatment successfully introduced 9.18% primary amine groups on titanium surfaces, significantly higher than the 4.67% achieved with silanisation. Despite the higher density of amine groups with plasma treatment, peptide immobilisation levels were comparable between the two methods, with 59.67 nmol on plasma-treated surfaces and 61.34 nmol on silanised surfaces. This suggests that although plasma treatment introduces more amine groups, these groups may be less stable, leading to similar peptide attachment levels.

Plasma treatment was also found to improve surface energy and wettability without altering the surface topography, thereby enhancing protein adsorption and supporting favorable cell behaviour. This method is advantageous over silanisation due to its efficiency, reduced toxicity, and lower costs, offering a more streamlined and cost-effective approach for functionalising surfaces.

In one part of this study, PEG was employed as a linker for AMPs, improving the mobility of these peptides on the surface at specific concentrations. This strategy aimed to merge antifouling and bactericidal properties while enhancing tissue integration and effectively inhibiting bacterial biofilm formation. The antimicrobial activity against four pathogenic bacterial strains showed more than 90% inhibition of bacterial growth. Surfaces grafted with PEG linkers demonstrated superior resistance to bacterial adhesion and colonisation compared to those without linkers, due to the increased mobility and flexibility of AMPs.

In addition, the study investigated the potential of HELP-based matrices as a linker and delivery system triggered by enzymatic activity in the surrounding environment. HELP linkers were used to facilitate the controlled release of AMPs. Upon exposure to elastase,

a significant release of the KR-12 peptide was observed from HELP-coated surfaces, highlighting the effective degradation and release mechanism provided by HELP.

The antibacterial efficacy of the functionalised surfaces relies on the interplay between the release of antimicrobial peptides and their permanent attachment to the surface. While the release mechanism, as observed with HELP linkers, enables a burst of antibacterial action in response to enzymatic activity, the immobilised peptides provide a sustained protective effect by preventing bacterial adhesion. This balance between transient antimicrobial release and long-term surface functionality is crucial for ensuring continuous protection against infections while maintaining biocompatibility. Future studies should further optimise this dual-action approach to enhance both the initial bactericidal impact and the long-term resistance of implants against biofilm formation.

The antimicrobial activity of surfaces functionalised with KR-12 was assessed against four clinically relevant bacterial strains: *S. aureus*, *S. epidermidis*, *E. coli*, and *P. aeruginosa*. The results demonstrated more than 90% inhibition of bacterial growth. Surfaces with PEG linkers showed an inhibition ratio of 44% due to their antifouling properties, while HELP linkers did not exhibit similar effects. However, when KR-12 was immobilised on surfaces with HELP linkers, the antimicrobial activity was significantly enhanced, attributed to the increased loading density and flexibility of the KR-12 peptides.

Cell viability and adhesion tests further confirmed the biocompatibility of plasma-treated surfaces, demonstrating comparable or even superior cell promotion compared to silanised surfaces. SEM and MTT assay results supported the effectiveness of integrating plasma treatment with peptide immobilisation for improved cell adhesion and antimicrobial performance.

In conclusion, plasma treatment has proven to be as effective as silanisation for functionalising surfaces with peptides while offering additional benefits such as faster processing, reduced toxicity, fewer chemical reactions, and lower costs. The study highlights the potential of plasma treatment combined with HELP-based linkers for developing advanced antimicrobial coatings with enhanced performance and biocompatibility for orthopaedic applications.

5.2. Future perspective

- **Optimising AMP immobilisation techniques**: While the current study has

demonstrated the efficacy of plasma treatment and silanisation for AMP immobilisation, future research should focus on optimising these techniques to enhance the stability and activity of immobilised peptides under physiological conditions. This includes exploring novel plasma parameters and chemical modifications that could further increase the density and stability of functional groups on implant surfaces.

- **Development of smart AMP-responsive coatings**: The integration of smart, stimuli-responsive AMP coatings presents an exciting area for future research. These coatings could be designed to release AMPs in response to specific environmental triggers such as changes in pH, temperature, or the presence of bacterial enzymes. Such systems would allow for on-demand, localised antimicrobial activity, minimising the risk of resistance and reducing the need for systemic antibiotic administration.

- **Exploration of advanced linker systems**: Future studies should investigate the use of advanced linker systems beyond PEG and HELP, which could further improve the flexibility and mobility of immobilised AMPs. New linker molecules with tunable length, flexibility, and degradation rates could be developed to fine-tune the interaction between AMPs and bacterial cells, optimising antimicrobial efficacy while promoting cell adhesion and tissue integration.

- **Polymicrobial infections are increasingly recognised as a significant challenge in implant-associated infections**: These infections often involve complex microbial communities, including bacteria, fungi, and other microorganisms, which interact synergistically to enhance biofilm formation and antibiotic resistance. Understanding how AMP coatings perform in the presence of multiple pathogens, including their ability to prevent biofilm formation and disrupt established microbial communities, will be crucial for developing more robust antimicrobial strategies.

- **Long-term *in vivo* studies and clinical trials**: To bridge the gap between *in vitro* findings and clinical applications, long-term *in vivo* studies and clinical trials are essential. These studies assess the durability, biocompatibility, and antimicrobial performance of AMP coatings over extended periods, providing critical data on their effectiveness in preventing peri-implant infections in real-world medical settings. Before progressing to animal studies, NC3Rs (National Centre for the Replacement, Refinement and Reduction of Animals in Research) can be applied to use alternative

models such as advanced 3D tissue-engineered systems, organ-on-chip models, or *ex vivo* approaches. These models can facilitate analysing the biological responses and improve experimental design, thereby reducing the need for animal testing.

- **Integration with computational design**: The use of computational design and artificial intelligence to predict the behaviour of AMP coatings and optimise peptide sequences for specific applications is a promising direction for future research. By combining experimental data with machine learning algorithms, researchers can accelerate the development of AMP coatings with tailored properties for various biomedical applications.
- **Multi-functional coatings**: Expanding the functionality of AMP coatings to include additional therapeutic properties, such as anti-inflammatory, pro-healing, or osteoinductive effects, could significantly enhance their clinical utility. Research into multifunctional coatings that can simultaneously prevent infection, promote tissue regeneration, and improve implant integration is a promising area for future investigation.
- **Customisation for specific medical devices**: As the field progresses, it will be important to customise AMP coatings for different types of medical devices and implant materials. This could involve tailoring the AMP sequence, immobilisation method, and coating thickness to optimise performance for specific applications, such as dental implants, joint replacements, or cardiovascular stents.
- **Regulatory and manufacturing considerations**: As AMP-coated implants move closer to clinical use, addressing regulatory hurdles and scaling up manufacturing processes will be essential. Future studies should focus on developing standardised protocols for AMP immobilisation that are reproducible, cost-effective, and compliant with regulatory requirements, ensuring a smooth transition from the laboratory to the clinic.

Appendix

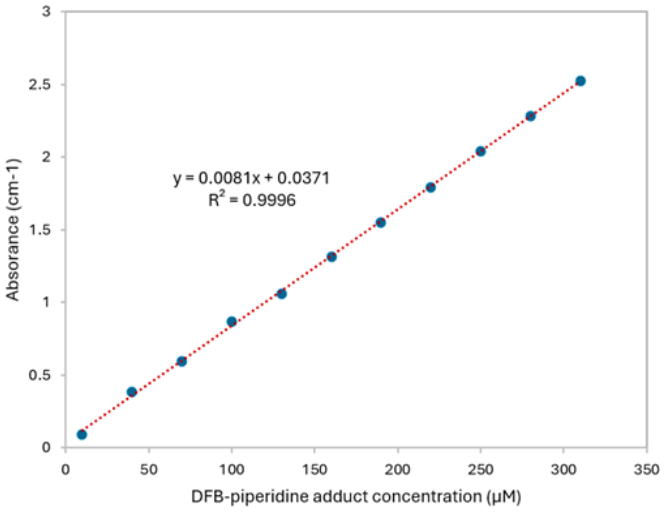
Supporting information

The Details of HELP polypeptide

HELP (clon. 22/3/2004) nel plasmide pEX8EL aa: 536 MW 44885.79 pI: 11.68

Sequence: MRGSHHHHHHGSAAAAAAAAKAAAKAAQFGL VPGVG VAPGVG VAPGVG VAPGVG LAPGVG VAPGVG VAPGVG VAPGIAPA AAAAAKAAAKAAQFGL VPGVG VAPGVG VAPGVG VAPGVG LAPGVG VAPGVG VAPGVG VAPGIAPA AAAAAKAAAKAAQFGL VPGVG VAPGVG VAPGVG VAPGVG LAPGVG VAPGVG VAPGVG VAPGIAPA AAAAAKAAAKAAQFGL VPGVG VAPGVG VAPGVG VAPGVG LAPGVG VAPGVG VAPGVG VAPGIAPA AAAAAKAAAKAAQFGL VPGVG VAPGVG VAPGVG VAPGVG LAPGVG VAPGVG VAPGVG VAPGIAPA AAAAAKAAAKAAQFGL VPGVG VAPGVG VAPGVG VAPGVG LAPGVG VAPGVG VAPGVG VAPGIAPA AAAAAKAAAKAAQFGL VPGVG VAPGVG VAPGVG VAPGVG LAPGVG VAPGVG VAPGVG VAPGIAPGV

a)



b)

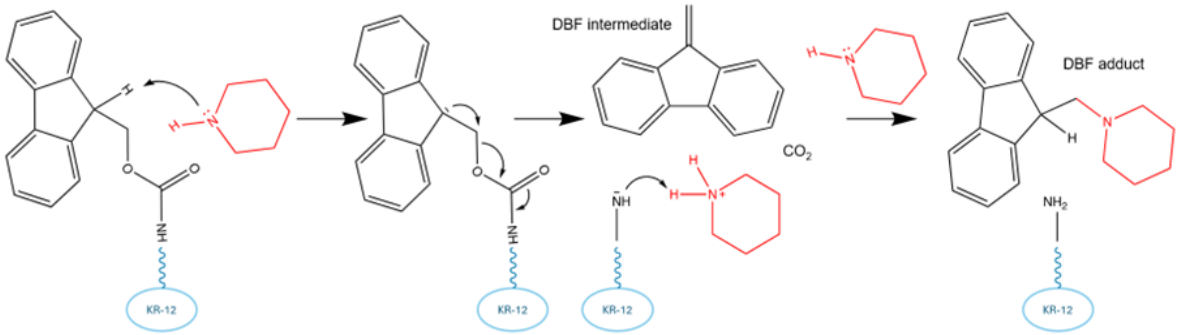


Figure S1. a) Calibration curve of dibenzofulvene-base adduct (µM) vs. absorbance, using 20% piperidine (Panel B) in DMF, b) Mechanism for Fmoc group removal from immobilised KR-12.

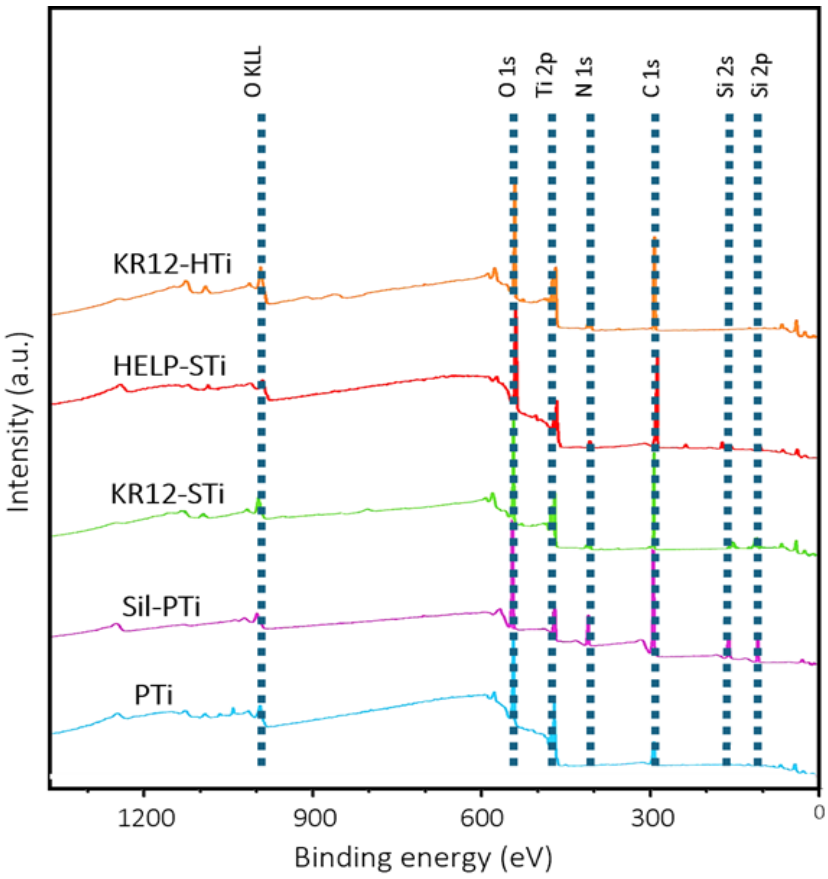


Figure S2. XPS survey spectra of modified surfaces PTi, Sil-PTi, KR12-STi, HELP-STi, and KR12-HTi with characteristic peaks of carbon (C), oxygen (O), nitrogen (N), silicon (Si), and titanium (Ti).